



**Politecnico
di Torino**

Politecnico di Torino

Corso di Laurea Magistrale in Ingegneria Meccanica

A.a. 2020/2021

Sessione di Laurea dicembre 2021

Model-based calibration of a dual -loop EGR CI engine fueled with conventional Diesel and HVO

Academic supervisors:

Prof. Stefano D'Ambrosio
Ing. Alessandro Mancarella
Ing. Andrea Manelli

Candidate:

Simone Marturana

*A mio nonno Mimmo...
...so che sarebbe fiero di me*

Acknowledgement

Grazie a Stefano, Alessandro e Andrea che mi hanno dato l'opportunità di svolgere questa attività, facendomi scoprire cosa fosse realmente l'attività di calibrazione motori. Mi sono stati accanto per tutta la durata di questa attività ed è stato un vero piacere lavorare con loro.

Grazie ai miei genitori e alla mia famiglia, senza i quali molto probabilmente non avrei neanche potuto intraprendere il percorso di studi che oggi mi ha portato dove sono. Questo traguardo è anche merito vostro.

Grazie ai miei amici che sono sempre presenti. So che sono felici per me ed è anche questo che mi spinge ad andare avanti.

Abstract

HVO represents an alternative fuel for diesel engines which can help to reduce the pollutants emissions and the CO_2 production. In the present thesis work, starting from a conventional 2.3 litre diesel engine for light duty application, a further *EGR* system was added, namely the *Long-Route (Low-Pressure)*. For each engine point, preliminary tests were performed in order to evaluate the limit values for the main engine parameters, which determined the domain region for the *DoEs*. The *DoEs* were prepared by means of *MBC Model MATLAB* toolbox and then run on the test bench. The acquired data from pollutants analyzers were post-processed in order to calculate brake specific mass emissions and used to create regression models. Statistical methods were adopted to estimate the goodness of the created models. With the aim to minimize the engine-out emissions of certain pollutant species, optimal calibrations were generated starting from the models and subsequently evaluated at the test bench. This procedure was performed both with conventional *diesel fuel* and with *HVO*, and the results were tested on the engine and compared to investigate the potential of *HVO*. To get further information about the domain region around the optimizations, lambda sweeps of these ones were performed, showing once again the benefits that come from the use of *HVO*.

Also, the addition of the *LP EGR* system to the original engine layout showed good results in NO_x reduction, even if it has led to more complexities in the management of the engine air quantity.

Contents

Acknowledgement.....	4
Abstract	7
List of figures	13
List of tables	17
List of equations	19
Nomenclature	21
Introduction	25
1. Test bench and engine instrumentation	27
1.1. Software component	27
1.2. Dynamometer	31
1.3. Engine	32
1.4. Engine instrumentation.....	33
1.4.1. Pressure sensors	33
1.4.2. Temperature sensors	35
1.4.3. Injectors current measurement system.....	37
1.4.4. Lambda sensors.....	37
1.4.5. Angular speed sensor	38
1.4.6. Intake air mass flow measurement.....	38
1.5. Engine cooling system.....	39
1.6. Fuel consumption measuring system.....	40

1.7. Exhaust emissions bench	42
1.7.1. NO _x measurement	43
1.7.2. CO measurement.....	43
1.7.3. HC measurement.....	45
1.7.4. O ₂ measurement	45
1.7.5. PM measurement	46
2. Exhaust Gas Recirculation	49
2.1. Short-Route (High Pressure) EGR	49
2.2. Long-Route (Low Pressure) EGR	50
2.3. F1A EGR systems	51
3. Diesel Particulate Filter	55
3.1. Structure.....	55
3.2. Filtering.....	56
3.3. Regeneration	57
4. HVO fuel	59
4.1. Context.....	62
4.2. State of the art.....	63
4.3. Effect of HVO on combustion.....	64
5. Experimental procedure.....	65
5.1. Preliminary tests	65
5.2. Design of experiment.....	73
5.2.1. Optimal DoEs creation.....	73
5.2.2. Main statistical parameters	76

5.2.3.	Main statistical functions	78
5.3.	Experimental tests.....	81
5.4.	Calculation of mass emissions.....	81
5.4.1.	Mass evaluation procedure	82
5.4.2.	Evaluation of the number of moles.....	83
5.4.3.	Post elaboration MATLAB software	87
5.5.	Regression models creation.....	87
5.6.	Calibrations generation.....	92
5.7.	Calibrations evaluation on test bench.....	94
5.8.	Diesel and HVO optimal calibrations.....	101
5.8.1.	Calibration optimization: 1250 [rpm] x 2 [bar]	102
5.8.2.	Calibration optimization: 2000 [rpm] x 9.6 [bar]	106
5.8.3.	Calibration optimization: 2250 [rpm] x 14.4 [bar]	109
6.	Lambda sweep of optimal calibrations.....	113
7.	Conclusions.....	117
	Bibliography.....	119

List of figures

Figure 1 – Example of AVL PUMA desktop 1	27
Figure 2 – Example of AVL PUMA desktop 2	28
Figure 3 – Example of AVL IndiCom desktop	28
Figure 4 – Example of INCA desktop	29
Figure 5 – Example of CAMEO desktop	30
Figure 6 – Example of CONCERTO desktop	30
Figure 7 - AVL APA 100 dynamometer	31
Figure 8 - F1A Engine	32
Figure 9 - Piezoelectric pressure sensor Kistler 6058A	33
Figure 10 - Piezoresistive pressure sensor Kistler 4007C	34
Figure 11 - Piezoresistive pressure sensor Kistler 4049B	35
Figure 12 - Thermocouple type-K	36
Figure 13 - Thermistor PT100	36
Figure 14 - Position of the cylinder head thermocouples	37
Figure 15 - Current measuring system Tektronix TCPA300	37
Figure 16 - Lambda sensor UEGO	38
Figure 17 - PicoTurn turbocharger speed sensor	38
Figure 18 - AVL Flowsonix Air	39
Figure 19 - CoolCon engine cooling system	40
Figure 20 - AVL KMA4000	41
Figure 21 - AVL AMA i60 emission bench	42
Figure 22 - CLD scheme	43
Figure 23 - IRD scheme	44
Figure 24 - FID scheme	45
Figure 25 - POD scheme	46
Figure 26 - AVL 415S Smoke meter	47
Figure 27 - Smoke meter characteristics	47
Figure 28 - High pressure EGR layout	50
Figure 29 - Low Pressure EGR layout	50
Figure 30 - Engine air scheme	52
Figure 31 - Three-way LP EGR valve	52

Figure 32 - F1A DPF	55
Figure 33 - Wall-through monoliths.....	56
Figure 34 - DPF scheme	57
Figure 35 – Preliminary EGR trade-off at fixed lambda @ 1250 [rpm] x 2 [bar]	68
Figure 36 - Preliminary EGR trade-off at fixed lambda @ 1500 [rpm] x 9 [bar]	69
Figure 37 – Preliminary EGR trade-off at fixed lambda @ 1750 [rpm] x 5 [bar]	70
Figure 38 - Preliminary EGR trade-off at fixed lambda @ 2000 [rpm] x 9.6 [bar]	71
Figure 39 – Preliminary EGR trade-off at fixed lambda @ 2250 [rpm] x 14.4 [bar]	72
Figure 40 – Example of DoE creation	74
Figure 41 – Example of 1D table EGR constraint.....	75
Figure 42 – Example of 3D Design Projection	75
Figure 43 – Example of PEV surface	76
Figure 44 - Example of use of stepwise regression	80
Figure 45 - Example of use of Box-Cox transformation	80
Figure 46 – Example of Response Model graphs.....	88
Figure 47 – Example of Response Surface.....	89
Figure 48 – Example of Predicted/Observed graph.....	89
Figure 49 - Example of a calibration generated by CAGE.....	93
Figure 50 - Differences between model and experimental data of Diesel optimizations	94
Figure 51 - Differential pressure on DPF of DoE 2250[rpm] x 14.4[bar] Diesel	95
Figure 52 - Cabin and air snorkel temperatures trend of DoE 2250[rpm] x 14.4[bar] Diesel	97
Figure 53 - Cabin and air snorkel temperatures trend of DoE 2250[rpm] x 14.4[bar] HVO	97
Figure 54 - EGR cooler inlet and outlet pressures of DoE 2250[rpm] x 14.4 [bar] Diesel	98
Figure 55 - Coolant water temperature of DoE 2250[rpm] x 14.4[bar] Diesel	99
Figure 56 - Lambda values of the repetition points of the DoE 2250[rpm] x 14.4[bar] Diesel.....	100
Figure 57 –Variations of Diesel and HVO optimizations respect to baseline @ 1250 [rpm] x 2 [bar]	102

Figure 58 - In-cylinder pressure and HRR of optimizations and baseline @ 1250 [rpm] x 2 [bar]	105
Figure 59 - Mass fraction burned of optimizations and baseline @ 1250 [rpm] x 2 [bar]	106
Figure 60 – Variation of Diesel and HVO optimizations respect to baseline @ 2000 [rpm] x 9.6 [bar]	107
Figure 61 - In-cylinder pressure and HRR of optimizations and baseline @ 2000 [rpm] x 9.6 [bar]	108
Figure 62 - Mass fraction burned of optimizations and baseline @ 2000 [rpm] x 9.6 [bar]	108
Figure 63 – Variation of Diesel and HVO optimizations respect to baseline @ 2250 [rpm] x 14.4 [bar]	109
Figure 64 - In-cylinder pressure and HRR of optimizations and baseline @ 2250 [rpm] x 14.4 [bar]	111
Figure 65 - Mass fraction burned of optimizations and baseline @ 2250 [rpm] x 14.4 [bar]	112
Figure 66 - Comparison of lambda trade-offs of Diesel and HVO optimizations @ 1250[rpm] x 2[bar]	114
Figure 67 - Comparison of lambda trade-offs of Diesel and HVO optimizations @ 2000[rpm] x 9.6[bar]	115
Figure 68 - Comparison of lambda trade-offs of Diesel and HVO optimizations @ 2250[rpm] x 14.4[bar]	116

List of tables

Table 1 - Dynamometer characteristics	31
Table 2 - Main engine parameters	32
Table 3 - Kistler 6058A characteristics	33
Table 4 - Kistler 4007C characteristics	34
Table 5 - Kistler 4007C characteristics	35
Table 6 - AVL KMA4000 characteristics	41
Table 7 – Main engine components.....	53
Table 8 - HVO and EN590 Diesel characteristics.....	61
Table 9 - Engine points tested and their base calibration.....	65
Table 10 – Starting engine calibrations for EGR sweeps of preliminary tests.....	66
Table 11 - Variations of HVO compared to Diesel fuel for preliminary tests	67
Table 12 - V values of DoEs	76
Table 13 - Model statistical parameters of DoE 1250[rpm] x 2[bar] HVO	90
Table 14 - Model statistical parameters of DoE 1250[rpm] x 2[bar] Diesel fuel.....	90
Table 15 - Model statistical parameters of DoE 2000[rpm] x 9.6[bar] HVO	91
Table 16 -Model statistical parameters of DoE 2000[rpm] x 9.6[bar] Diesel fuel.....	91
Table 17 - Model statistical parameter of Doe 2250[rpm] x 14.4[bar] HVO.....	92
Table 18 - Model statistical parameters of DoE 2250[rpm] x 14.4[bar] Diesel fuel.....	92
Table 19 - Temperatures comparison between two DoE	97
Table 20 - Differences in the use of the exhaust flap @ 1250 [rpm] x 2 [bar].....	103
Table 21 - Diesel, HVO and baseline calibrations @ 1250 [rpm] x 2 [bar].....	104
Table 22 – Combustion parameters of optimizations and baseline @ 1250 [rpm] x 2 [bar]	104
Table 23 - Diesel, HVO and baseline calibrations @ 2000 [rpm] x 9.6 [bar].....	107
Table 24 - Combustion parameters of optimizations and baseline @ 2000 [rpm] x 9.6 [bar]	109
Table 25 – Diesel, HVO and baseline calibrations @ 2250 [rpm] x 14.4 [bar]	110
Table 26 - Combustion parameters of optimizations and baseline @ 2250 [rpm] x 14.4 [bar]	111

List of equations

(2. 1)	46
(4. 1)	61
(5. 1)	66
(5. 2)	77
(5. 3)	77
(5. 4)	77
(5. 5)	77
(5. 6)	77
(5. 7)	77
(5. 8)	78
(5. 9)	78
(5. 10)	78
(5. 11)	79
(5. 12)	82
(5. 13)	82
(5. 14)	82
(5. 15)	82
(5. 16)	82
(5. 17)	83
(5. 18)	83
(5. 19)	83
(5. 20)	83
(5. 21)	83
(5. 22)	84
(5. 23)	84
(5. 24)	84
(5. 25)	84
(5. 26)	84
(5. 27)	84

(5. 28)	84
(5. 29)	84
(5. 30)	84
(5. 31)	85
(5. 32)	85
(5. 33)	85
(5. 34)	85
(5. 35)	85
(5. 36)	86
(5. 37)	86
(5. 38)	86
(5. 39)	86
(5. 40)	86
(5. 41)	94
(5. 42)	101
(5. 43)	101
(5. 44)	101
(5. 45)	103

Nomenclature

<i>AC</i>	Alternate current
<i>BMEP</i>	Brake mean effective pressure
<i>bsfc</i>	Brake specific fuel consumption
<i>bTDC</i>	Before top dead centre
CF_{cooler}	Dry-wet conversion factor
<i>CFPP</i>	Cold filter plugging point
<i>CI</i>	Compression ignition
<i>CLD</i>	Chemiluminescence detector
<i>CN</i>	Combustion noise
<i>CPO</i>	Crude palm oil
<i>DC</i>	Direct current
<i>DF</i>	Diesel fuel
<i>DL</i>	Dual-loop EGR
<i>DOC</i>	Diesel oxidation catalyst
<i>DoE</i>	Design of experiment
<i>DPF</i>	Diesel particulate filter
<i>DT1</i>	Dwell time between the main and the first pilot injection
<i>DT2</i>	Dwell time between the main and the second pilot injection
<i>ECU</i>	Electronic control unit
<i>EGR</i>	Exhaust gas recirculation
<i>EU</i>	European Union
<i>FAME</i>	Fatty acid methyl esters
<i>FFA</i>	Free fatty acids
<i>FID</i>	Flame ionization detector
<i>FSN</i>	Filter smoke number
<i>H</i>	Hydrogen
H_{low}	Lower heating value
H_{abs}	Absolute air humidity
<i>HC</i>	Unburned hydrocarbon

<i>HP</i>	High pressure
<i>HRR</i>	Heat release rate
<i>HVO</i>	Hydrotreated vegetable oil
<i>ICE</i>	Internal combustion engine
<i>ID</i>	Ignition delay
<i>IMEP</i>	Indicated mean effective pressure
<i>IRD</i>	Infrared detector
<i>K</i>	Equilibrium constant for water-gas reaction
<i>k</i>	Parameter of Box-Cox transformation
<i>LP</i>	Low pressure
\dot{m}	Mass flow rate
<i>M</i>	Molecular weight
M_x	Molar mass of the pollutant species X
M_{exh}	Exhaust gas average molecular weight
\dot{m}_{exh}	Mass-flow rate of exhaust gases
\dot{m}_{fuel}	Fuel mass-flow rate
<i>MFB</i>	Mass fraction burned
<i>MFB 10</i>	10% of mass fraction burned
<i>MFB 50</i>	50% of mass fraction burned
<i>MFB 90</i>	90% of mass fraction burned
n_{eng}	Rotational speed of the engine
NO_x	Generic nitrogen oxide pollutants
n_j	Number of moles of the specie j
n_{turbo}	Rotational speed of the turbocharger
p_{boost}	Relative engine boost pressure
p_{bTC}	Pressure before turbine
p_{rail}	Rail pressure
<i>PEV</i>	Predicted error variance
<i>PFAD</i>	Palm fatty acid distillate
<i>PID</i>	Proportional integrative derivative
<i>PM</i>	Particulate matter

<i>PMEP</i>	Pumping mean effective pressure
<i>POD</i>	Paramagnetic oxygen detector
<i>PRESS</i>	Predicted residual error sum of square
q_{pil1}	Quantity of the pilot injection number 1
q_{pil2}	Quantity of the pilot injection number 2
<i>SAF</i>	Sustainable aviation fuel
<i>SSE</i>	Sum of squared estimate of errors
<i>SSR</i>	Residual sum of squares
<i>SST</i>	Total sum of squares
R^2	Coefficient of determination
R^2_{Adj}	Adjusted coefficient of determination
<i>RMSE</i>	Root mean square error
<i>SOC</i>	Start of combustion
SOI_m	Start of injection of the main injection
SOI_{pil1}	Start of injection of the first pilot injection
SOI_{pil2}	Start of injection of the second pilot injection
<i>T</i>	Temperature
T_{intake}	Temperature at the intake manifold
<i>THC</i>	Total unburned hydrocarbon
<i>UEGO</i>	Universal exhaust gas oxygen
<i>VGT</i>	Variable geometry turbine
<i>W</i>	Brake power output
<i>W-G</i>	Water-gas
<i>X</i>	Any of the pollutant species; mass fraction
[<i>X</i>]	Volume fraction of the pollutant specie X
{ <i>X</i> }	Mass fraction of the pollutant specie X
{ \dot{X} }	Mass-flow rate of the pollutant specie X
{ <i>X</i> } _{bs}	Brake specific mass emissions of the pollutant specie X
X_b	Mass fraction burned
<i>y</i>	Response model
<i>ZLEV</i>	Zero and low emission vehicle

α	Air-fuel ratio
λ	Relative air-fuel ratio
η_{bth}	Brake thermal efficiency

Introduction

Environmental problems related to air pollution have led to an increasing attention to internal combustion engines' emissions. In January 2019, European Union has set new rules that will ensure that from 2030 onwards new cars will emit on average 37.5% less CO_2 and new vans will emit on average 31% less CO_2 compared to 2021 levels. Between 2025 and 2029, both cars and vans will be required to emit 15% less CO_2 . The Parliament and the Council agreed on a mechanism to encourage the sale of more *ZLEV (Zero and Low Emissions Vehicles)*, such as fully electric or plug-in hybrid cars.

Even if modern technologies have made possible a continuous improvement both of after-treatment systems and engines design, these solutions seem not to be enough to overcome future pollutant emissions standards. Because of this, it is necessary to improve *ICEs (Internal Combustion Engine)*, trying to make them increasingly environment friendly.

Due to this, during this thesis work, model-based calibrations optimizations were performed in order to get a reduction of the main pollutant species and a reduction of fuel consumption. Tests were performed both with *EN590 Diesel* and with *Hydrotreated Vegetable Oil (HVO)*, to investigate the behaviour of this kind of diesel fuel on a light duty engine.

HVO has potential to emerge as an alternative fuel to mineral diesel due to its favourable properties. The ability to produce *HVO* from non-edible feedstock benefits the well-to-wheel carbon dioxide emissions, which reportedly can be reduced by 90% when compared to diesel fuel. As shown by Hunicz et al., *HVO* has similar properties to diesel fuel, so its application is not limited to small-scale blends, as with *FAME (Fatty acid methyl ester)*. Thus, *HVO* can fully utilise the existing fuel infrastructure and is currently available as stand-alone.

Advanced biofuels are one of the tools that can help limit CO_2 emissions in the transport sector, so much so that the *European Union* promotes their use by means of specific directives such as the *RED (Renewable Energy Directive) II* of December 2018.

Biofuels are one of the solutions available to us when it comes to limiting CO_2 emissions from transport. In order for them to be truly sustainable, however, it is important that they no longer be produced from raw materials that would otherwise be used for food or for which dedicated crops have to be created, taking up valuable agricultural land.

1. Test bench and engine instrumentation

The experimental tests carried on during this thesis work were performed at the dynamic test bench located at the *Dipartimento di Energia* at the *Politecnico di Torino*. Most software and hardware components of the test bench are *AVL*. During this chapter all the main important systems concerning the test bench are discussed.

1.1. Software component

In the control room of the dynamic test bench are located the PCs with the software necessary to control and make the test bench work.

By means of *AVL PUMA* software, it is possible to manage all the systems necessary to perform the tests, e.g., to control the engine working point, to dialogue with the emission bench and the fuel measuring system, monitor the engine cooling system and to get information about pressures and temperatures of the engine. Through *PUMA* it is possible to acquire the interested engine's parameters, to control electro-valves which regulate the cooling/warming of the engine coolant water, to dialogue with the *fuel consumption measuring system*, exhaust emissions bench, engine instrumentation and *ECU*.

In Figure 1 and Figure 2 are shown the two desktops in which *PUMA* runs.

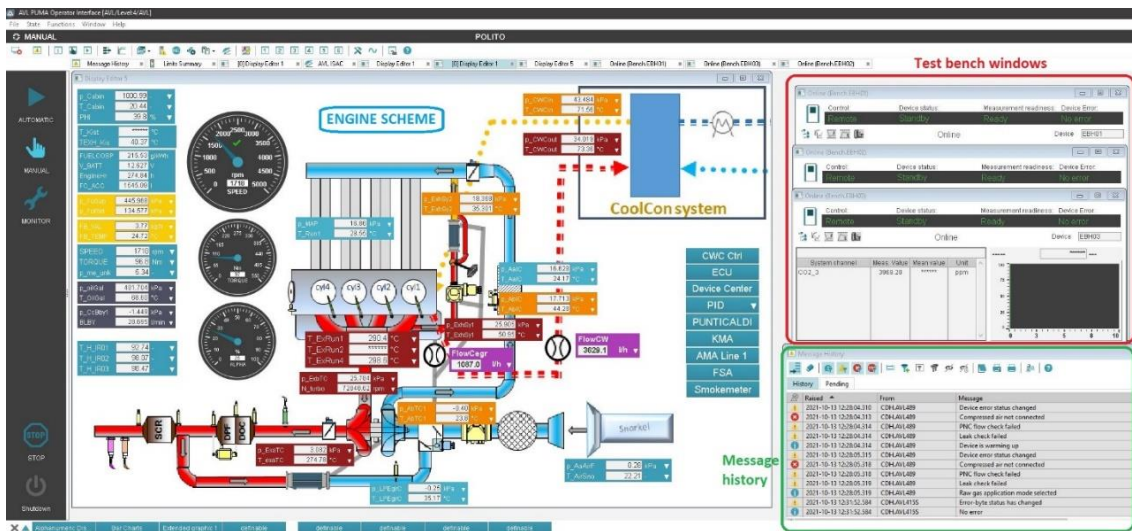


Figure 1 – Example of AVL PUMA desktop 1



Figure 2 – Example of AVL PUMA desktop 2

By means of *AVL IndiCom* software it is possible to get the in-cylinder pressure tracks which come from high-frequency sensors and so the real time *HRR* is calculated. *IndiCom* also provide to acquire current signals from current clamp, giving information about fuel injections.

In Figure 3 is shown the desktop in which runs *IndiCom*.

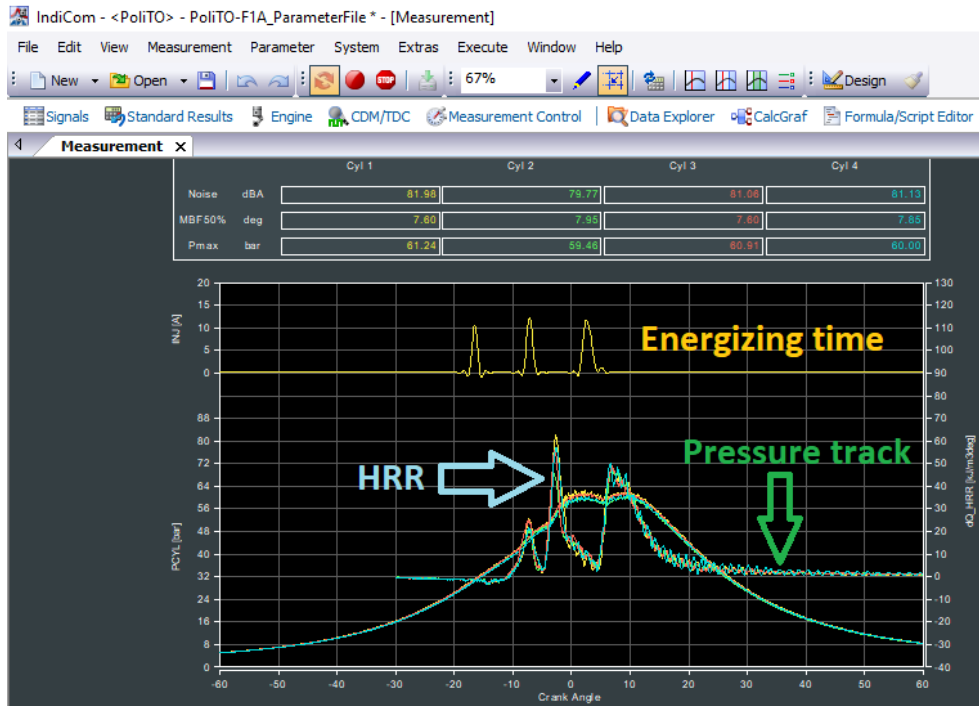


Figure 3 – Example of AVL IndiCom desktop

By means of *INCA* software, which is connected to the engine *ECU*, it is possible to control and modify the engine calibration, changing maps and parameters, e.g., *rail pressure* (p_{rail}), *SOI*, *VGT* position, *EGR* actuation, *dwell time*, pilots' injection quantities (q_{pil}), etc. An example of *INCA* desktop is presented in Figure 4, in which are visible the p_{rail} map, the actuators maps, the window concerning the injection parameters, the pressure drop across the *DPF*, the measure from *lambda* sensor and many other engine data.

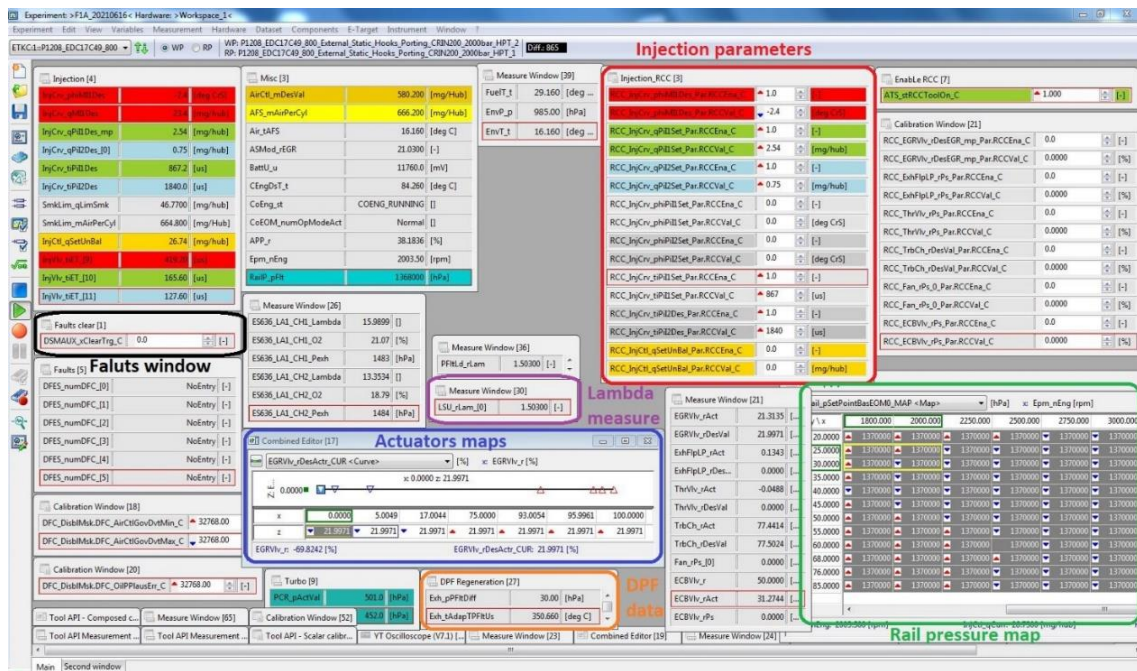


Figure 4 – Example of INCA desktop

By means of *CAMEO* software it is possible to implement the variation list and to program all the steps of the *DoE*. This software provides to follow these steps completely by itself, setting engine calibrations, running the emissions measurements and acquiring the data. In Figure 5 is shown the *Run Test* window of *CAMEO* during the running of a *DoE*.

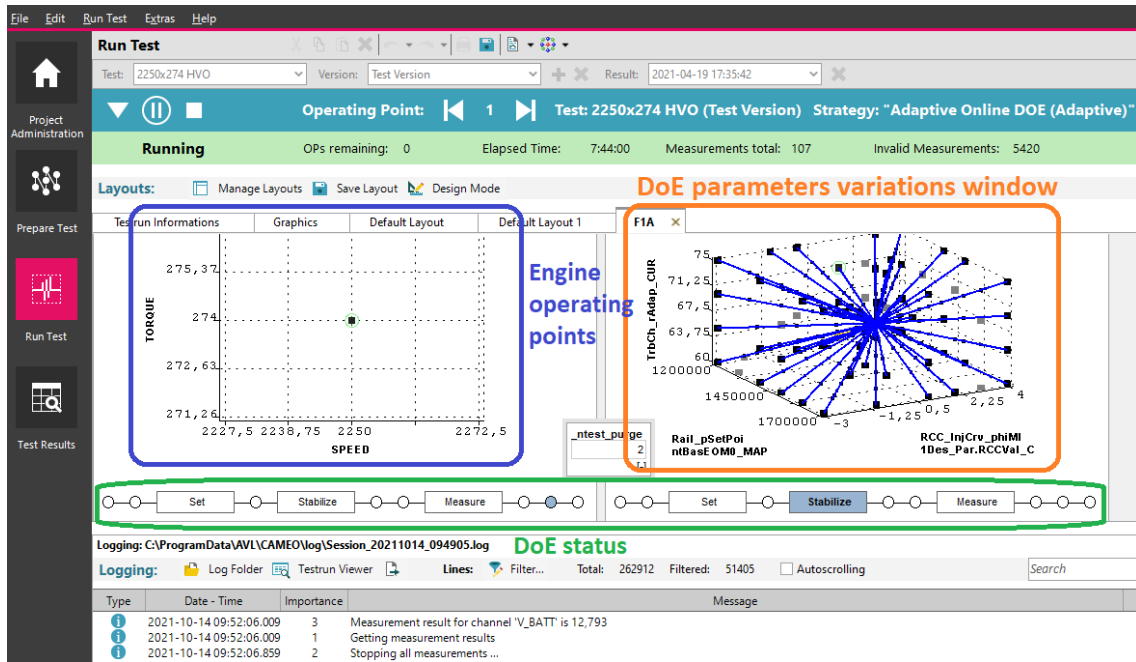


Figure 5 – Example of CAMEO desktop

By means of *AVL CONCERTO* software, emissions values measured and all the data regarding the engine and the test bench were collected. It allows also to display the quantity of interest after acquiring, like pollutants emissions and fuel consumption, as shown in Figure 6.

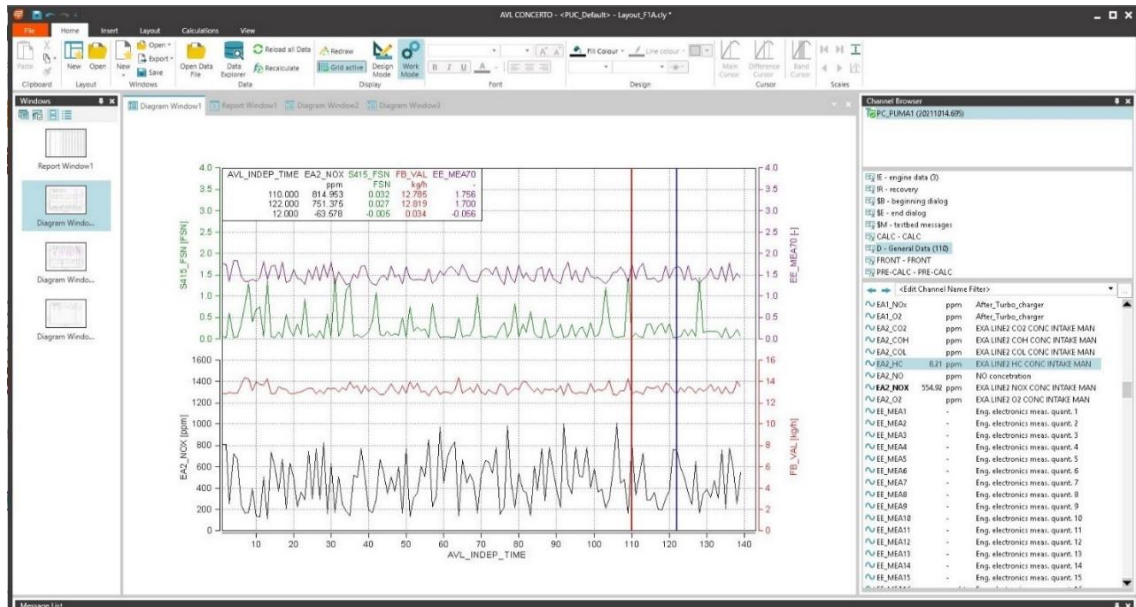


Figure 6 – Example of CONCERTO desktop

1.2.Dynamometer

The test bench is equipped with an *AVL APA 100 dynamometer*, which is a reversible electric machine. It can work both as a motor, carrying on the engine and permitting to evaluate its friction, and as a brake. Linked to the engine flywheel by means of a removable joint, it allows to make the engine work under specific load and speed conditions, adjustable by the user. This dynamometer can also operate in dynamic conditions in order to simulate load and speed transients.

In Figure 7 is shown the dynamometer and in Table 1 its main characteristics.



Figure 7 - AVL APA 100 dynamometer

<i>Characteristic</i>	<i>Value</i>
<i>Max angular speed</i>	12000 rpm
<i>Max torque</i>	525 Nm
<i>Max power</i>	200 kW
<i>Mass moment of inertia</i>	0.32 kg * m ²

Table 1 - Dynamometer characteristics

1.3.Engine

The engine tested is the variable geometry turbocharged Diesel *FIA FPT* designed for light duty vehicles (*Ducato*). In Table 7 are listed the main engine parameters and the *FIA engine* in shown in Figure 8.

<i>Engine parameters</i>	<i>Value</i>
<i>Bore</i>	88 mm
<i>Stroke</i>	94 mm
<i>Connecting rod length</i>	146 mm
<i>Compression ratio</i>	16.3
<i>Displacement</i>	2.3 l
<i>Number of cylinders</i>	4
<i>Firing order</i>	1-3-4-2
<i>Emission standard</i>	Euro 6 d final
<i>Max. power</i>	102 kW
<i>Max. torque</i>	400 Nm
<i>Supercharging</i>	Variable Turbine Geometry
<i>Exhaust gas recirculation</i>	LP and HP, water cooled
<i>Exhaust system</i>	DOC, DPF
<i>Fuel injection</i>	Common rail

Table 2 - Main engine parameters



Figure 8 - FIA Engine

1.4.Engine instrumentation

Engine is equipped with temperature, pressure and flow sensors which mensuration values can be monitored through *PUMA* software in real time.

1.4.1. Pressure sensors

In-cylinder pressure sensors

To get information about in-cylinders pressures, piezoelectric pressure sensors are installed instead of glow plugs by mean of an adaptor. The used ones are the high-frequency *Kistler 6058A* type. Piezoelectric pressure sensors are made of quartz crystal, which is exposed, through a diaphragm, to the combustion chamber environment. Quartz crystal reacts to a mechanical compression by producing an electric voltage; in this way, an electric voltage proportional to the in-cylinder pressure is obtained. Then an amplifying and filtering of this electric signal are performed.

In Figure 9 is shown the piezoelectric sensor in question and in Table 3 its main characteristics.



Figure 9 - Piezoelectric pressure sensor Kistler 6058A

<i>Characteristics</i>	<i>Value</i>
<i>Measuring range</i>	0 – 250 bar
<i>Overload</i>	300 bar
<i>Operating temperature range</i>	-50 – 400 °C

Table 3 - Kistler 6058A characteristics

Intake manifold pressure sensors

To get information about intake manifold pressure, a piezoresistive pressure sensor is here installed. The used one is *Kistler 4007C*. Piezoresistive pressure sensors working principle is based on Wheatstone bridge which generates an electric signal proportional to the applied pressure.

In Figure 10 is shown the piezoresistive sensor in question and in Table 4 its main characteristics.



Figure 10 - Piezoresistive pressure sensor Kistler 4007C

<i>Characteristics</i>	<i>Value</i>
<i>Measuring range</i>	0 – 250 bar
<i>Overload</i>	400 bar
<i>Operating temperature range</i>	-40 – 200 °C

Table 4 - Kistler 4007C characteristics

Exhaust manifold pressure sensors

To get information about exhaust manifold pressure, a piezoresistive pressure sensor is here installed. The used one is *Kistler 4049B*. Due to the high temperature reached by the exhaust manifold (over 500°C), this pressure sensor is water cooled. The measurement element is situated in an oil-filled cavity separated by a steel diaphragm, placed within a cooled jacket; thanks to this, the internal temperature is nearly independent from the hot gas one.

In Figure 11 - Piezoresistive pressure sensor Kistler 4049B is shown the piezoresistive sensor in question and in Table 5 its main characteristics.



Figure 11 - Piezoresistive pressure sensor Kistler 4049B

<i>Characteristics</i>	<i>Value</i>
<i>Measuring range</i>	0 – 10 bar
<i>Overload</i>	25 bar
<i>Operating temperature range</i>	0 – 1100 °C

Table 5 - Kistler 4007C characteristics

1.4.2. Temperature sensors

Temperature sensors employed in this engine instrumentation are of two types: *thermocouples* and *thermistors*.

Thermocouples

Thermocouple consists of two dissimilar electrical conductors forming an electrical junction. Its working principle is based on *Seebeck effect*, according to which, when an electric conductor is subjected to a thermal gradient, an electric charge displacement is induced, consequently an electric voltage, proportional to the thermal gradient, can be measured. Thermocouples can be of different types depending on the temperature levels and the materials used for the conductors; for this engine instrumentation, *type-K* have been used, which can be exposed to temperatures up to 1260 °C. In order to get temperature's information in the regions and engine's components of interest, thermocouples have been mounted at the intake runner, exhaust runners, after turbine, after *LP EGR cooler*, before and after *HP EGR cooler*, after *turbocharger* and before and after *intercooler*.

In Figure 7 thermocouple *type-K* is shown.

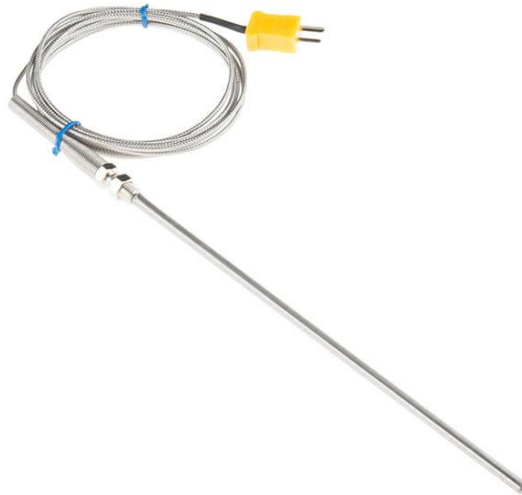


Figure 12 - Thermocouple type-K

Thermistors

Thermistors are made of semiconductor material whose resistivity is inversely proportional to their temperature and this change is measured by *Wheatstone bridge*. By sending an electrical current, the drop voltage across the thermistor is related to the variation of resistance, and by means of calibration, it can be linked to the temperature. In this engine instrumentation, *PT100* thermistors have been employed to monitor fluids temperature, such as engine, *EGR* and *intercooler* cooling water.

In Figure 13 a thermistor *PT100* is shown.

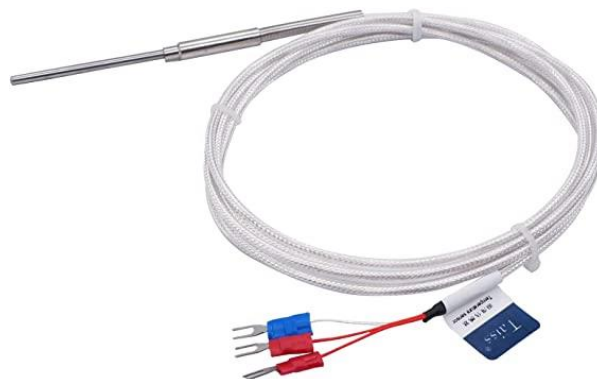


Figure 13 - Thermistor PT100

In Figure 14 is shown the positioning of the thermocouples installed on the cylinder head to monitor the combustion chamber temperature in three different points.

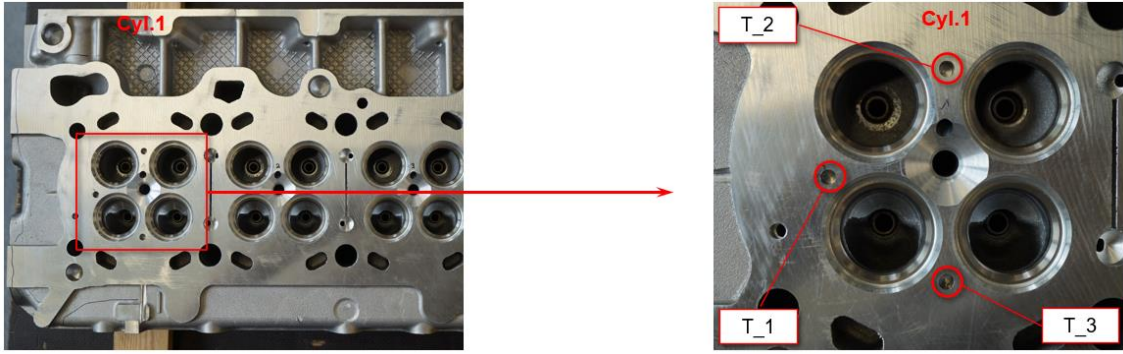


Figure 14 - Position of the cylinder head thermocouples

1.4.3. Injectors current measurement system

In order to get current signal corresponding to the injection rate of the injectors, a current measurement system *Tektronix TCPA300* has been installed. This system consists in an amplifier and an AC/DC current probe. Thanks to the connection with *IndiCom* software, it is possible to see on-screen oscilloscope.

In Figure 15 the amplifier and its probe are shown.



Figure 15 - Current measuring system Tektronix TCPA300

1.4.4. Lambda sensors

Lambda sensors UEGO (universal exhaust gas oxygen) have been employed to measure the oxygen concentration in air flow.

In addition to its standard *lambda* sensor at the exhaust pipe, another one has been installed, and both are before *DOC*. In order to investigate the *EGR* flow coming from *HP* and *LP* circuits, additional *lambda* sensors were mounted, one at intake pipe and one after the *intercooler*.

In Figure 16 the *lambda* sensor is shown.



Figure 16 - Lambda sensor UEGO

1.4.5. Angular speed sensor

A *PicoTurn* angular speed sensor has been installed at the turbocharger. It exploits the eddy current reduction technique: it directly senses each vane of the turbocharger wheel with a speed sensor that is mounted in a hole bored into the turbocharger housing. To get turbocharger speed is important also because it is linked to the engine boost level.

In Figure 17 the *PicoTurn* sensor is shown.



Figure 17 - PicoTurn turbocharger speed sensor

1.4.6. Intake air mass flow measurement

An *AVL Flowsonix* has been mounted at the engine intake pipe to get an accurate measurement of air consumption. It uses two ultrasound pulses, one propagating into the

air flow and one against it; the system measures the acceleration of the sound pulse travelling with the air flow, as well as the deceleration of the sound pulse travelling against the air flow. By comparing the two results, the mass air flow through the intake can be assessed, with a measurement uncertainty of less than 1%.

In Figure 18 is shown the device in question.



Figure 18 - AVL Flowsonix Air

1.5.Engine cooling system

The engine has not its own cooling system so, in order to monitor the coolant water temperature, an external cooling system, called *CoolCon*, has been installed. This consists in a manually variable head pump, a water-water heat exchanger, a heater and an electro valve to regulate the cooling water flow.

Engine coolant water coming out from the engine passes through the heat exchanger where is cooled by the external cooling water; the flow of this last one fluid is regulated thanks to the electro valve. It in turn is monitored from *PID* system; by setting *PID*'s parameters and temperature target, it will provide to reach and to maintain the desired engine water temperature. *PID* parameters and temperature target can be varied by user from *PUMA* interface.

It is also present a heater which provides to make the engine water temperature grow, used to accelerate the warm-up phases.

In Figure 19 is shown the engine cooling system.



Figure 19 - CoolCon engine cooling system

1.6. Fuel consumption measuring system

For the real-time engine fuel consumption measuring the test bench is equipped with an *AVL KMA4000*. Fuel, stored in an external drum, is moved to the test bench tank by an external pump when *PUMA* software is switched to “*Manual*”; for safety reasons, every time the test bench is switched to “*Monitor*”, the fuel inside the internal tank is moved back to the drum by a return line. From the test bench tank, the fuel is aspirated, by another pump, and comes inside the measuring system where it passes through a bubble detector and, if it necessary, the *KMA4000* asks to the user to run a bubble separation: it will be performed by the instrument itself and provide to remove air from fuel. Then the fuel is filtered and passes through a heat exchanger, a density sensor and a volume flow rate meter. All these parameters are directly visible by the *KMA* windows on *PUMA*. Fuel pressure is maintained constant by means of a pressure relief valve. The measuring system provide also to manage the fuel coming from the return line of the injection system. An additional heat exchanger is installed in the test bench in order to maintain quite constant the fuel temperature.

In Figure 20 is shown the fuel consumption measurement system and in Table 6 its main characteristics.

<i>Characteristics</i>	<i>Value</i>
<i>Flow rate measure range</i>	0.02 – 380 kg/h
<i>Density measure range</i>	0.5 – 2.0 g/cm ³
<i>Volume flow rate measure error</i>	± 0.1 %
<i>Density measure error</i>	± 0.03 %
<i>Mass flow rate measure error</i>	± 0.1 %

Table 6 - AVL KMA4000 characteristics



Figure 20 - AVL KMA4000

1.7.Exhaust emissions bench

The analysis of raw exhaust gases is performed by an *AVL AMA i60 emission bench*, which provide to measure the concentration of CO , NO_x , HC , CO_2 and O_2 . It consists of three measuring probes: one installed downstream the *DOC* and one upstream to measure pollutants concentration; the third is mounted at the intake to measure CO_2 and O_2 concentrations to evaluate *EGR* rate. Probes are heated and maintained at the constant temperature of $190^{\circ}C$ to avoid condensation of chemical species on the walls. Tanks with specified concentrations of gases are connected to the emission bench in order to perform the analyzers calibration (zero and span gas).

When *AVL AMA i60* is switched to “*Measure*”, its internal pumps aspire the raw gases through the probes. Since particulate matter is not measured by this instrument and it can damage the analyzers, it must be removed: in order to do this, raw gas passes through a ceramic filter. After this, depending on the type of measurement, raw gas passes through a second filtering stage: in case of dry measurement the filtering stage consists of a paper filter; in case of wet measurement, it consists of a metallic filter.

In Figure 21 is showed the emission bench.



Figure 21 - *AVL AMA i60 emission bench*

What concerns *PM* measuring it is entrusted to an *AVL Smoke Meter*, which is separated from the previous one.

1.7.1. NO_x measurement

The NO_x emissions measurement is performed by the *CLD* (*Chemiluminescence detector*). In the chamber of the reactor a vacuum pump provides to control the pressure; here exhaust gas meets the ozone particles generated by an ozonizer. The NO molecule reacts with O_3 giving rise to NO_2 molecules electronically excited; this will return to its base state by emitting a light radiation, which is measured by a photoelectric device and turned to an electric signal. With this procedure only NO concentration can be measured; to get also the NO_x concentration it is necessary to let the raw gas pass through a catalytic converter, which provides to transform NO_2 to NO , and then proceeding with the measurement.

The scheme of *CLD* is shown in Figure 22.

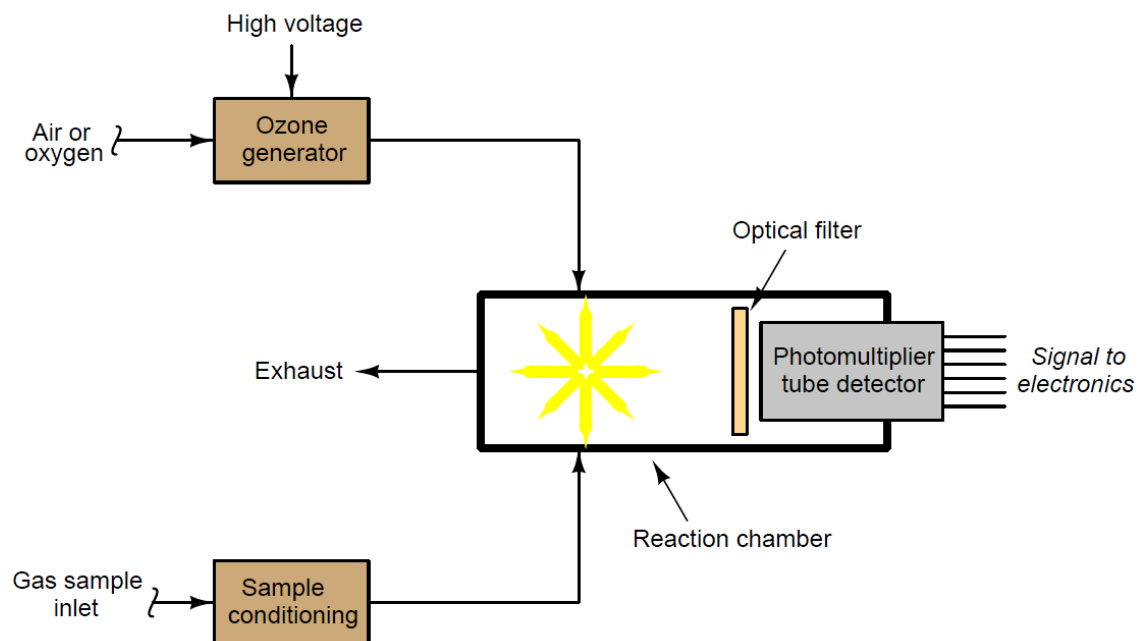


Figure 22 - CLD scheme

1.7.2. CO measurement

The CO emissions measurement is performed by the *IRD* (*Infrared Detector*). Its working is based on the principle for which a gas, exposed to infrared radiations, absorbs only that one with a certain wavelength, related to the atomic composition of the specie. In this

analyzer, two volumes with two different gases are exposed to an infrared radiation produced by an emitter. In one cell flows the exhaust gas coming from the engine; the other one is filled with a reference gas, usually nitrogen or pure air. These volumes are separated by a flexible membrane which forms one of the two plates of a capacitor. Due to the different nature of the gases inside the two cells, the radiations absorption will be different; in particular it is proportional with the concentration of the specie. This causes a thermal gradient, and so different pressure levels, between the two side of the flexible membrane, which will react by deflecting: this deflection varies the characteristic of the capacitor, and it can be related to a current signal.

A chopper is inserted between infrared source and the cells: it consists of a disc with holes which rotates at a constant angular speed. The chopper alternatively stops and let the radiation pass, in order to get a cyclic variation of the signal of the diaphragm. Thanks to this it is possible to convert a DC electrical signal into an AC signal, since AC amplification are more suitable to perform high signal amplification.

Since absorption spectra of CO_2 has an overlap with that one of CO for a certain range of wavelength, a filter containing great quantity of the interference gas is positioned after the sample cell to minimize this undesired effect.

The scheme of *IRD* is shown in Figure 23.

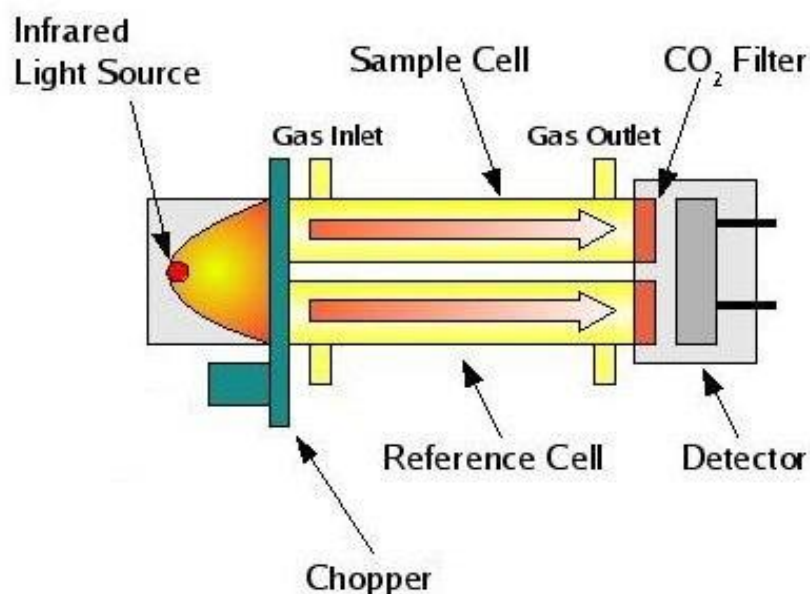


Figure 23 - IRD scheme

1.7.3. HC measurement

The *HC (unburned Hydrocarbons)* emissions measurement is performed by the *FID (Flame Ionization Detector)*. It is based on the principle that a pure hydrogen flames burning in air, generates a negligible number of ions, while an hydrocarbons combustion produces a quite strong ionization. The analyzers is made of a burner in which exhaust gas flows through the flame produced by the combustion of hydrogen and pure air. The unburned hydrocarbons present in the exhaust gas, generate an ionization proportional to the number of burned carbon atoms. Due to these ions, an electric current flow can be measured between the two electrodes of the instrument.

The scheme of *FID* is shown in Figure 24.

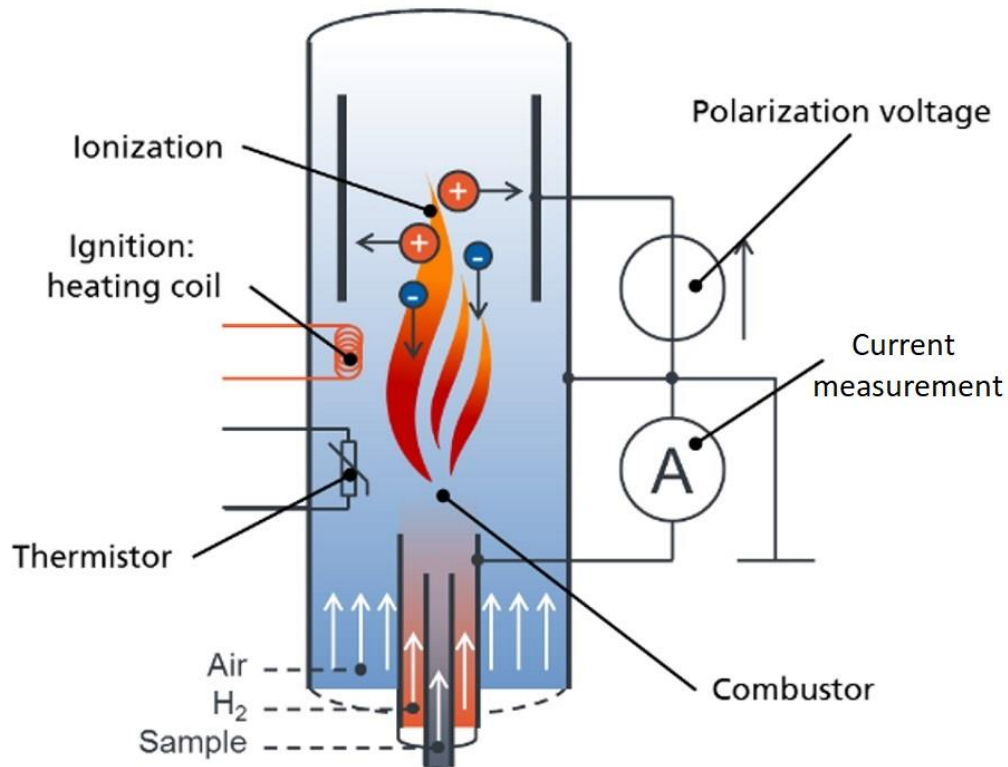


Figure 24 - FID scheme

1.7.4. O₂ measurement

The *O₂* concentration measurement is performed by the *POD (Paramagnetic Oxygen Detector)*. It exploits the paramagnetic behaviour of the oxygen molecules. The system is composed by a torsion bar, with two spheres at extremities, embedded in a magnetic field. This one varies according to the oxygen concentration, modifying the repulsion force on the spheres and so the angular position of the bar. The system will provide to

restore the reference angular position by energizing a solenoid connected to the bar; the solenoid current demand is directly connected to the oxygen concentration.

The scheme of *POD* is shown in Figure 25.

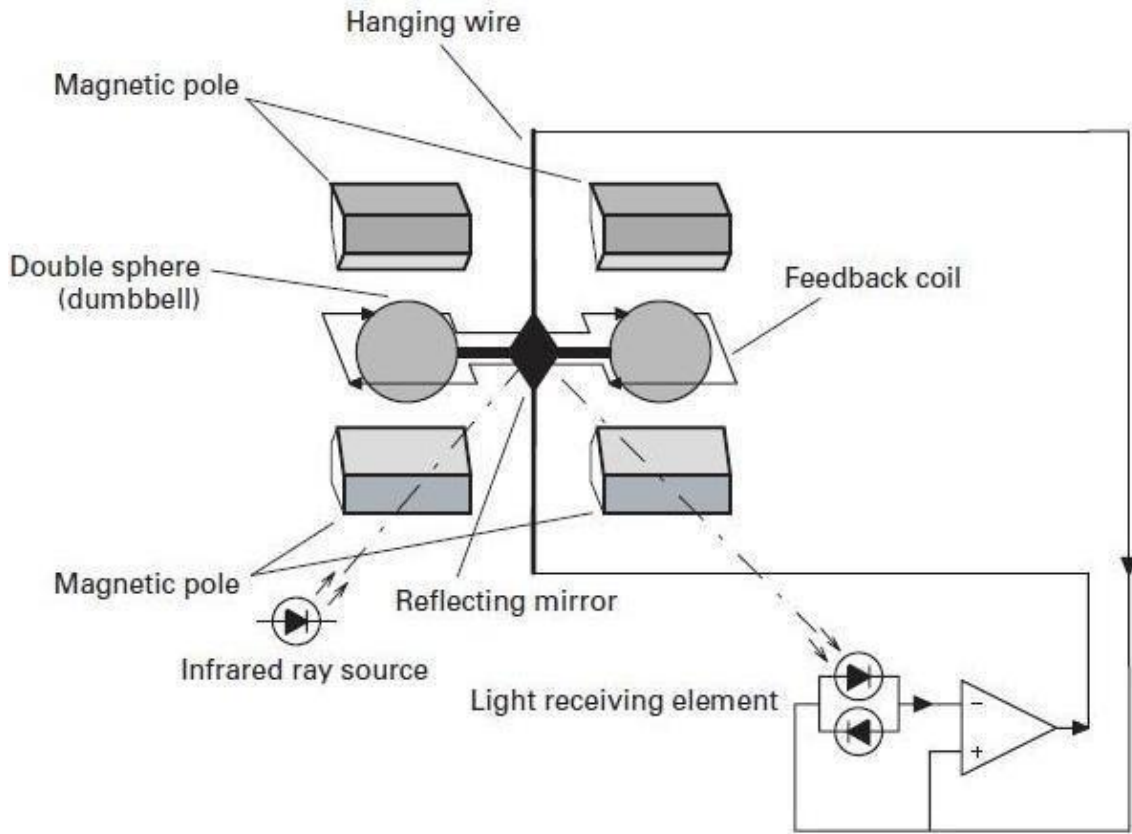


Figure 25 - *POD* scheme

1.7.5. PM measurement

The analysis of *soot* emissions is performed by an *AVL 415S Smoke meter*. A diaphragm pump collects a precise sample of exhaust gas and make it pass through a white paper tape: this causes the fouling of the paper. This last one is then illuminated by a light source, and a photoelectric sensor measures the reduction of reflectance of the filter, due to the blackening caused by the *soot*.

The result of the measurement is a *Filter Smoke Number (FSN)* indicating of *soot* emission; it is calculated as it follows:

$$FSN = \left(1 - \frac{I/I_0}{I_{clean}/I_0} \right) A \quad (2.1)$$

where: I_0 is the *light intensity on the filter*; I is the *light intensity reflected from the filter* after its blackening; I_{clean} is the *light intensity reflected from the clean filter*.

In Figure 26 is shown the *smoke meter* and in Table 6 its main characteristics.



Figure 26 - AVL 415S Smoke meter

<i>Characteristic</i>	<i>Value</i>
<i>Measured range</i>	0 to 10 FSN
<i>Detection limit</i>	0.002 FSN or 0.02 mg/m ³
<i>Maximum exhaust temperature</i>	600 °C
<i>Ambient conditions</i>	5 to 55°C / max. 95% relative humidity

Figure 27 - Smoke meter characteristics

2. Exhaust Gas Recirculation

Exhaust Gas Recirculation (EGR) is an emission control strategy allowing significant engine-out NO_x emission reductions. It is a method by which a portion of engine's exhaust gas is returned to the combustion chamber. This effect is mainly due to the lower oxygen levels and to the reduction of temperatures reached during the combustion process. This reduction is obtained through three effects:

- 1- *Dilution effect*. Flame temperature reduction operated by the dilution of the fresh air charge with burned gas. It is due to a less mass ratio between oxygen and fuel in the burning zone, interfering with fuel oxidation. This is the dominant effect.
- 2- *Thermal effect*. Burned gas, composed primarily of CO_2 and water, have a higher thermal capacity respect to fresh air, composed primarily of O_2 and N_2 ; therefore, the thermal capacity of the charge increases.
- 3- *Chemical effect*. Due to the lower temperature reached, dissociation phenomenon become less relevant, and this cause a slight increase of the temperature. This effect is the less important.

Since the *EGR* gas are at higher temperatures, this determines an increase in of the charge temperature; at high *EGR* rates, this might lead to an increase of NO_x emissions due to excessively high intake manifold temperature. For this reason, two coolers, one for *Low Pressure* and one for *High Pressure EGR*, are installed.

The main *EGR* architectures used are two: *Short-Route* and *Long-Route EGR*.

2.1.Short-Route (High Pressure) EGR

Exhaust gas is taken before the turbine inlet and deflected towards the intake manifold; gas is cooled by means of an *EGR* cooler, which also has a by-pass circuit to avoid *EGR* gas cooling during engine warm-up. The *EGR* rate is proportional to the pressure drop across the engine, i.e., between the exhaust and the intake manifold; therefore, the recirculated quantity can be limited. To overcome to this drawback, a *throttle valve*, positioned after the *intercooler*, provides to decrease the intake manifold pressure in order to enhance the *EGR* rate.

In Figure 28 is schematized the *short-route EGR* circuit.

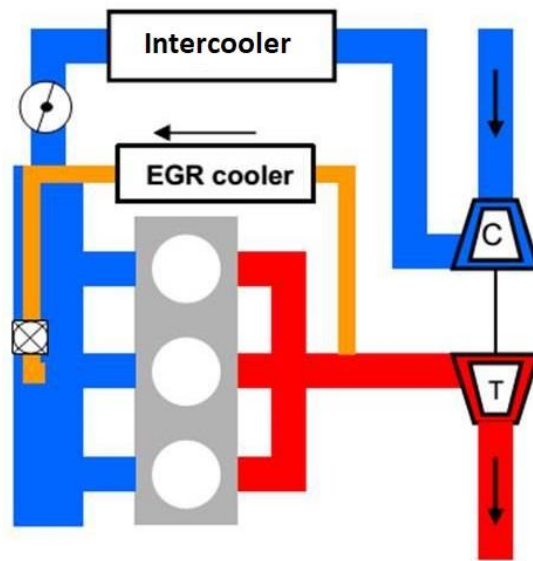


Figure 28 - High pressure EGR layout

2.2. Long-Route (Low Pressure) EGR

Exhaust gas is taken at the outlet of the after-treatment system. It passes through an *EGR cooler* and it is recirculated at the inlet of the compressor. This system allows a greater *EGR* rate than the *HP* one, because the pressure level at the exhaust is always higher than ambient pressure present at the inlet of the compressor. The drawback is the slow response to the transient, due to the long track of the gas.

In Figure 29 is schematized the *long-route EGR* circuit.

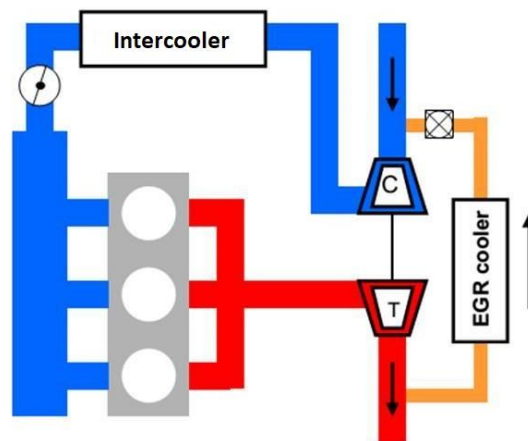


Figure 29 - Low Pressure EGR layout

2.3.F1A EGR systems

F1A engine has both two *EGR* circuits; this complicates the engine layout and its air control but allows to investigate their effects on pollutants and *brake specific fuel consumption (bsfc)*. During the tests, in addition to the use alternatively only the *LP* or only the *HP*, a blending of them has been used.

Originally the only *EGR* circuit present on the engine was the *HP* one; afterwards the *LP* one was added. Besides the mechanical processing necessary to equip the engine with an additional *EGR* system, also the electric control of the *LP* valve and its position feedback had to be made; in order to do this, the actuator and control of the exhaust flap was used. For this reason, the *ECU* control variable corresponding to the *LP EGR* valve is “*ExhFlap*”, while the one corresponding to the exhaust flap is “*ExhFan*”, which belonged to a fan present in the exhaust pipe.

HP EGR rate is controlled by a valve with position feedback; it allows the exhaust gas to pass directly from the exhaust manifold to the intake, after being cooled by the *HP EGR Cooler*.

What concerns *LP EGR*, exhaust gas, coming from turbine outlet, is withdrawn at the outlet of the *DOC*. It passes through the *LP EGR cooler* and finally arrives at the compressor inlet. The ratio between *LP EGR* and fresh air rate is regulated by a three-way valve with position feedback.

In Figure 30 is schematized the engine air circuit and the two *EGR* systems, while in Table 7 are listed the main engine components concerning the previous scheme.

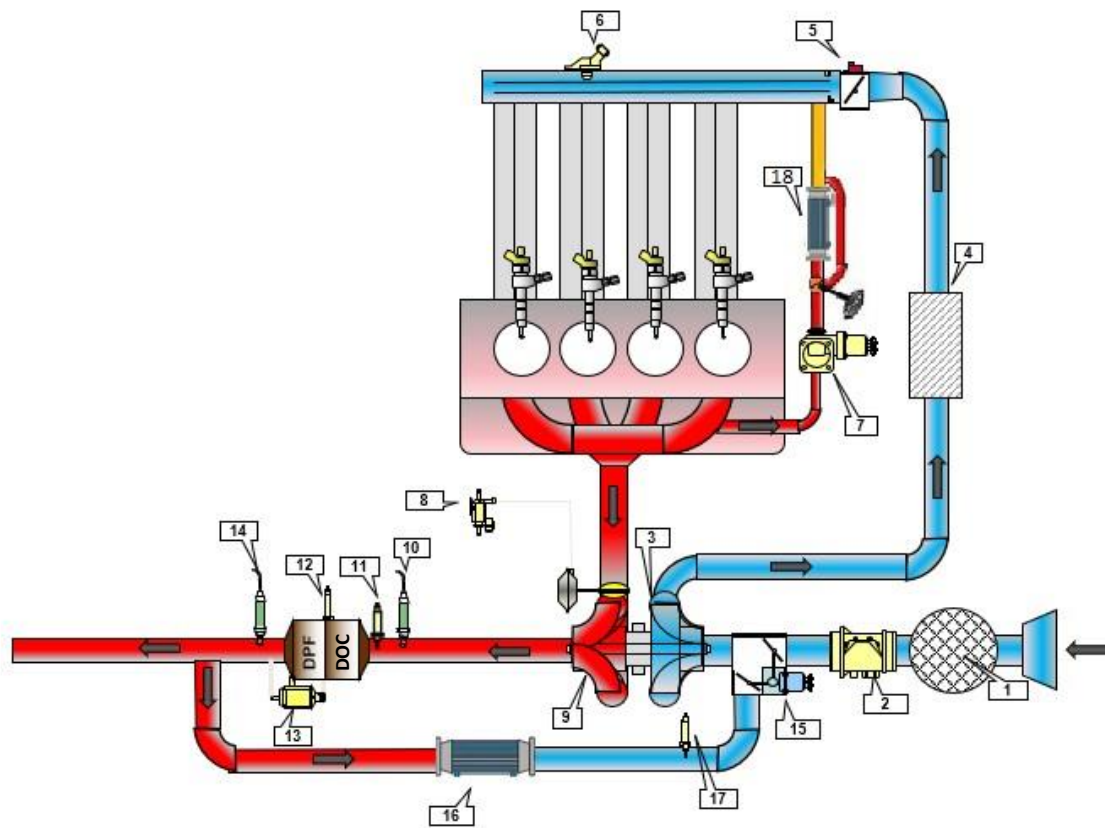


Figure 30 - Engine air scheme

In Figure 31 is shown the three-way valve adopted to regulate the *LP EGR* rate.

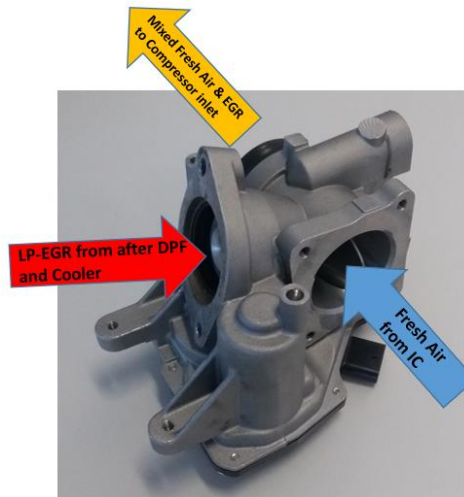


Figure 31 - Three-way LP EGR valve

N.	Engine component
1.	<i>Air filter</i>
2.	<i>Air flow meter (mass and temperature)</i>
3.	<i>Compressor</i>
4.	<i>Intercooler</i>
5.	<i>Throttle Valve Actuator with position feedback</i>
6.	<i>Intake manifold pressure and temperature sensor</i>
7.	<i>HP EGR valve with position feedback</i>
8.	<i>VGT Turbocharger actuator</i>
9.	<i>VGT Turbocharger with position feedback</i>
10.	<i>Lambda sensor #1</i>
11.	<i>Inlet catalyst temperature sensor</i>
12.	<i>Inlet DPF temperature sensor</i>
13.	<i>DPF differential pressure sensor</i>
14.	<i>Lambda sensor #2</i>
15.	<i>LP EGR valve (3-way) with position feedback</i>
16.	<i>LP EGR Cooler</i>
17.	<i>LP EGR Cooler outlet temperature sensor</i>
18.	<i>HP EGR Cooler</i>

Table 7 – Main engine components

3. Diesel Particulate Filter

Diesel Particulate Filter (DPF) is a device that physically captures all the solid particles coming out from the engine.

F1A engine is equipped with a *DOC* closed coupled *DPF* shown in Figure 32.



Figure 32 - F1A DPF

3.1. Structure

DPF are usually of the wall-through type and typically utilizes a cordierite or silicon carbide or aluminium titanate wall-flow particulate filter substrate, with channels alternatively plugged at the ends, to force the gas through the porous walls; by means of this, particulate matter is mechanically trapped and separated from the exhaust gas flow. The most significant differences between the three materials lay in the thermal expansion coefficient and in the thermal conductivity: during soot burning, the hotter regions tend to expand, compressing the colder ones and generating mechanical stresses inside the component. These are the main drawbacks of silicon carbide; for these reasons it is not generally possible to build a monolithic *SiC* filter, but it is usually made up of small square segment.

The two types of monoliths most frequently used in automotive applications are shown in Figure 33.

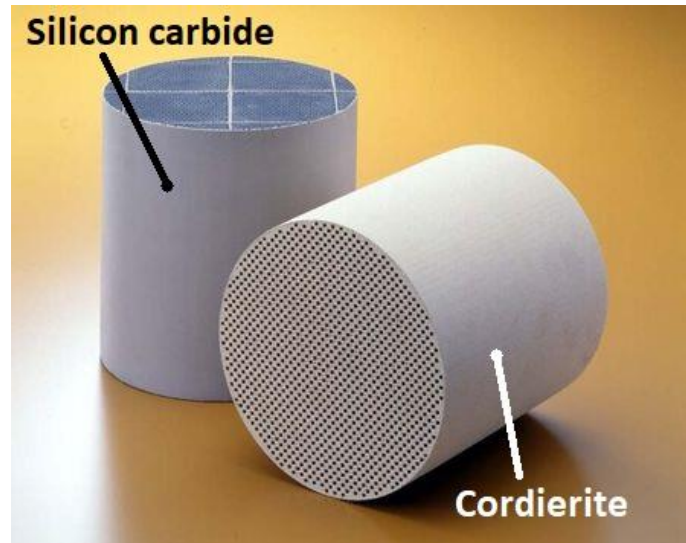


Figure 33 - Wall-through monoliths

3.2. Filtering¹

Particles separation from exhaust gas takes place with two filtering ways:

- 1- **Deep bed filtration:** after transport to the filter grain surface, particles are then attached to the surface of the grain by a variety of mechanisms. These mechanisms depend greatly on the chemical characteristics of the filter system. The forces involved in attachment can be divided into two groups. One group consists of the London-Van der Waals attraction force and the electric double-layer force; these forces are called long-range forces, as they influence transport and attachment even when particles are separated from the filter by 100nm. The second group of forces is the Born repulsion force and hydration force; they are called short-range forces due to their influence on particles being dominant only if the particles within 5 nm from filter surface.
- 2- **Surface separation filtering:** filter pores dimensions must be smaller than particles dimensions, in order to perform this kind of filtering. In the first phase, particles with greater dimensions remain attached on the filter surface. In this way,

¹

[1] G. Keir, V. Jegatheesan and S. Vigneswaran, “Deep bed filtration: modelling theory and practice,” *Research gate*, 2009.

the particles clog the filter pores, by forming a layer called “cake”, which initially contributes to increase the filtering efficiency.

DPFs usually work with a combination of these two kinds of filtering ways.

A scheme of *DPF* and its working principle are shown in Figure 34 .

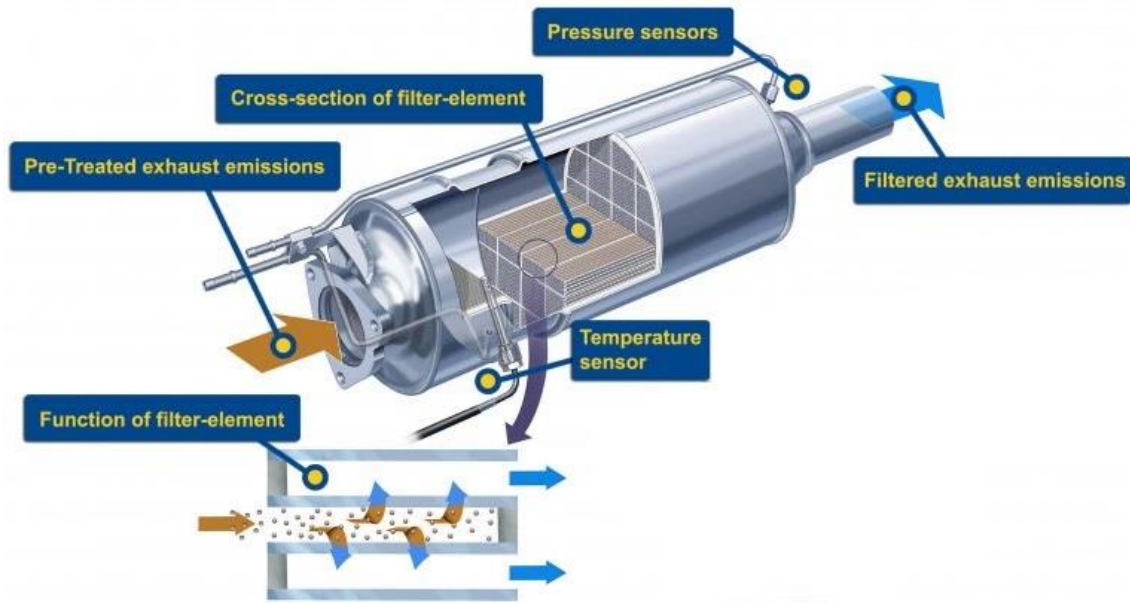


Figure 34 - *DPF* scheme

3.3.Regeneration

During its working, *DPF* collects particulates, but an excess of *soot* attached on the filter surface may cause an excessively high exhaust gas drop pressure, which would negatively affect the engine working. Therefore, *DPF* have to provide a way of removing particulates from the filter, to restore its *soot* collection capacity. The way to do this is called “*regeneration*” and it can be performed continuously, during regular operation of the engine, or periodically, after a pre-determined quantity of *soot* has been accumulated. During the periodical regeneration, called also “*forced regeneration*”, the *ECU* implements firstly a different fuel injection strategy, activating the “*after*” injections, to increase the *DPF* inlet temperature; obviously the main injection quantity has to be adjusted to satisfy the torque demand. If this is not enough to reach the target temperature, the *ECU* activates the “*post*” injections, which consist in very-late fuel injections that will not burn inside the combustion chamber but along the exhaust line.

During the tests, to avoid any unexpected variation on the injection strategy, unwanted by the user, the possibility of the *ECU* to intervene on the injection strategy, in order to perform the *DPF* forced regeneration, was disabled. For this reason, during the use of the test bench, the drop pressure across the *DPF* was monitored. When necessary, the forced regeneration was performed making work the engine at high speed and medium-high load; the recommended engine working point for regeneration was 3500 rpm x 206 Nm.

4. HVO fuel

As described in the article “*Ecofining: turning organic waste into biofuel*”, available to the ENI website, the *Ecofining*TM system, patented by ENI, allows to transform raw materials of biological origin into biofuels, known in technical terms as *HVO* (*Hydrotreated Vegetable Oil*). The process itself is very flexible, meaning that it can be used to treat different types of feedstocks, from vegetable oils to animal fats and even used cooking oils and algal oils. Unlike traditional biofuels produced from crops that could otherwise be used for food, advanced biofuels process waste and crops that do not take land away from agriculture, such as algae, straw, crude glycerine, shells, agricultural and forestry clippings, and organic waste from separate collections. Unlike the conventional biodiesel production process, *Ecofining*TM also produces a high-quality biofuel that contains no oxygenated components and has a high cetane number, meaning improved performance, regardless the feedstock used. Conventional biodiesel - technically referred to as *FAME* - production plants use the *transesterification* process whereby incoming triglycerides are treated with methanol to obtain a product whose characteristics depend heavily on the type of raw material used. Two other major limitations of this system are the difficulty integrating it into existing refineries and the production of crude glycerine, which can only be enhanced following an expensive purification process. The *Ecofining*TM technology overcomes these obstacles by replacing *transesterification* with a different chemical process consisting of two subsequent stages - *hydrogenation* and *isomerisation* - the former involving treating the initial feedstock with hydrogen to eliminate oxygen and saturate the double bonds, the latter “restructuring” the resulting paraffins to improve their cold properties².

Despite the more expensive production process of *HVO*, with a *CAPEX* (Capital expenditure) of typically 1-1,2€/L (assuming a ~227M litre facility), compared to a *CAPEX* of f 0,4-0,5 €/L (~136M litre facility) for *FAME*, *HVO* shows some clear competitive advantages when compared to *FAME* fuels³.

² ENI, “Ecofining: turning organic waste into biofuel,” [Online]. Available: <https://www.eni.com/en-IT/operations/biofuels-ecofining.html>.

³ C. Nicolais and A. Del Pia, *Biofuels: NextChem innovative proposition to drive the future of transportation*, NextChem, 2020.

The significant differences in terms of chemical structure between *FAME* and traditional diesel, explains why this type of biofuel is used only as drop-in elements in diesel (usually with a ration between 5-20%). Therefore, performance issues typically restrict high blending of *FAME* with petroleum diesel. Using an excessive amount of *FAME* as diesel blending may in fact damage rubber components in older vehicles and cause filter blockage.

HVO is a paraffinic compound, and the lack of aromatics rings is the reason of the reduced emitted particulate matter. On the other hand, *Diesel Fuel (DF)* has a complex paraffinic-olefin-aromatic structure.

In principle, biobased diesel fuel component can be used in three ways:

- 1- To add a couple percent of biocomponent into diesel fuel. This is a common approach with ester-type biodiesel fuels (*FAME*), and the amount is currently limited to maximum 5 vol-% by the *EN 590:2004* standard.
- 2- To blend tens of percent of biocomponent into diesel fuels. This is possible with *HVO* without compromising fuel quality, exhaust emissions and engine operation. In fact, the fuel blend, will be premium grade, since *cetane number* is increased and aromatic content is decreased.
- 3- To use *HVO* as a pure fuel in order to reduce exhaust emissions.

In Table 8 are listed the main features of the *HVO* compared to the ones of *EN590* Diesel fuel. The lower density and viscosity of *HVO* respect to diesel fuel, support spray propagation and mixture formation.

<i>Characteristic</i>	<i>Unit of measure</i>	<i>EN590</i>	
		<i>Diesel</i>	<i>HVO</i>
<i>Density at 15°C</i>	<i>kg/m³</i>	830.60	777.80
<i>Kinematic viscosity</i>	<i>mm²/s</i>	2.969	2.646
<i>Dynamic viscosity</i>	<i>Pa · s</i>	$2.47 \cdot 10^{-3}$	$2.06 \cdot 10^{-3}$
<i>Cetane number</i>	-	54.60	79.60
<i>Monoaromatic</i>	<i>% v/v</i>	20.10	0.50
<i>Polyaromatic</i>	<i>% v/v</i>	3.00	0.00
<i>Total aromatic</i>	<i>% v/v</i>	23.10	0.00
<i>Flammability</i>	<i>°C</i>	74.0	60.5
<i>Lower heating value</i>	<i>MJ/kg</i>	42.65	44.35
<i>Hydrogen</i>	<i>% m/m</i>	13.72	15.00
<i>Carbon</i>	<i>% m/m</i>	86.67	85.00
<i>Oxygen</i>	<i>% m/m</i>	0.61	0.00
<i>Sulphur</i>	<i>mg/kg</i>	6.50	0.53
<i>FAME</i>	<i>% v/v</i>	5.00	0.05
<i>Chemical formula</i>	-	$C_{13}H_{24.80}O_{0.07}$	$C_{13}H_{27.33}$

Table 8 - HVO and EN590 Diesel characteristics

As can be seen from Table 8, *DF* and *HVO* have different lower heating values and densities. During the tests carried on in this thesis work, the engine *ECU* calculates by itself the *ET* to set in order to meet the load demand; the *ET* will be different even if the same engine point is running, depending on the used fuel. Considering the nozzles opening for a different time with the passage of a lower density fuel (i.e., *HVO*), means a smaller injected fuel mass; on the other side, this reduction, would be compensated from the greater heating value of *HVO*. For this reason, to evaluate the improvements given by this alternative fuel, it is necessary to consider the *brake thermal efficiency* η_{bth} , defined as:

$$\eta_{bth} = \frac{W}{\dot{m}_{fuel} * H_{low}} \quad (4.1)$$

where W is the brake power output, \dot{m}_{fuel} is the fuel mass flow and H_{low} is lower heating value of the fuel.

4.1.Context

Since July 2019 the *Total* refinery of La Mede and the *ENI*'s plan of Gela (Sicily), converted into *HVO* production. As can be seen from the article “*Waste based biofuels, waste based feedstock*” realized by the *Greenea* team, the profitability of the *HVO* plant business model is driven by the fact that the final product of the hydrotreatment process is of higher quality than the *ENI4214* biodiesel standard. This is achieved with the cheapest feedstock possible such as *CPO* (*Crude Palm Oil*), *PFAD* (*Palm Fat Acid Distillate*) or high *FFA* (*Free Fatty Acid*) animal fat. *PFAD* is a by-product from palm oil production, while, during the process of refining *CPO*, *FFA* are removed⁴. Although the *PFAD* is a by-product from the palm oil production, it has considerable value, and is more or less 100% utilized. It is used as feedstock for many different products for animal feeds, laundry soaps, the oleochemical industry, and combustion for local power/process heat⁵. In order to achieve the *EU* standard requirements, the producers of *first-generation* biofuels (*FAME*) need to process a mix of vegetable oils with at least 50% of rapeseed oil while an *HVO* plant can run fully on palm oil or *PFAD* and still reach the *European Union* standards. A *first-generation* plant, while using the same low-quality feedstock from palm, would be able to produce biodiesel with *CFPP* (*Cold Filter Plugging Point*) +12°C which is out of the *EU* standard even in the summer; the *CFPP* is defined as the lowest temperature at which a given volume of pure biodiesel still passes through a standardized filter within 60 seconds⁶.

Always *Greenea* highlights that, apart from the reasons connected to the *HVO*'s superior quality over regular fossil diesel, the investments are also caused by financial and social reasons. Fossil oil refineries in Europe are facing overcapacity and liquidity issues which limit the profitability of the plants. Conversion to *HVO* allows them to become profitable and compete more successfully on the market.

At the same time conversion of no-longer-profitable plants into *HVO* units saves thousands of workplaces by preventing closures. It results in an improved social image of these companies and gives them some political advantage. This phenomenon is especially visible in the south of Europe (*ENI* in Italy, *Total* in the south of France) while

⁴ ZERO and Rainforest foundation Norway, *Palm fat acid distillate in biofuels*, 2016.

⁵ A. G. M. Top, “Production and utilization of palm fatty acid distillate (PFAD),” *Lipid Technology*, 2010.

1. ⁶ G. Knothe, *Microalgae-based biofuels and bioproducts*, Elsevier, 2005.

not so much in the UK, for example. This is predominantly due to higher social responsibility of the big companies in these countries and higher governmental pressures connected with the social aspect of their activities.

4.2.State of the art

The first *HVO* refinery in Europe was invested by *Neste* in 2007. In 2011, tall oil based *HVO* was introduced in Sweden. Today *HVO* is the third most common biofuel in the world (after ethanol and *FAME*) with 3.5 million tonnes of standalone production per year and is expected to increase to 10 million tonnes by 2030. In Europe, several refineries have been re-constructed to treat *HVO* instead of fossil feedstocks, e.g., *ENI* has converted their refinery in Venice, (Italy) to annually produce 0.4 billion litres. Today's largest feedstock globally for producing *HVO* is palm oil. In EU, *HVO* plants are under construction in Sweden (*StI*) and France (*Total*), to annually produce 0.3 and 0.7 billion litres respectively. Further *HVO* plants are planned in Finland (*UPM*) and Italy (*ENI*) to annually produce 0.7 and 0.8 billion litres of *HVO* respectively.⁷

HVO can also be upgraded to sustainable aviation fuel (*SAF*). *AltAir Fuels* supplies *HVO*-based *SAF* and produces around 13 million litres per year. Many initiatives are taken world-wide for producing *SAF* in the near future.

Globally there is currently 3.5 million tonnes of standalone *HVO* production per year and is expected to increase to 10 million tonnes by 2030. In 2019 Europe consumed around 1.8 million tonnes of *HVO*; France was the biggest consumer, followed by Norway, Spain and Sweden. It is expected that Europe's consumption will grow to circa 7 million tonnes which is a combination of consumer demand and legislative changes leading to European refiners to use *HVO* more and more for blending requirements. Nowadays, *Neste* have a production capacity of circa 2.4 million tonnes per year across refineries in Finland, Singapore and Rotterdam. They have around 200 retail stations across Finland, where the public can use *HVO* in their cars and have expanded their product into service stations across Estonia, Latvia and Netherlands in Europe, as well as taking their product across the world to the US with availability in Oregon.⁸

⁷ ETIP Bioenergy, *Hydrogenated vegetable oil*, 2020.

⁸ *HVO – the revolutionary new renewable superfuel: the future of energy or a fashionable alternative?*, WPGGroup, 22 September 2021

4.3. Effect of HVO on combustion

Pechout et al. have seen that for *HVO*, the *HRR* occurs earlier with higher peak compared to diesel fuel, and a reduced premixed combustion phase. It results in more rapid development and advance of combustion, particularly at low speed and loads. This is attributable to its higher *Cetane number*, which allows to obtain a smaller *ID* (*ignition delay*), up to 45% shorter than *DF* as reported from *Alkhatat et al.*, and similar or lower NO_x compared to diesel. The *ID*, known as the period from the *start of fuel injection (SOI)* and the *start of combustion (SOC)*, is an important parameter which characterizes the initiation of combustion process and consequently its development in Diesel engines, with consequences on engine's performance and pollutants. Since the *SOC* is more dependent on the application and the ignition behaviour of the fuel under investigation, the definition of the *ID* can vary and depends on the researcher; in this thesis work, the *SOC*, has been defined as the point in which the *HRR* curve visually starts to increase. This parameter mainly depends on chemical factors, which are related to the fuel structure and its properties, and also on physical factors, which are related to the engine operating conditions. Controlling ignition delay time could be a clue to improve engine efficiency and to decrease *bsfc* and exhaust emissions. As *Alkhatat et al.* have observed, decreasing *ID* allows to reduce NO_x emissions; this because shorter *ID* leads to longer time available for the combustion development and lower peak in-cylinder pressure.

Surface tension and *viscosity* also have a considerable effect on *physical ID* due their influence on *atomization*. The effect of less dynamic viscosity of *HVO* makes its atomization process faster and forming smaller droplet diameter, that efficiently forms a combustible mixture.

The chemical composition of *HVO* has relevant effect on the reduction of the *chemical ID*. This is due to the *long-chain paraffins*, with no aromatic contents, which constitute *HVO*. The longer the paraffin chains, the more sites where *H* atom can migrate, leading to faster branching followed by shorter time for auto-ignition.

Hulkkonen et al. performed comparative studies of spray parameters of diesel fuel and *HVO*; it was observed that *HVO's penetration distance* was slightly shorter, while *spray cone angle* was up to 2° wider.

Pechout et al. also show that the *maximum pressure slope* seems to be slightly lower for most of engine regimes, suggesting little reduction of *combustion noise (CN)*.

5. Experimental procedure

The experimental procedure followed during this thesis activity consists of a series of steps, which are described during this chapter.

The engine operating points tested, with their base calibration with diesel fuel, are the five showed in Table 9 .

<i>Speed</i>	<i>BMEP</i>	<i>Torque</i>	<i>Load</i>	<i>p_{rail}</i>	<i>VGT</i>	<i>q_{pil1}</i>	<i>DTI</i>	<i>SOI_m</i>
<i>[rpm]</i>	<i>[bar]</i>	<i>[Nm]</i>	<i>[%]</i>	<i>[bar]</i>	<i>[%]</i>	<i>[mg/str]</i>	<i>[μs]</i>	<i>[°bTDC]</i>
1250	2	36	13.1	610	87	1.94	1090	-2.8
1500	9	165	47.1	1100	78	4.95	1140	-7.2
1750	5	90	25.7	1015	90	2.7	940	-3.4
2000	9.6	163	46.6	1370	77.5	2.54	867	-2.4
2250	14.4	274	78.3	1450	67	1.22	715	-2.4

Table 9 - Engine points tested and their base calibration

From all these, the comparisons with *HVO* requested by *ENI* concerned only the engine points $1250[rpm] \times 1.9[bar]$, $2000[rpm] \times 9.6[bar]$ and $2250[rpm] \times 14.4[bar]$, corresponding, respectively, to low, medium and high load. Due to this, only for these the *DoE*, the optimizations and the *HVO* comparisons were performed, while the preliminary tests were run for all five points.

5.1.Preliminary tests

The first step is the individuation of the range values for *Design of Experiment (DoE)* for the main engine variables. In order to do this, preliminary tests have been performed for each engine point of interest. The preliminary procedure can be schematized as follow:

1. Starting from the base calibration of the engine at a fixed stationary point, the λ value has been kept fixed, while exploring different combinations of *High*

Pressure (HP) and Low Pressure (LP) actuators: HP only, LP only and Dual Loop (DL, i.e., a combination of HP and LP).

2. These EGR configurations have been explored with different λ values.
3. The best calibrations have been selected to perform additional single-parameter sweeps, by keeping λ value constant, to find limits for the DoE test plans: SOI_m , p_{rail} , VGT actuator position, q_{pil1} and DTI.

Thanks to this procedure, experimental trade-offs of main pollutants and *bsfc* have been carried out.

In Figure 35, Figure 36, Figure 37, Figure 38 and Figure 39 are shown the experimental trade-offs for fixed λ varying HP and LP EGR proportion. The values in the graphs are normalized respect to the reference condition for reservedness reasons, which corresponds to the same engine point performed with Diesel fuel at the base calibration, and they have been evaluated accordingly to the Equation (5. 1):

$$Perc. var [\%] = \frac{x_{preliminary}}{x_{baseline}} \quad (5. 1)$$

Already from these preliminary tests, the benefits of using HVO, instead of conventional Diesel fuel, are evident. The most interesting thing is that, in preliminary tests, no change in calibration has been performed: this simulates the realistic eventuality in which, in a common Diesel engine, the fuel is switched without introduce any variations of the calibration. Yet in this situation, as can be seen from the graphs, HVO shows advantages in terms of pollutants emission, *bsfc* and CN respect to the traditional Diesel fuel.

The calibrations which seemed to best from the preliminary tests and that have been the starting points to conduct the EGR sweeps here proposed, are listed in Table 10.

Engine point					HP	LP			
	SOI_m	p_{rail}	VGT	EGR	EGR	q_{pil1}	DTI	λ	
[rpm x bar]	[°bTDC]	[bar]	[%]	[%]	[%]	[mg/str]	[μs]	[-]	
1250 x 2	-2.8	610	90.0	11.0	89.0	1.9	1090	2.25	
1750 x 5	-3.4	1015	90.0	12.0	60.0	0.73	940	1.80	
1500 x 9	-5.5	1200	90.0	5.0	20.0	5.0	1140	1.40	
2000 x 9.6	-2.4	1370	77.5	3.0	65.0	2.5	867	1.40	
2250 x 14.4	2.4	1450	67.0	4.0	26.0	1.2	715	1.40	

Table 10 – Starting engine calibrations for EGR sweeps of preliminary tests

In Table 11 are summarized the percentual variations of *HVO* compared to diesel fuel, at the minimum NO_x value, concerning pollutant, *bsfc* and *CN* of the preliminary tests. They show how *HVO* plays an important role on reduction of *HC* and *CO* especially significant at low load, and of *soot*, especially significant at high load. *HVO* also improve *bsfc* for the reasons explained in Chapter 4.3. A minor variation in *CN* has been also measured. The values in green are the ones for which *HVO* shows the greatest advantages.

<i>Speed x BMEP</i>	<i>Soot</i>	<i>CO</i>	<i>HC</i>	<i>bsfc</i>	<i>CN</i>
<i>[rpm x bar]</i>	<i>[%]</i>	<i>[%]</i>	<i>[%]</i>	<i>[%]</i>	<i>[dBA]</i>
<i>1250 x 2</i>	- 48	- 48	- 60	- 2.4	- 0.3
<i>1750 x 5</i>	- 44	- 25	- 31	- 3	- 1.4
<i>1500 x 9</i>	- 48	- 18	- 37	- 2.7	- 1.7
<i>2000 x 9.6</i>	- 36	- 7.6	- 17	- 2.4	- 0.8
<i>2250 x 14.4</i>	- 31	- 0.5	- 7	- 2.7	- 0.4

Table 11 - Variations of *HVO* compared to Diesel fuel for preliminary tests

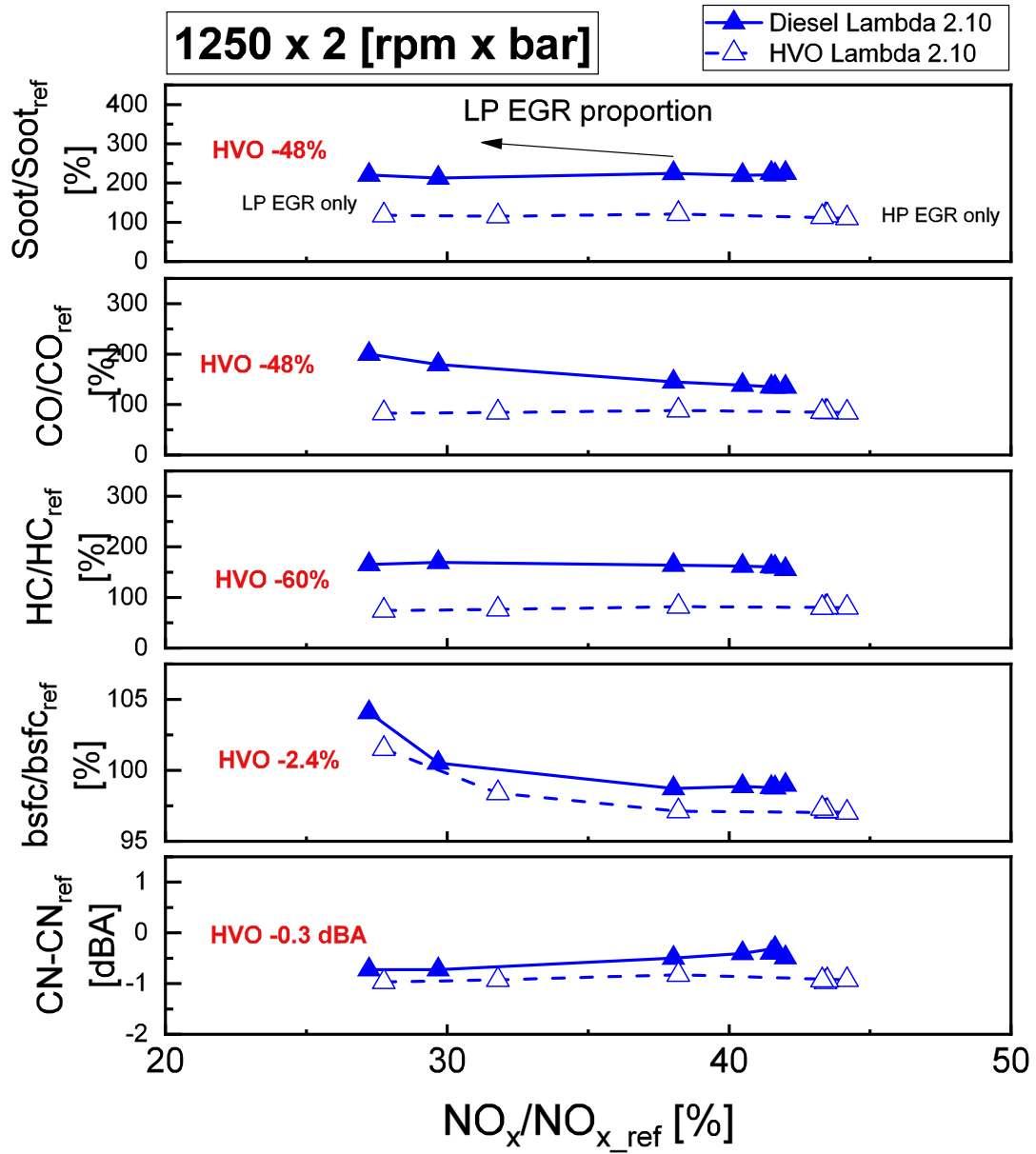


Figure 35 – Preliminary EGR trade-off at fixed lambda @ 1250 [rpm] x 2 [bar]

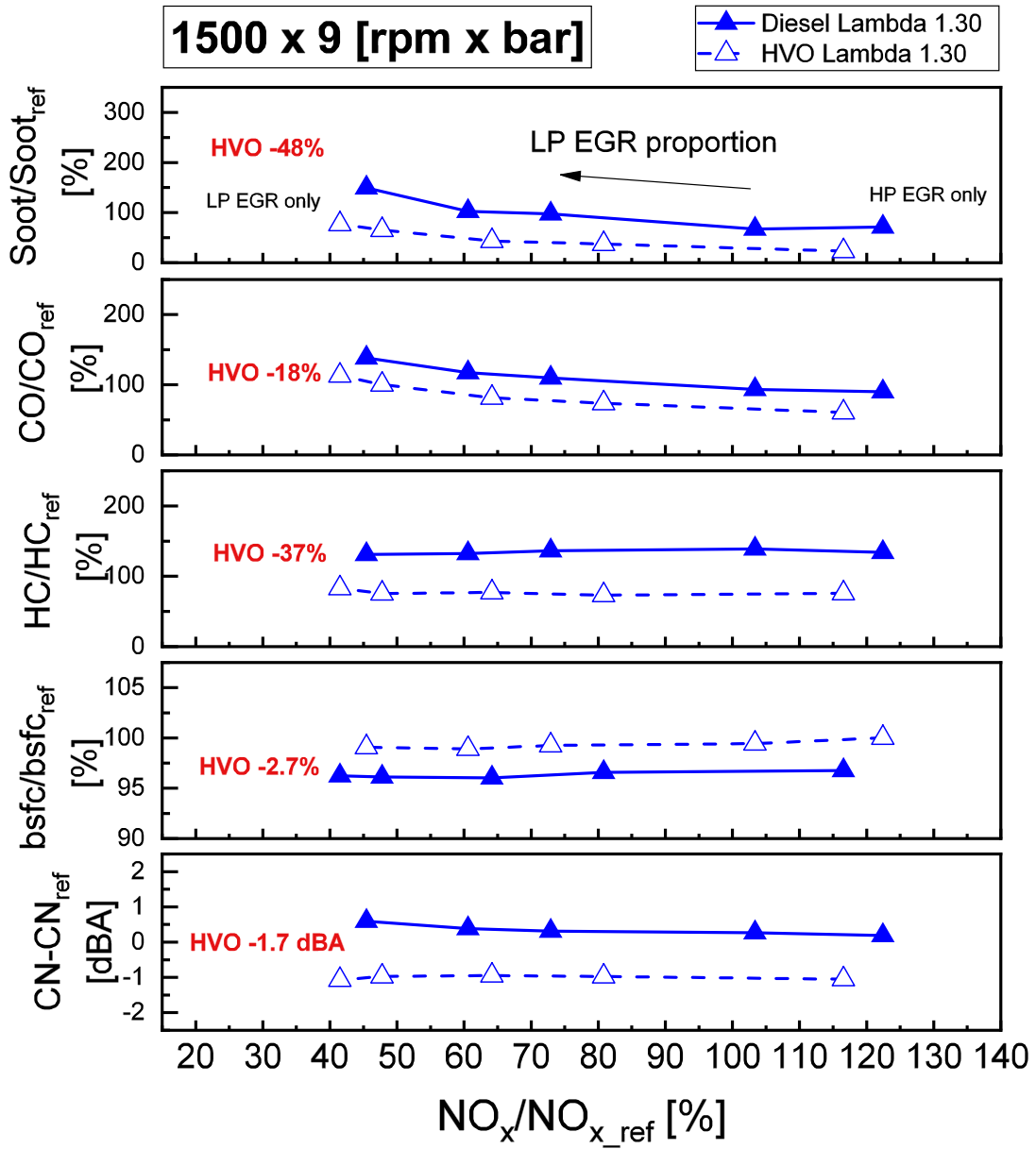


Figure 36 - Preliminary EGR trade-off at fixed lambda @ 1500 [rpm] x 9 [bar]

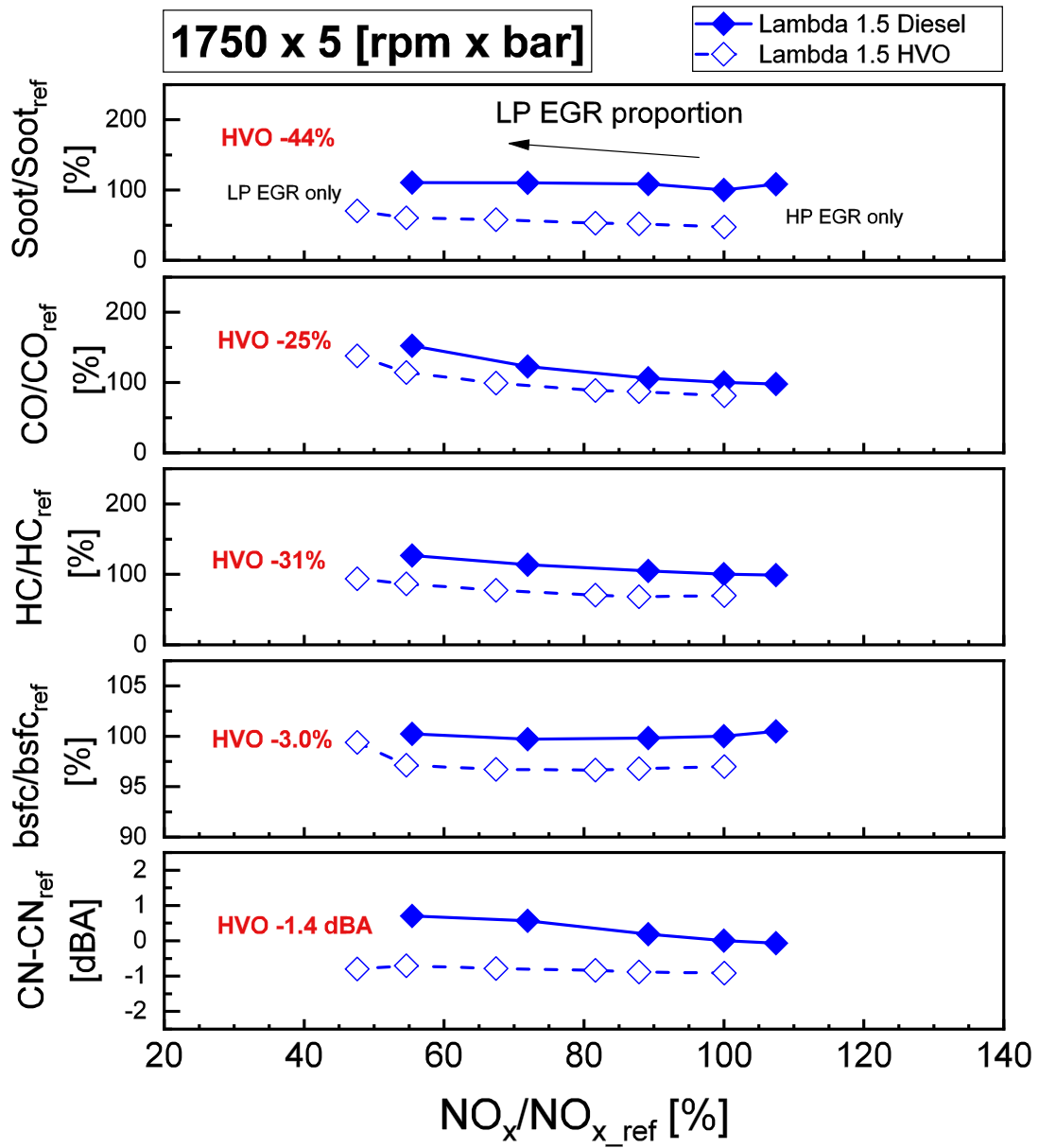


Figure 37 – Preliminary EGR trade-off at fixed lambda @ 1750 [rpm] x 5 [bar]

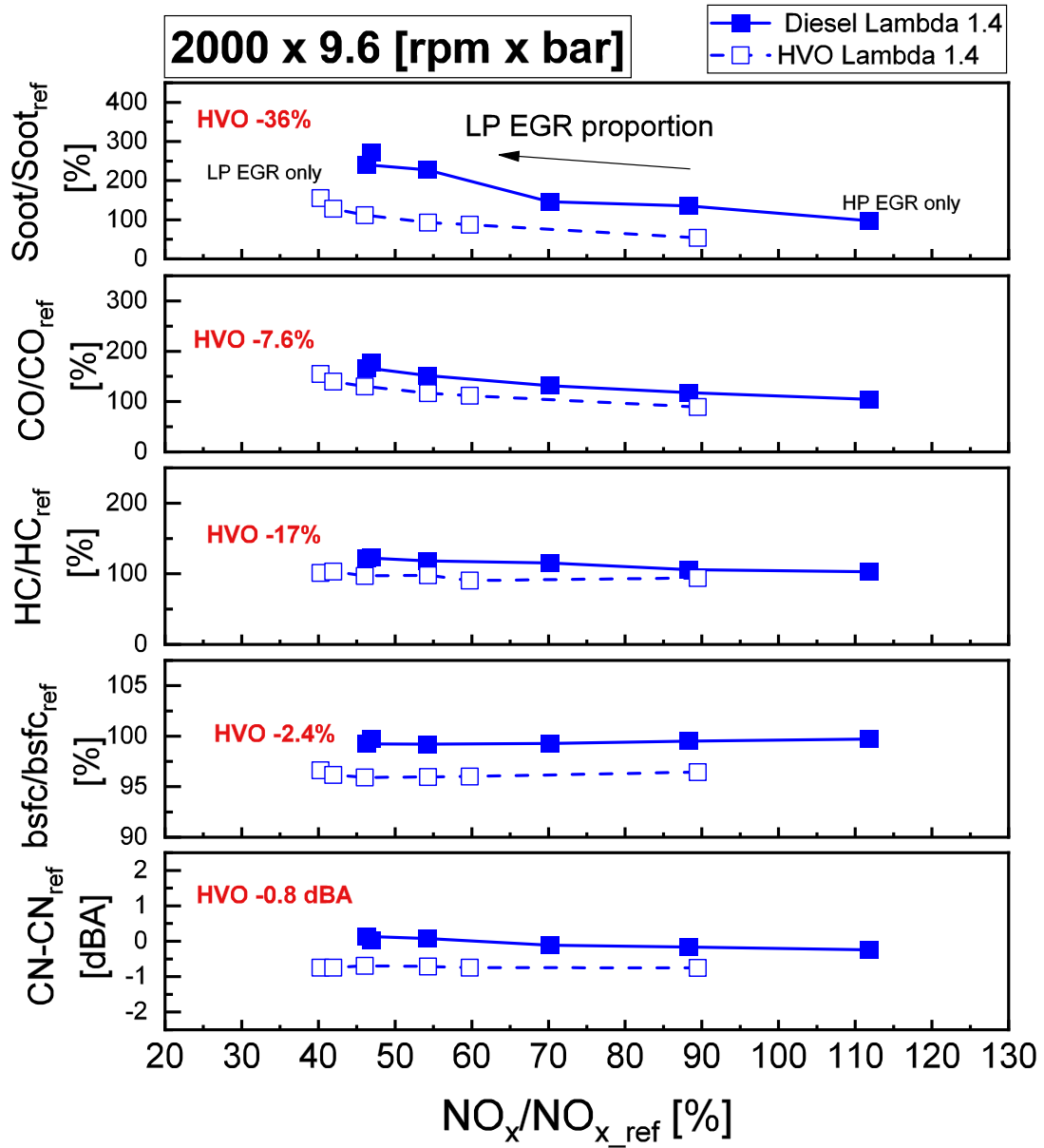


Figure 38 - Preliminary EGR trade-off at fixed lambda @ 2000 [rpm] x 9.6 [bar]

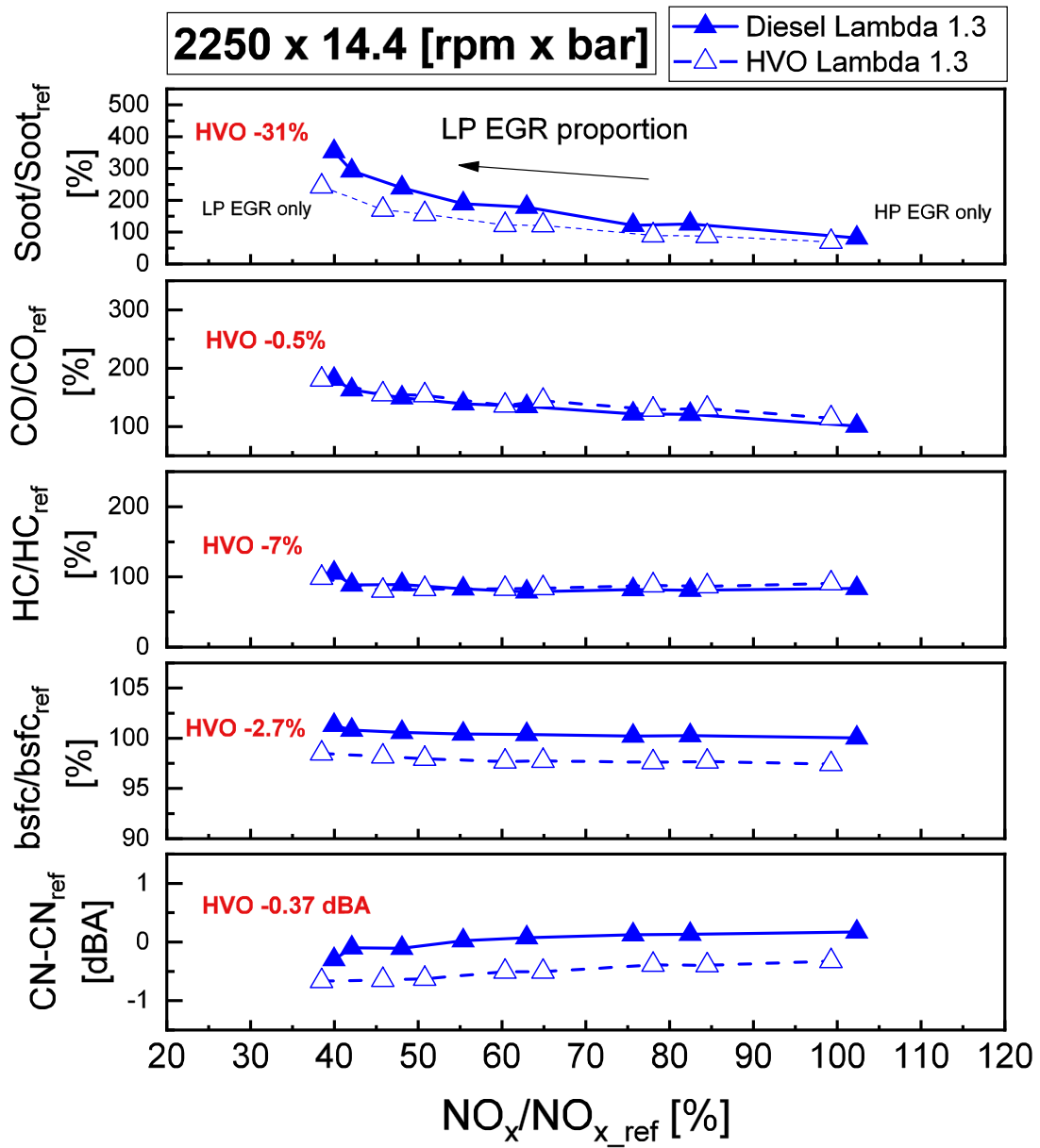


Figure 39 – Preliminary EGR trade-off at fixed lambda @ 2250 [rpm] x 14.4 [bar]

5.2. Design of experiment

The term *Design of Experiment (DoE)* is a branch of applied statistics that deals with planning, conducting and analysing controlled tests to evaluate the factors that control the values of parameters. It allows for multiple input factors to be manipulated, determining their effect on a desired output. By manipulating multiple input at the same time, *DoE* can identify important interactions that may be missed when experimenting with one factor at a time. If all possible combinations are investigated it is called Full factorial, while, if only a portion is investigated, it is called Fractional factorial. In *ICE* environment the parameters under investigation are too many to perform a full factorial *DoE* or to change them one at a time on base of the user experience; the first solution would lead to a very expensive and time-consuming procedure, while the second one would not be sufficient to reach the new European standards concerning pollutant, CO_2 emissions and *bsfc*. A strategically planned and executed *DoE* may provide a great deal of information about the effect on a response variable due to one or more factors.

5.2.1. Optimal DoEs creation

During this thesis work, *Optimal design* was chosen as method for *DoE* construction, in particular the *V-Optimal*. The optimal design goal is to estimate statistical model, which parameters are without bias and with minimum variance. *V-Optimal* minimizes the mean value of *PEV* in the design region.

DoE were planned by mean of *MBC Model* toolbox of *MATLAB* software. The procedure followed to create the *DoEs* is the following:

1. The input factors were inserted, specifying their maximum and minimum limits.
2. Constrains were added to limit *DoEs* region, e.g., 1-D maps of *HP* and *LP EGR* in order to maintain an acceptable range values of λ .
3. Optimal design was selected.
4. Linear model was chosen.
5. *V-Optimal* was selected as optimality criteria and many additional points to *DoE* design were added in order to improve the future model.
6. For each factor, the number of levels (number of values that the factor can assume) was imposed.
7. The program is launched to optimizing design to attain minimum *V-Optimal* value.

8. The created *DoE* and its statistical properties are showed. In function of these last ones, the *DoE* is accepted or otherwise changed.

The number of input factors and the levels of each of them, were set trying on one side to perform the minimum number of tests, and on the other side, to explore more points as possible of the domain region. This led, during this thesis work, to chase as number of input factors of *DoEs*, seven engine parameters, and as number of levels a reasonable one depending on the considered quantity: for example, *SOI* levels was set to change $1\text{ }^{\circ}\text{CA}$ at time, *p_{rail}* levels differ from each other by 100 bar and *q_{pil}* by 1 mg/str .

With reference to point 5 of the previous list, it has been noticed that, for this kind of experiments, the number of tests to be performed is around 130; this number allows to get a low value of *PEV* even at the boundaries, usually chosen lower than 0.20. This is shown in Figure 43 by means to the tool *Prediction Error Variance Viewer*, thanks to which it is possible to see the *PEV* values in function of the *DoE* parameters on a 3D graph.

In Figure 40 and Figure 41 are shown the *MBC* windows concerning the *DoE* creation and an example of a 1D table constrain relating upper limit *EGR*.

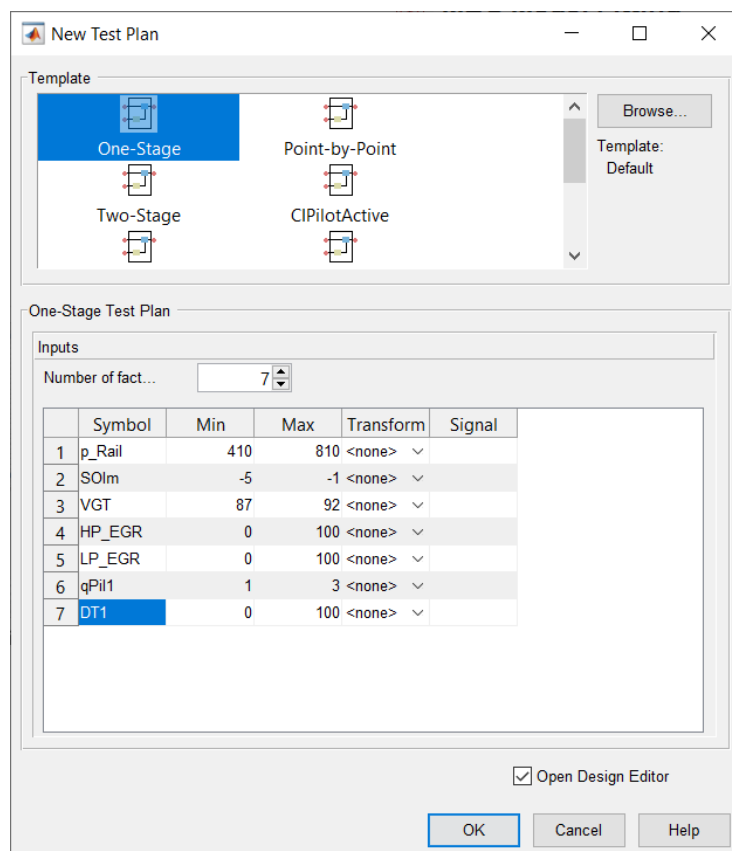


Figure 40 – Example of *DoE* creation

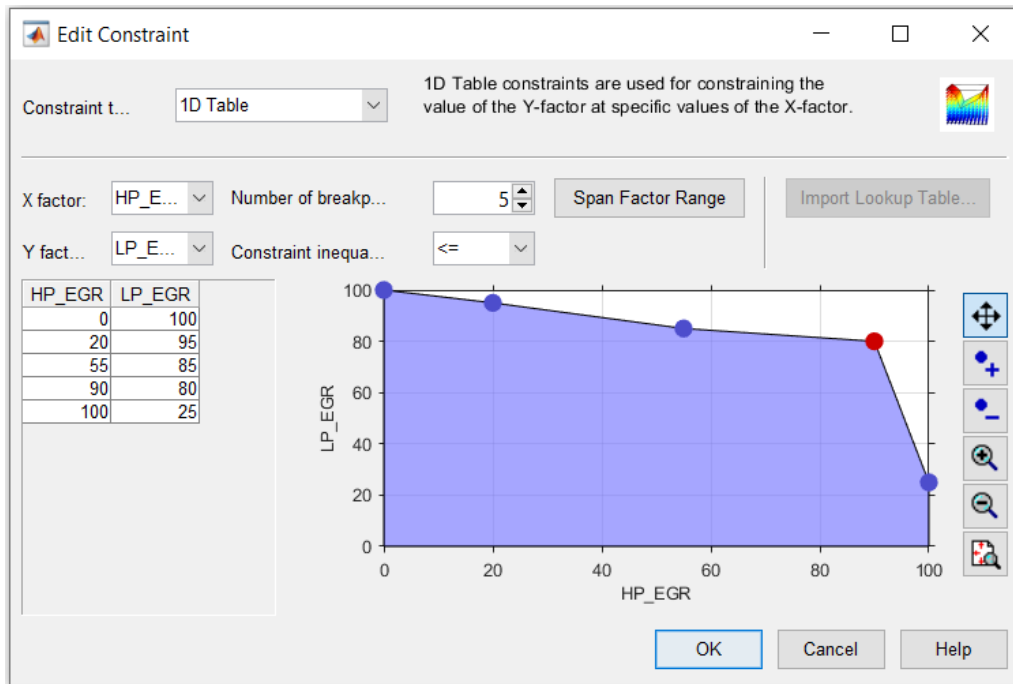


Figure 41 – Example of 1D table EGR constraint

The points of the created *DoE* can be seen on a *3D Design Projection*, as shown in Figure 42.

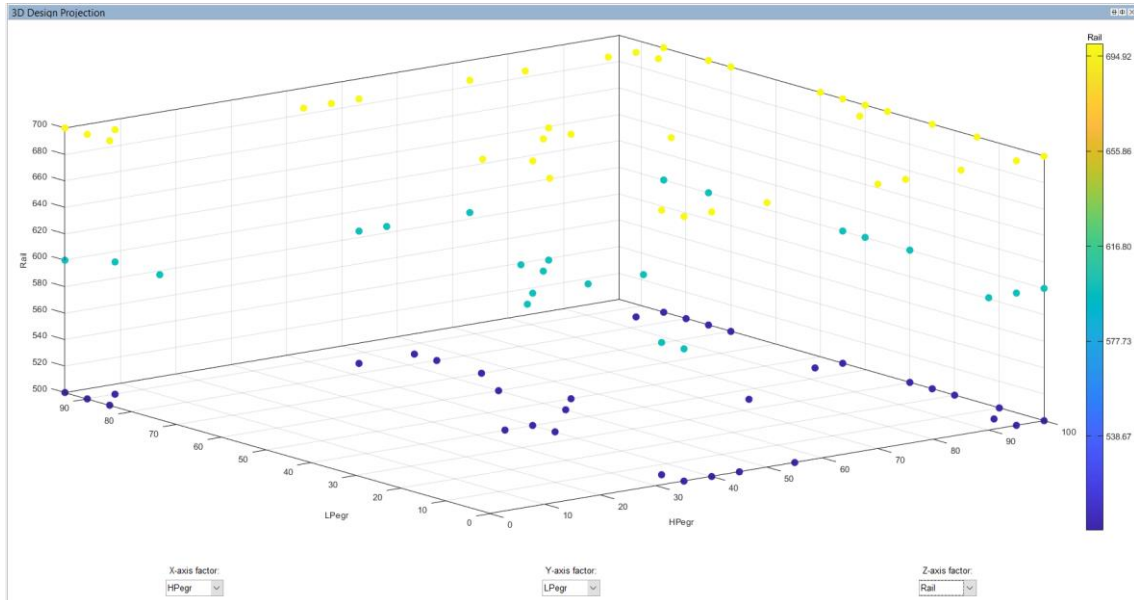


Figure 42 – Example of 3D Design Projection

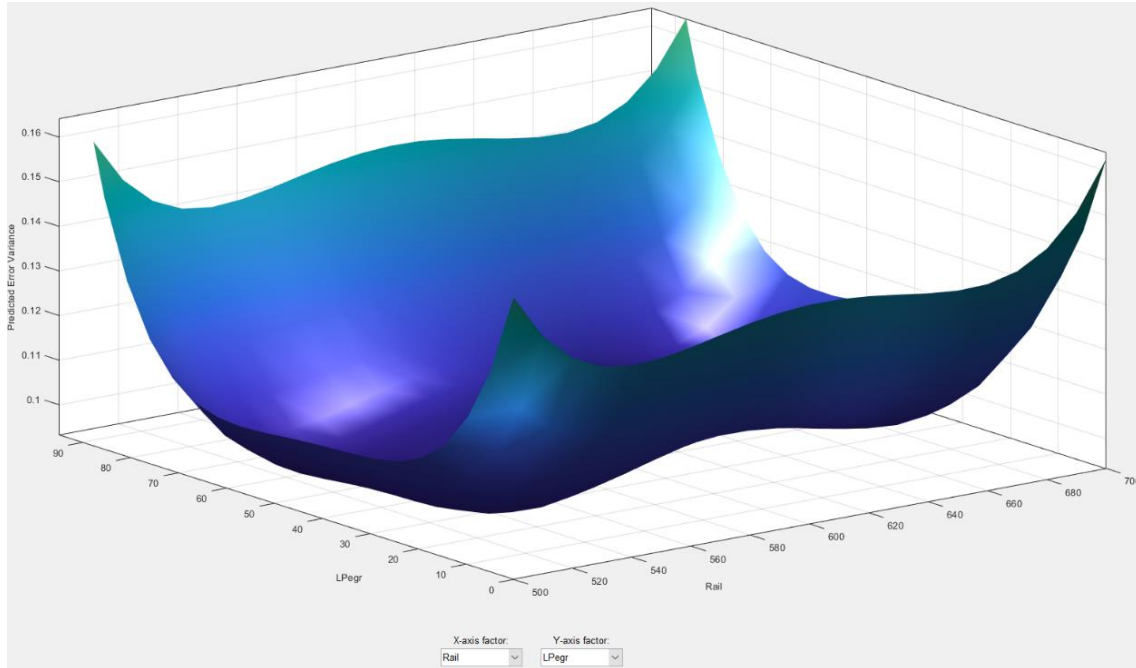


Figure 43 – Example of PEV surface

For all the *DoEs* run during this thesis activity, are reported, on Table 12, the values of *V*.

<i>Speed x BMEP</i>	<i>V value</i>	
<i>[rpm x bar]</i>	<i>Fuel</i>	<i>[-]</i>
1250 x 2	Diesel	0.183
	HVO	0.184
2000 x 9.6	Diesel	0.173
	HVO	0.172
2250 x 14.4	Diesel	0.403
	HVO	0.538

Table 12 - *V* values of *DoEs*

5.2.2. Main statistical parameters

To evaluate the goodness of the models created during this thesis work, it was necessary to observe some statistical parameters. The most important are the following.

- *Coefficient of determination R^2* : it describes the proportion between the data variation and the statistical model correctness. It measures the variance fraction of the dependent variable which the R^2 refers on. Its value can vary from 0 – which corresponds to the minimum fitting of the model variable with

experimental results – and 1 – representing the best fitting value. It is evaluated starting from to other statistical parameters: *SSR* and *SST*.

$$R^2 = \frac{SSR}{SST} \quad (5. 2)$$

- *Residual sum of square SSR*: it is the sum of squared residuals of regression.

$$SSR = \sum_{i=1}^n (\tilde{y}_i - \bar{y})^2 \quad (5. 3)$$

Where \tilde{y}_i is the *i-th value estimated by the model* and \bar{y} is the *average among overall observed data*.

- *Total sum of squares SST*: it is the *sum of residual squares of the variable mean*.

$$SST = \sum_{i=1}^n (y_i - \bar{y})^2 \quad (5. 4)$$

Where y_i is the *i-th observed datum*.

- *Sum of squared estimate of errors SSE*: it indicates the amount of variability that the model is not able to detect.

$$SSE = \sum_{i=1}^n (y_i - \tilde{y}_i)^2 \quad (5. 5)$$

- *R² adjusted R²_{Adj}*: it takes into consideration the proportion of the observed data variability explained by its predictor variable.

$$R^2_{Adj} = 1 - \frac{\frac{SSE}{n-p}}{\frac{SST}{n-1}} \quad (5. 6)$$

Where n represents the *number of considered tests*, while p is the *number of explanatory variables in the model*, not including the constant term.

- *Predicted residual error sum of square PRESS*: it is a form of cross-validation used to provide a summary measure of the fit of a model to a sample of observations that were not themselves used to estimate the model.

$$PRESS = \sum_{i=1}^n (y_i - \tilde{y}_{i-1})^2 \quad (5. 7)$$

Applying *PRESS* statistic on R^2 it is possible to evaluate the prediction of the model:

$$PRESS R^2 = 1 - \frac{PRESS}{SST} \quad (5.8)$$

- *Root mean square error RMSE*: it is a measure of accuracy to quantify the differences between values predicted by a model and the values observed. Low values of *RMSE* reflect great accuracy.

$$RMSE = \sqrt{\frac{\sum_{i=1}^n (y_i - \hat{y}_i)^2}{n}} \quad (5.9)$$

Applying *PRESS* statistic on *RMSE* it is possible to define *PRESS RMSE*:

$$PRESS RMSE = \sqrt{\frac{\sum_{i=1}^n (y_i - \hat{y}_{(i)})^2}{n}} \quad (5.10)$$

5.2.3. Main statistical functions

To improve the quality of the model it was necessary to resort to some statistical functions. The two used during this thesis work are described in this chapter.

- *Stepwise regression*⁹. The procedure iteratively constructs a sequence of regression models by adding or removing variables at each step. The criterion for adding or removing a variable is usually expressed in terms of a partial *F-test* (*Fisher test*). Let f_{in} be the value of the F-random variable for adding a variable to the model and let f_{out} be the value of the F-random variable for removing a variable from the model. We must have $f_{in} \geq f_{out}$, and usually $f_{in} = f_{out}$. Stepwise regression begins by forming a one-variable model using the regressor variable that has the highest correlation with the response variable. This will also be the regressor producing the largest *F-statistic*.

⁹ D. C. Montgomery and G. C. Runger, "Aspects of multiple regression modeling," in *Applied statistics and probability for engineers*, John Wiley & Sons, Inc., 2003.

In general, at each step, the set of remaining candidate regressors is examined, and the regressor with the largest partial F-statistic is entered; then, the partial *F-statistic* for each regressor in the model is calculated and the regressor with the smallest observed value of F is deleted if the observed $f < f_{out}$. The procedure continues until no other regressors can be added to or removed from the model.

- **Box-Cox transformation¹⁰**. Generally, transformations of the response variable are used for stabilizing response variance, making the distribution of the response variable closer to the normal distribution and improving the fit of the model to the data. In particular, the power family of transformation $y^* = y^k$ is very useful to reach good results, where k is the parameter of the transformation to be determined and y is the response. *Box* and *Cox* have shown how the transformation parameter k may be estimated simultaneously with other model parameters. The theory underlying their method uses the method of maximum likelihood. The computational procedure consists of performing, for various values of k , a standard analysis of variance on

$$y^{(k)} = \begin{cases} \frac{y^k - 1}{k * \dot{y}^{k-1}} & k \neq 0 \\ \dot{y} * \ln(y) & k = 0 \end{cases} \quad (5. 11)$$

where $\dot{y} = \ln^{-1} \left[\frac{\sum \ln(y)}{n} \right]$ is the geometric mean of the observations. The maximum likelihood estimation of k is the value for which the *error sum of square (SSE)* is a minimum. This value of k is usually found by plotting a graf of *SSE* versus k and then reading the value of k that minimizes *SSE* from the graph. In using the *Box-Cox* method, is recommended that experimenter uses simple choice for k , because, e.g., the practical difference between $k = 0.5$ and $k = 0.58$ is likely to be small, but the square root transformation ($k = 0.5$) is much easier to interpret. In addition, values of k close to unity would suggest that no transformation is necessary.

Both these procedures were performed via *MBC Model MATLAB* toolbox, and the examples of their use during this thesis activity is shown in Figure 44 and in Figure 45.

¹⁰ D. C. Montgomery, Design and analysis of experiments, Jhon Wiley and Sons, Inc., 2013.

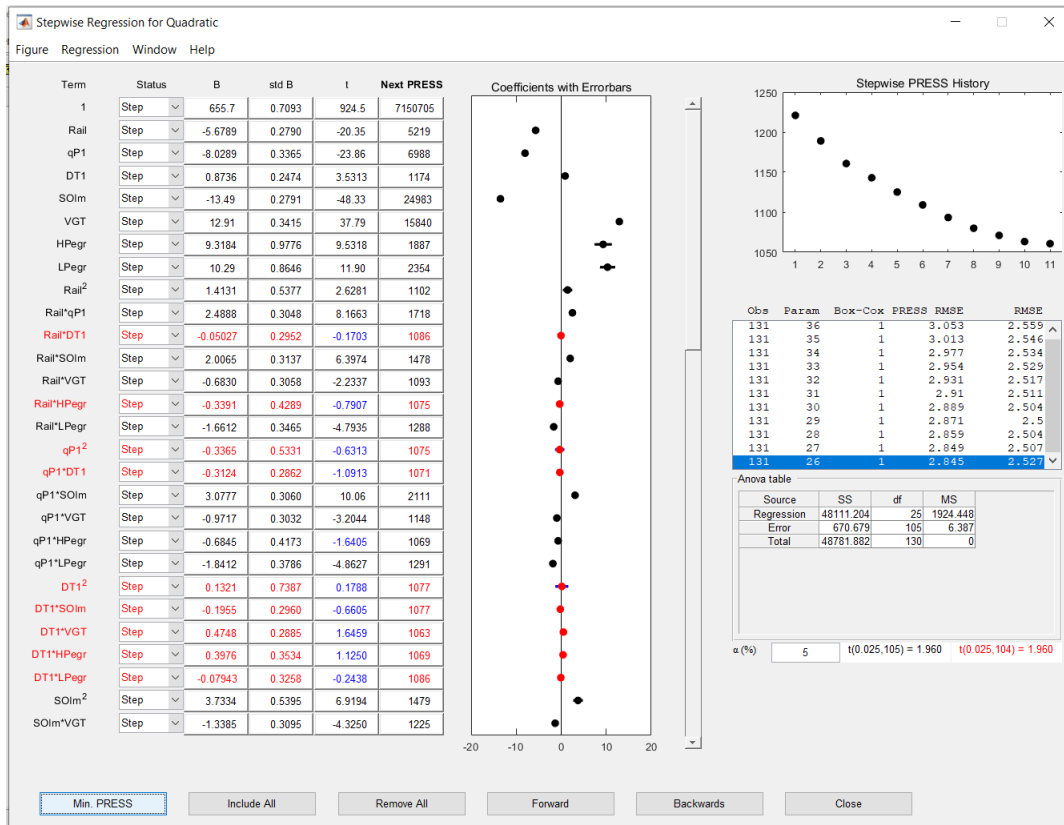


Figure 44 - Example of use of stepwise regression

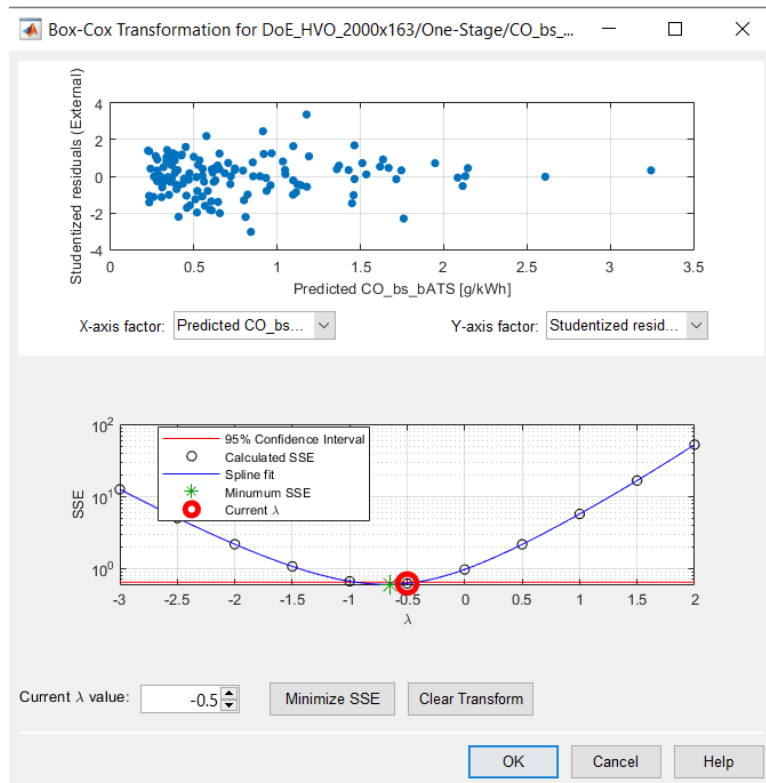


Figure 45 - Example of use of Box-Cox transformation

5.3. Experimental tests

Once the *DoE* is created, repetition point was added: it consists of an engine calibration which is repeated after a certain number of tests (in this case every eleven test), in order to monitor the trend of experiment. In this way, from the data acquired by this repetition points, it is possible to investigate if any drift affects the experiment, e.g., monitoring pressure drop across *DPF*, λ value or emissions values to understand if *DPF* loading is leading to a different *EGR* rate with the same calibration.

The variation list is so created and implemented on *AVL CAMEO* software: it allows to create the procedure to execute the *DoE*, and it will be followed automatically by the software. *CAMEO* is in fact connected to all the systems present in the test bench and it can access to the *ECU* parameters. The tests execution is structured as it follows:

1. Engine calibration coming from *DoE* design is set.
2. A stabilization time is waited in order to let every transient extinguished, e.g., variation of intake manifold temperature due to different *EGR* actuators position.
3. The measure of emissions is launched for a sampling period of sixty seconds, after which, the average values are acquired.
4. After the measurement, the new engine calibration is set, and the procedure is repeated.

To ensure a good measure repeatability of emissions bench, every four tests, purge procedure is launched: it consists of an air flow passing through the analyzers in order to clean them.

5.4. Calculation of mass emissions

The measured exhaust gas emissions, coming from laboratory's analyzers, are measured in volume fraction (ppm). It is so necessary to calculate mass emission, in order to perform comparisons. During this thesis work, this aim has been achieved by means of a *MATLAB* code containing the evaluation procedure illustrated by *S. D'Ambrosio*, *R. Finesso* and *E. Spessa*; in Chapter 5.4.1 and Chapter 5.4.2, this procedure is reported.

5.4.1. Mass evaluation procedure¹¹

In order to calculate mass emissions, it is necessary to know the molar concentration of all the constituents of the exhaust gases. The relation between *volume fraction* $[X_{wet}]$ and the corresponding *mass fraction* $\{X\}$ is:

$$\{X\} = \frac{M_x}{M_{exh}} \cdot [X_{wet}] \quad (5.12)$$

where M_x is the molar mass of the pollutant species X and M_{exh} is the *exhaust gas average molecular weight*:

$$M_{exh} = \frac{\sum_j (n_j \cdot M_j)}{\sum_j n_j} \quad (5.13)$$

Being, respectively, M_j and n_j the *molar mass* and the *number of moles* of each chemical species j at the exhaust.

The *mass-flow rate of X* is expressed as

$$\{\dot{X}\} = \dot{m}_{exh} \cdot \{X\} \quad (5.14)$$

Being \dot{m}_{exh} the *mass-flow rate of exhaust gases*.

Brake specific mass emissions can be expressed as:

$$\{X\}_{bs} = \frac{\dot{m}_{exh} \cdot \frac{M_x}{M_{exh}} \cdot [X_{wet}]}{W} \quad (5.15)$$

where W is the *power output* of the engine.

For steady-state operations, the *exhaust gas flow rate* can be computed as:

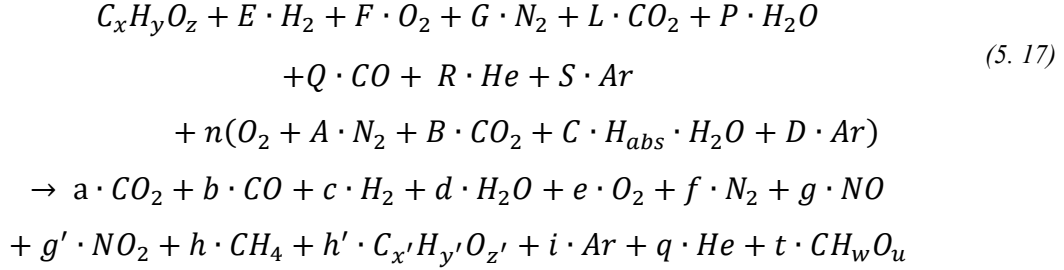
$$\dot{m}_{exh} = \dot{m}_{fuel} \cdot [1 + \alpha \cdot (1 + H_{abs} \times 10^{-3})] \quad (5.16)$$

Being \dot{m}_{fuel} the *fuel mass-flow rate*, α the *air-fuel ratio* experimentally measured by means of *Lambda UEGO sensor* and H_{abs} the *air humidity*, measured by a hygrometer.

¹¹ S. D'Ambrosio, R. Finesso and E. Spessa, "Calculation of mass emissions, oxygen mass fraction and thermal capacity of the inducted charge in SI and diesel engines from exhaust and intake gas analysis," *Elsevier*, 2010.

5.4.2. Evaluation of the number of moles¹²

In order to evaluate the number of moles of the exhaust species it is necessary to recall the combustion reaction:



where coefficients E, F, G, L, P, Q, R and S are introduced to account for the composition of gaseous fuel mixtures which cannot be represented only with the average formula of the generic hydrocarbon $C_x H_y O_z$. n is the number of moles of oxygen that react with fuel in Eq. (5.17). The coefficient A, B , and D take into account respectively the presence of N_2, CO_2 and Ar in the combustion air and they can be evaluated as:

$$A = \frac{[N_2]_{amb}}{[O_2]_{amb}} \approx 3.72745 \tag{5.18}$$

$$B = \frac{[CO_2]_{amb}}{[O_2]_{amb}} \approx 0.00143 \tag{5.19}$$

$$D = \frac{[Ar]_{amb}}{[O_2]_{amb}} \approx 0.04439 \tag{5.20}$$

From the absolute humidity H_{abs} of the air, the coefficient C can be expressed as follows:

$$C = \frac{M_{air,dry}/M_{H_2O}}{[O_2]_{amb}} \times 10^{-3} \approx 0.00767 \tag{5.21}$$

Regarding the combustion products, the measurements of the exhaust volume concentrations of $CO_2, CO, O_2, NO, NO_2, CH_4$ and $C_{x'} H_{y'} O_{z'}$, are available from the analyzers, together with soot level estimation coming from the smoke meter. $C_{x'} H_{y'} O_{z'}$

¹² S. D'Ambrosio, R. Finesso and E. Spessa, "Calculation of mass emissions, oxygen mass fraction and thermal capacity of the inducted charge in SI and diesel engines from exhaust and intake gas analysis," *Elsevier*, 2010.

is a general composition for the average *unburned non-methane hydrocarbon*, while CH_wO_u is an average composition of *soot*.

The concentrations of CO_2 , CO and O_2 are measured through *IRD* and *POD* on a dry basis, being the water vapor extracted from the exhaust gas, by means of a cooler, before entering the analyzers. The coefficient a , b and e are evaluated as follow:

$$a = [CO_2]_{dry} \cdot n_{tot,dry} \cdot CF_{cooler} \quad (5. 23)$$

$$b = [CO]_{dry} \cdot n_{tot,dry} \cdot CF_{cooler} \quad (5. 22)$$

$$e = [O_2]_{dry} \cdot n_{tot,dry} \cdot CF_{cooler} \quad (5. 24)$$

where:

$$n_{tot,dry} = a + b + c + e + f + g + g' + h + h' + i + q \quad (5. 25)$$

$$CF_{cooler} = \frac{n_{tot,dry} + n_{H_2O,cooler}}{n_{tot,dry}} \quad (5. 26)$$

The concentration of NO , NO_2 , CH_4 and $C_{x'}H_{y'}O_{z'}$, on a dry basis, can be measured as:

$$g = [NO]_{dry} \cdot n_{tot,dry} \cdot CF_{cooler} \quad (5. 27)$$

$$g' = [NO_2]_{dry} \cdot n_{tot,dry} \cdot CF_{cooler} \quad (5. 28)$$

$$h = [CH_4]_{dry} \cdot n_{tot,dry} \cdot CF_{cooler} \quad (5. 29)$$

$$h' = \frac{[THC]_{dry} - [CH_4]_{dry}}{x'} \cdot n_{tot,dry} \cdot CF_{cooler} \quad (5. 30)$$

CH_4 and THC volume fractions are expressed as C_1 equivalent based on the measurements of FID analyzer. NO and NO_2 are measured by means of CLD instruments.

As regards the soot term, the filter smoke number (FSN) measured by the smoke meter, is closely related to the mass carbon emission per unit volume (C_{soot}), therefore:

$$C_{soot} = p_0 \frac{t \cdot M_{PM}}{(a + b + c + d + e + f + g + g' + h + h' + i + q) \tilde{R}T_0} \quad (5.31)$$

$$= f(FSN)$$

where p_0 and T_0 are the standard pressure and absolute temperature, \tilde{R} is the ideal gas constant and $f(FSN)$ a correlation between C_{soot} and FSN developed by the smoke meter manufacturer. M_{PM} is the soot molecular weight, and for the average soot molecule CH_wO_u it is $M_{PM} = M_C + wM_H + uM_O$.

Finally:

$$t = C_{soot} \frac{\tilde{R}T_0}{p_0 \cdot M_{PM}} (a + b + c + d + e + f + g + g' + h + h' + i + q) \quad (5.32)$$

$$= \Gamma (a + b + c + d + e + f + g + g' + h + h' + i + q)$$

where:

$$\Gamma = C_{soot} \frac{\tilde{R}T_0}{p_0 \cdot M_{PM}} \quad (5.33)$$

Six other relations can be derived from the balance equations for the various atomic species, respectively C , H , O , N , Ar , and He :

$$x + L + Q + n \cdot B = a[1 - \Gamma] + b[1 + \Gamma] + c\Gamma + d\Gamma + e\Gamma \quad (5.34)$$

$$+ f\Gamma + g\Gamma + g'\Gamma + h[1 + \Gamma] + h'[x' + \Gamma] + i\Gamma + q\Gamma$$

$$y + 2E + 2P + 2nCH_{abs} = aw\Gamma + bw\Gamma + c[2 + w\Gamma] \quad (5.35)$$

$$+ d[2 + w\Gamma] + ew\Gamma + fw\Gamma + gw\Gamma + g'w\Gamma + h[4 + w\Gamma]$$

$$+ h'[y' + w\Gamma] + iw\Gamma + qw\Gamma$$

$$\begin{aligned}
& z + 2F + 2L + P + Q + 2n + 2n \cdot B + n \cdot CH_{abs} \\
= & a[2 + u\Gamma] + b[1 + u\Gamma] + cu\Gamma + d[1 + u\Gamma] + e[2 + u\Gamma] + fu\Gamma \\
& + g[1 + u\Gamma] + g'[2 + u\Gamma] + hu\Gamma + h'[z' + u\Gamma] + iu\Gamma + qu\Gamma
\end{aligned} \tag{5.36}$$

$$2G + 2n \cdot A = 2f + g + g' \tag{5.37}$$

$$S + n \cdot D = i \tag{5.38}$$

$$R = q \tag{5.39}$$

Hence, a further equation is required to solve the resulting algebraic system. The methods used to evaluate the number of moles of the exhaust species and of oxygen reacting with fuel, used in the MATLAB code, is the *Water-gas (W-G) reaction method*; the equation derived from the equilibrium constant of the water-gas reaction, added to the previous set, is:

$$K = \frac{[CO] \cdot [H_2O]}{[CO_2] \cdot [H_2]} = \frac{b \cdot d}{a \cdot c} \tag{5.40}$$

Once the algebraic system was solved, the mass emissions, worked out in term of brake specific mass emissions, were evaluated.

5.4.3. Post elaboration MATLAB software

This procedure, which leads to get the mass emissions, is performed by a post elaboration *MATLAB* software. The duty of the code is summarized as follow:

1. The txt file containing the *DoE*, for which the mass emissions have to be computed, must be selected.
2. The instrument used to get soot emission has to be selected; in this case it is *S415 FSN Smoke Meter*.
3. Which line of *AMA* test bench used to measure CO_2 has to be specified.
4. The position of the two *AMA* test bench lines has to be specified. In this case, the line 1 was connected to the exhaust pipe before the after-treatment system, while the line 2, after the after-treatment system.
5. The program evaluates the brake specific quantities, following the procedure described in Chapter 5.4.1 and Chapter 5.4.2., creating an Excel file.

5.5. Regression models creation

Thanks to *MBC Model Fitting MATLAB* toolbox, data collected from *DoEs* were then used to create the statistical models by fitting the data. These models concern all the *pollutant species*, CO_2 , *CN*, *bsfc* and λ .

The goodness of the models can be evaluated thanks to the statistical parameters discussed in Chapter 5.2.2.

The procedure followed to evaluate the models is here described:

1. Thanks to *stepwise* function the *PRESS* R^2 is minimized.
2. An *outliers detection* procedure is performed.
3. If the value of R^2 is greater than 0.85 the model is classified as good, and the procedure ends here, otherwise it follows.
4. In case of R^2 smaller than 0.85, all the deleted test, both the ones classified as outliers and the ones rejected by the stepwise function, are reintroduced.
5. A *Box-Cox transformation* is performed.
6. The *stepwise* function is again utilized to minimize *PRESS* R^2 .
7. The *outliers detection* procedure is performed
8. If R^2 value is greater than 0.85, the model is classified as good, and the procedure ends here, otherwise should be necessary to change the model.

During this thesis work it happened that, for some models, especially for *HC*, the value of R^2 was very low, e.g., quite 0.5. This was explained with the concentration of *HC* emitted by the engine: because of this low quantity produced, the accuracy of the analyzer can influence the measure, leading to a statistical model of low quality. Nevertheless, this was not an important problem, because all the generated calibrations were tested on the test bench, and the real *HC* emissions were measured and compared to those predicted ones.

The generated *Response Models* will appear as shown in Figure 46: in particular, in this figure, is represented the engine point 2000 x 9.6 [rpm x bar] run with *HVO*.

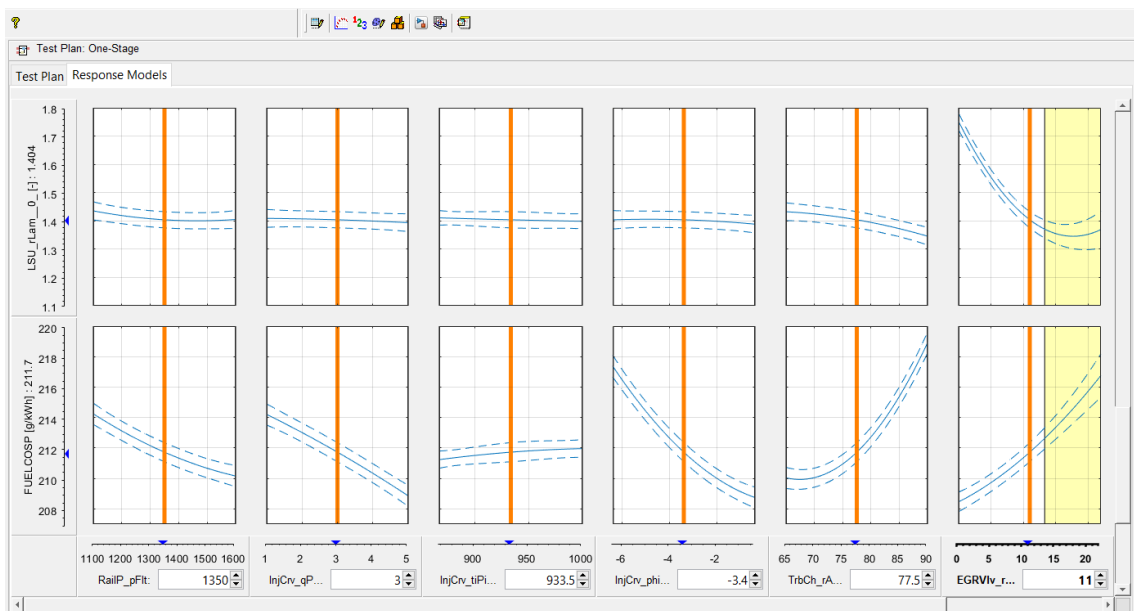


Figure 46 – Example of Response Model graphs

The models are so available and examinable. In particular, the *Response Surfaces* of them can be shown, which gives a graphical interpretation of the model. In Figure 47 is shown an example of the *response surface* of the *soot* model in function of p_{rail} and *SOI* of the main injection for the engine point 2000 x 9.6 [rpm x bar] run with *HVO*.

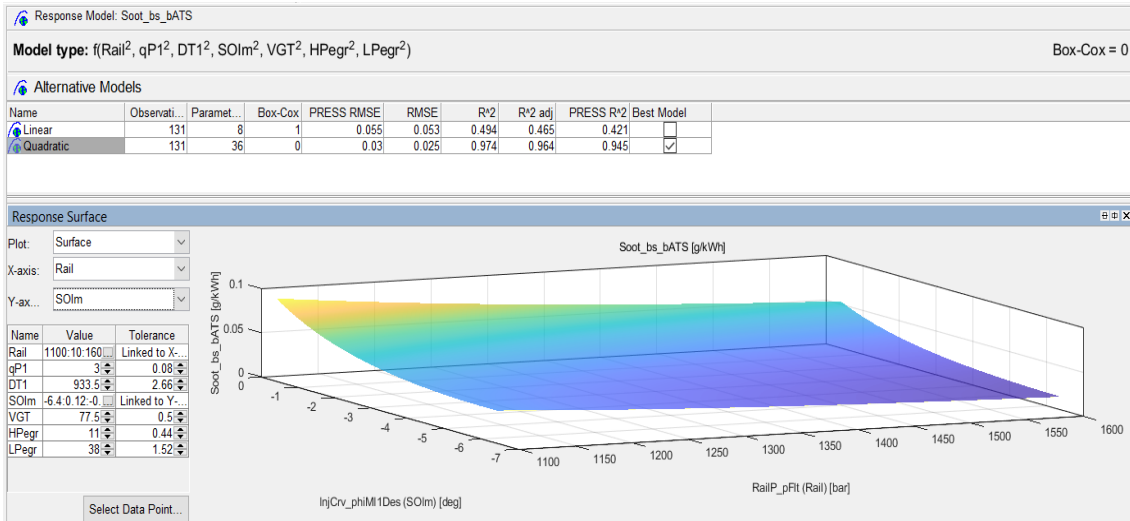


Figure 47 – Example of Response Surface

An important tool that allows to give a first graphical evaluation of the created model is the *Predicted/Observed* graph: it plots the predicted value of a certain variable in function of the real ones; theoretically, for a perfect model, all the points of the graph would lie on the bisector. In Figure 48 is shown an example of *predicted/observed* graph for *bsfc* for the engine point 2000 x 9.6 [rpm x bar] run with *HVO*: in this case, quite all the points are well scattered among the bisector; this means that the model has a good fit of the experimental data.

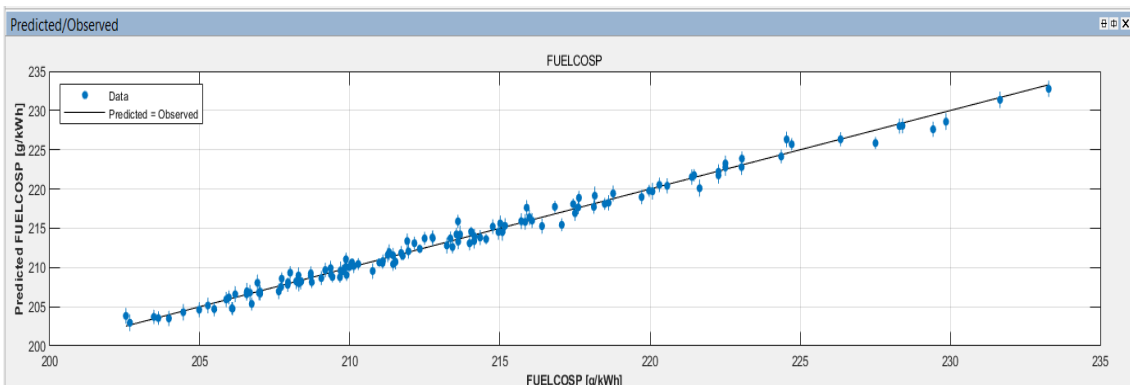


Figure 48 – Example of Predicted/Observed graph

All the main statistical parameters, discussed in Chapter 5.2.2, concerning the models of the *DoEs* run during this thesis work, are shown in Table 13, Table 14, Table 15, Table 16, Table 17 and Table 18.

<i>Parameter</i>	<i>Box-Cox</i>	<i>PRESS RMSE</i>	<i>RMSE</i>	<i>R²</i>	<i>R² adj</i>	<i>PRESS R²</i>
<i>CO₂</i>	1	7.325	6.313	0.804	0.742	0.651
<i>CO</i>	1	0.291	0.242	0.893	0.860	0.795
<i>BSFC</i>	1	2.242	1.879	0.824	0.769	0.670
<i>HC</i>	1	0.051	0.043	0.820	0.764	0.671
<i>λ</i>	1	0.156	0.126	0.893	0.860	0.783
<i>Noise</i>	1	0.355	0.299	0.962	0.950	0.929
<i>NO_x</i>	1	0.408	0.335	0.906	0.877	0.816
<i>Soot</i>	-0.5	0.012	0.009	0.936	0.916	0.873

Table 13 - Model statistical parameters of DoE 1250[rpm] x 2[bar] HVO

<i>Parameter</i>	<i>Box-Cox</i>	<i>PRESS RMSE</i>	<i>RMSE</i>	<i>R²</i>	<i>R² adj</i>	<i>PRESS R²</i>
<i>CO₂</i>	1	7.417	6.648	0.781	0.710	0.637
<i>CO</i>	-1	0.616	0.487	0.865	0.822	0.731
<i>bsfc</i>	1	2.492	2.185	0.781	0.710	0.620
<i>HC</i>	1.5	0.209	0.196	0.559	0.493	0.415
<i>λ</i>	-1	0.168	0.133	0.903	0.871	0.785
<i>Noise</i>	1	0.519	0.432	0.926	0.902	0.858
<i>NO_x</i>	1	0.359	0.327	0.903	0.890	0.866
<i>Soot</i>	-0.5	0.017	0.015	0.891	0.873	0.846

Table 14 - Model statistical parameters of DoE 1250[rpm] x 2[bar] Diesel fuel

<i>Parameter</i>	<i>Box-Cox</i>	<i>PRESS RMSE</i>	<i>RMSE</i>	<i>R²</i>	<i>R² adj</i>	<i>PRESS R²</i>
<i>CO₂</i>	1	3.053	2.559	0.987	0.983	0.975
<i>CO</i>	-0.5	0.184	0.153	0.971	0.960	0.941
<i>bsfc</i>	1	1.033	0.868	0.988	0.983	0.976
<i>HC</i>	1	0.006	0.005	0.816	0.778	0.718
<i>λ</i>	1	0.048	0.040	0.985	0.979	0.969
<i>Noise</i>	1	0.273	0.222	0.990	0.987	0.980
<i>NO_x</i>	1	0.368	0.302	0.981	0.973	0.960
<i>Soot</i>	0	0.030	0.025	0.974	0.964	0.945

Table 15 - Model statistical parameters of DoE 2000[rpm] x 9.6[bar] HVO

<i>Parameter</i>	<i>Box-Cox</i>	<i>PRESS RMSE</i>	<i>RMSE</i>	<i>R²</i>	<i>R² adj</i>	<i>PRESS R²</i>
<i>CO₂</i>	1	3.259	2.753	0.983	0.977	0.967
<i>CO</i>	-0.5	0.222	0.204	0.937	0.928	0.915
<i>bsfc</i>	1	1.066	0.893	0.984	0.979	0.969
<i>HC</i>	1	0.018	0.017	0.544	0.485	0.412
<i>λ</i>	1	0.051	0.043	0.983	0.977	0.968
<i>Noise</i>	1	0.277	0.234	0.992	0.989	0.984
<i>NO_x</i>	1	0.372	0.317	0.981	0.975	0.965
<i>Soot</i>	0	0.040	0.036	0.960	0.954	0.945

Table 16 - Model statistical parameters of DoE 2000[rpm] x 9.6[bar] Diesel fuel

<i>Parameter</i>	<i>Box-Cox</i>	<i>PRESS</i>	<i>RMSE</i>	<i>R²</i>	<i>R² adj</i>	<i>PRESSR²</i>
<i>CO₂</i>	1	1.733	1.451	0.996	0.994	0.991
<i>CO</i>	1	0.220	0.179	0.852	0.793	0.685
<i>bsfc</i>	1	0.638	0.542	0.995	0.993	0.990
<i>HC</i>	1	0.004	0.003	0.917	0.884	0.828
<i>λ</i>	1	0.031	0.026	0.980	0.972	0.960
<i>Noise</i>	1	0.214	0.176	0.993	0.990	0.986
<i>NO_x</i>	1	0.376	0.315	0.977	0.968	0.953
<i>Soot</i>	1	0.014	0.012	0.854	0.796	0.697

Table 17 - Model statistical parameter of Doe 2250[rpm] x 14.4[bar] HVO

<i>Parameter</i>	<i>Box-Cox</i>	<i>PRESS</i>	<i>RMSE</i>	<i>R²</i>	<i>R² adj</i>	<i>PRESSR²</i>
<i>CO</i>	-0.5	17.369	865.526	0.954	0.947	0.935
<i>bsfc</i>	1.0	1.661	1.498	0.952	0.944	0.931
<i>HC</i>	0.0	0.009	0.009	0.436	0.394	0.351
<i>λ</i>	1.0	0.039	0.037	0.964	0.959	0.952
<i>Noise</i>	1.0	0.242	0.215	0.990	0.988	0.985
<i>NO_x</i>	1.0	0.374	0.337	0.975	0.971	0.964
<i>Soot</i>	0.0	0.109	0.101	0.959	0.953	0.943

Table 18 - Model statistical parameters of DoE 2250[rpm] x 14.4[bar] Diesel fuel

5.6. Calibrations generation

Once created the models, the next step is to create the optimal calibration for the selected engine point. During this thesis work, this operation was performed by means of *CAGE* *MATLAB* toolbox, which allows to export the created models and to generate the calibration in function of them. The procedure which leads to this is here described:

1. Export the generated model to *CAGE* environment.
2. Select the model to minimize, e.g., the NO_x emissions.
3. Add constraints for the other parameters, for example a limit value for soot emissions or *bsfc*; in this way, *CAGE* will try to give a calibration with the lowest level of soot, without exceeding the upper value chase for *soot* and *bsfc*. During this step was also added the *EGR* limits in order to avoid finding out a calibration in that region.
4. Run the optimization. If it is possible to respect the added constraints, *CAGE* will return a calibration which minimize the selected parameter.

Different *optimizations* were run for each engine point, changing the variable to minimize and the *constraints*. The aim was to optimize the pre-existing engine calibration, implemented in the *ECU* by the *FPT Industrial Research & Development centre* in *Arbon* (Switzerland); for this reason, firstly the engine points were run as they were, i.e., with their *base-calibration*. Starting from this baseline, many optimizations were executed. The *optimizations* consisted in finding the minimum value of a chosen pollutant (e.g., NO_x) keeping constant the values of other ones and equal to that of the *base-calibration*; these were the *constrains* for the *optimizations*. At the end of this procedure, a data set of different calibrations was obtained.

In the windows *Results Surface* and *Objective Contours* of *CAGE* is possible to check the founded calibration and to change the variables on the axis to examine their values. In Figure 49 is shown an example of a calibration generated by *CAGE*, in which the target was to minimize NO_x emissions.

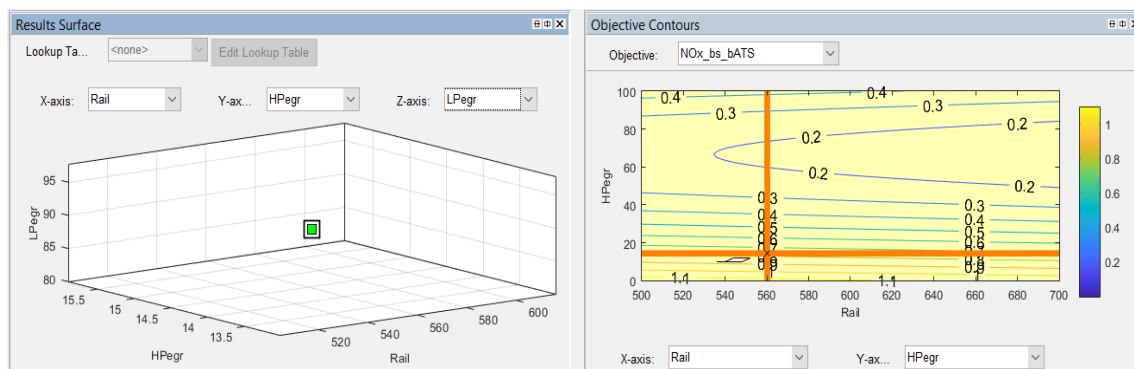


Figure 49 - Example of a calibration generated by *CAGE*

5.7. Calibrations evaluation on test bench

Once the calibrations were generated, they were evaluated at the test bench. This allowed to make some considerations by comparing the predicted values with the experimental ones.

In Figure 50 are shown, for *bsfc*, *pollutants* and *CN* the percentual differences of these quantities between the experimental and the model values. Each figure corresponds to different engine point and fuel used; for each graph are presented only few optimizations for sake of clarity.

The *percentual variations*, shown in Figure 50, have been evaluated with Equation (5.41):

$$\text{Perc. var [\%]} = \frac{x_{\text{experimental}} - x_{\text{model}}}{x_{\text{model}}} \quad (5.41)$$

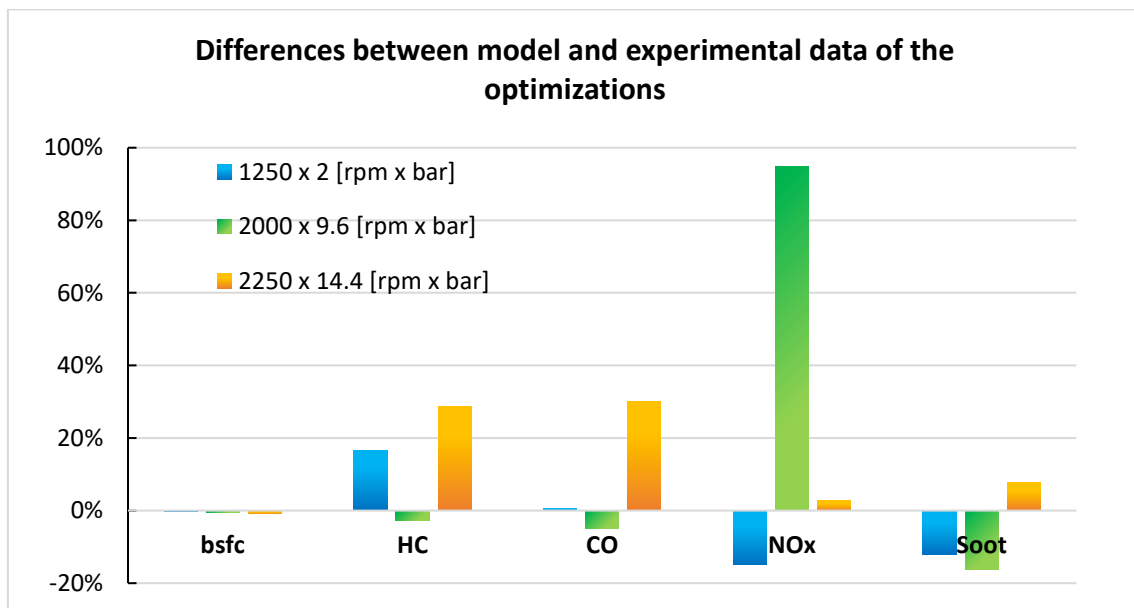


Figure 50 - Differences between model and experimental data of Diesel optimizations

From Figure 50 it can be seen that the major differences between the values predicted by the model and the experimental data, concern pollutant emission. The order of magnitude of these differences is about 20%. What concerns the 2000 [rpm] x 9.6 [bar] optimization, a difference of 95% on NO_x has been revealed (which means that the experimental value is almost two time greater than the predicted one); even if it is a very big discrepancy, the situation would appear clear looking at the absolute values (not here reported for

reservedness reasons): indeed, this value results too low to be realistic for the state of the art of the nowadays engines, so, even if the experimental value of NO_x emissions is double respect to the model one, it still remain a good value. This can be confirmed looking at the Figure 60 in Chapter 5.8, where a reduction of almost 20% of NO_x emission, respect to base calibration, has been noted thanks to this optimization.

Factors which lead to discrepancies between pollutants are many and all of them have as a consequence changes of α value. As well-known from the literature, pollutant species *formation mechanisms* have a strong dependence with α . The factors the mostly influenced fluctuations of air-fuel ratio of the tests led on during this thesis working are here discussed:

- **Loading of DPF.** Th *soot* production of the engine affects the cleaning level of the *DPF*, so the backpressure at the exhaust manifold can be different even if the same calibration is set (at the same engine point); this led to a different *EGR rate* and so to different λ values. The calibration generated by the optimization toolbox provides to set the actuators positions on specific values, but this does not consider the different pressure drops that can be present at the *DPF*. All this means that, small differences of the dirtying levels of the soot filter, may influence the quantity of exhaust gas recirculated and so the values of NO_x and *soot* emitted.

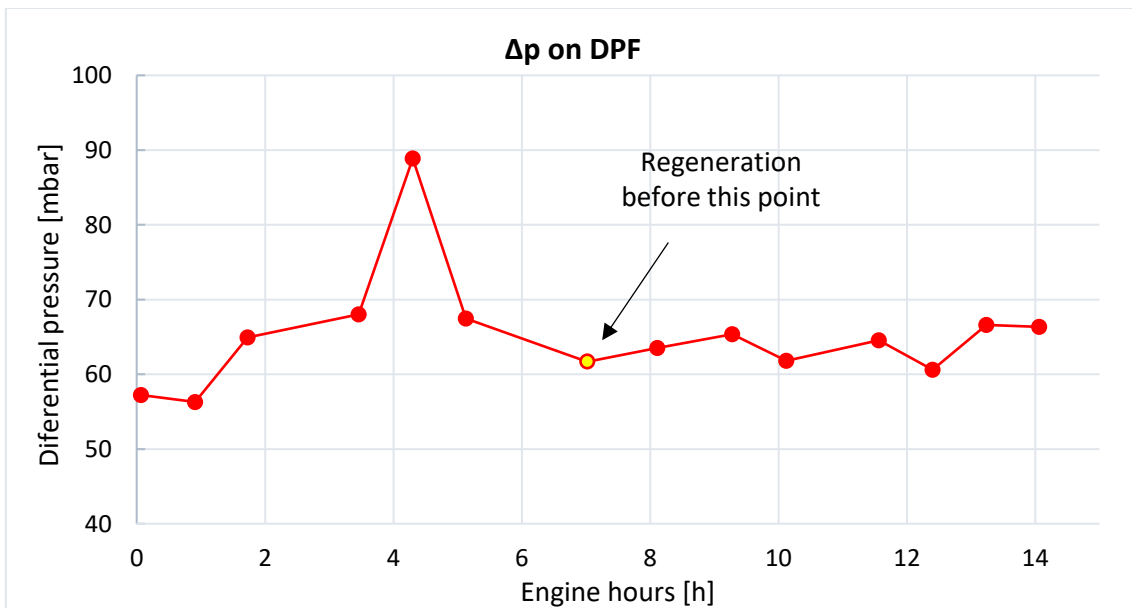


Figure 51 - Differential pressure on DPF of DoE 2250[rpm] x 14.4[bar] Diesel

In Figure 51 is shown the trend of the pressure drop across the *DPF* of the repetition points of a *DoE*: it starts from a “low” value, with *DPF* clean, and shows an increasing trend; some engine points can be interested by high *soot* levels production, which dirties the *filter* causing an increase of the *DPF* back-pressure. In the figure, it is also shown how the pressure goes back to low value after a forced regeneration.

- ***Drift of cabin and snorkel temperature.*** This failure of the air conditioning of the cabin and of the combustion air during this working thesis, led to add this further data disturbance. In dependence of the day in which tests were run, the temperature inside the cabin of the test bench could vary. In addition to this, starting from an initial “low” temperature, due to the running engine, the temperature of the cabin was in a slowly growing trend. This means that a test, performed at late afternoon, was at a different cabin temperature respect to the same test performed at early morning. The snorkel is the pipe that connects the intake manifold, upstream the air filter, to the external environment, providing the combustion air to the engine; higher temperatures levels at the snorkel, and more in general inside the cabin, lead a to lower density of the aspired air from the engine, and so a lower air mass, with the same actuators’ positions and turbocharging conditions, how stated from the *equation of state for ideal gases*. In addition, in absence of air cabin cooling, some hot engine component, e.g., the exhaust line, became heat source for other near components, contributing to their heating.

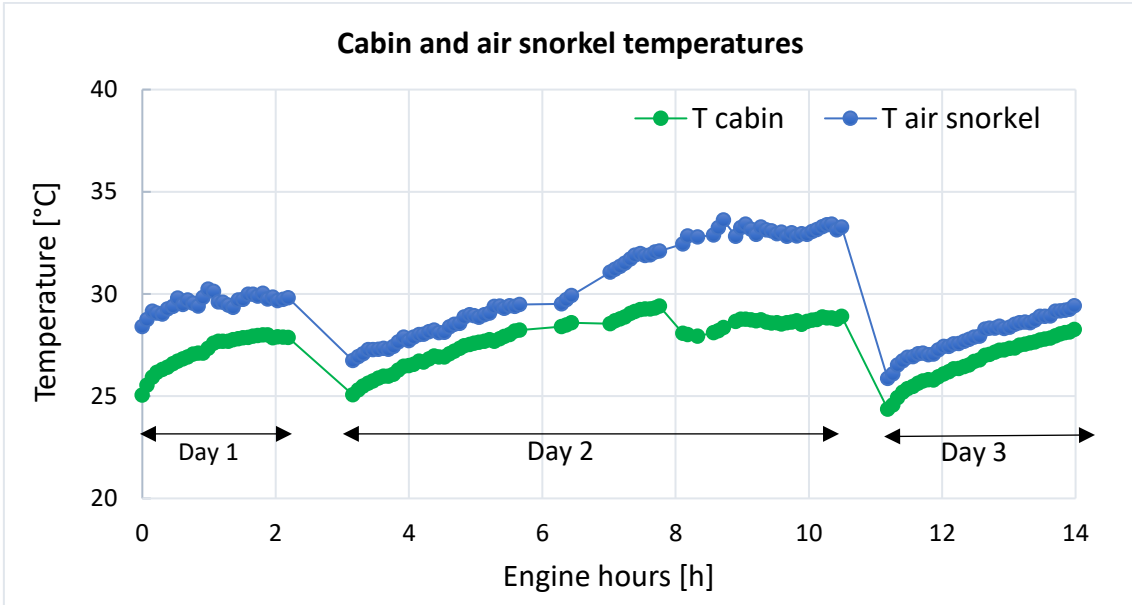


Figure 52 - Cabin and air snorkel temperatures trend of DoE 2250[rpm] x 14.4[bar] Diesel

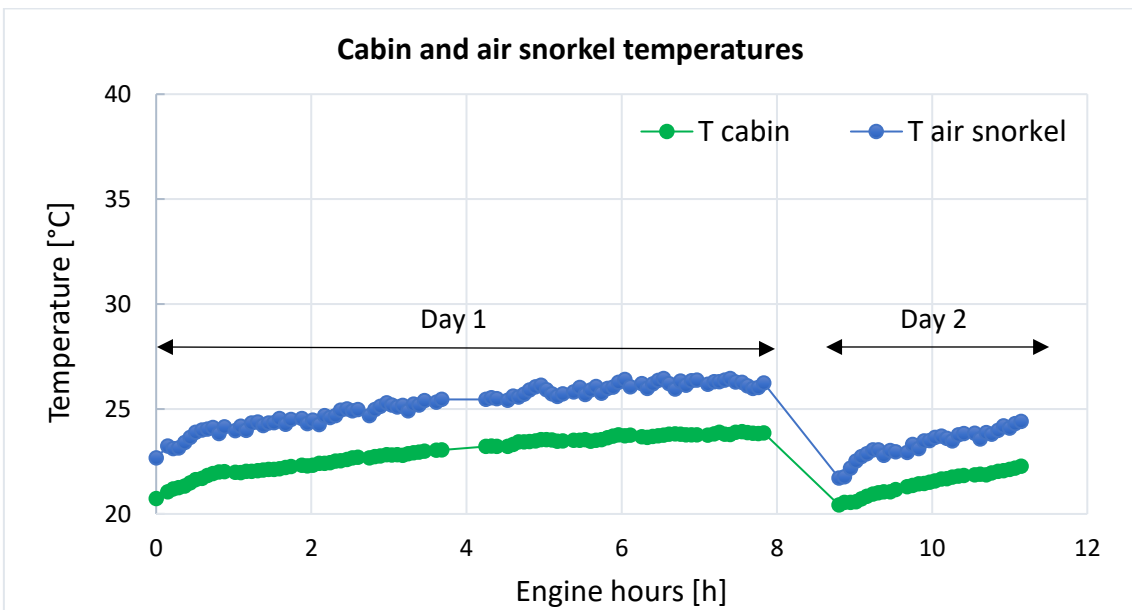


Figure 53 - Cabin and air snorkel temperatures trend of DoE 2250[rpm] x 14.4[bar] HVO

DoE 2250 x 14.4 [rpm x bar]	T cabin [°C]		T air snorkel [°C]	
	<i>Initial</i>	<i>Max</i>	<i>Initial</i>	<i>Max</i>
<i>Diesel</i>	25.1	29.4	28.4	33.6
<i>HVO</i>	20.7	23.9	22.7	26.5

Table 19 - Temperatures comparison between two DoE

In Figure 52, Figure 53 and Table 19 two different *DoE* are shown: since they were performed in different period of the year, they show different initial and maximum temperatures, both for the cabin and the snorkel air. The *HVO DoE*, run with a lower external temperature, and so with lower cabin and snorkel air temperature, show an increasing trend of the temperatures less marked respect to the *Diesel DoE* (run with a higher external temperature). These temperatures trends affect the variability of the *regression model* and λ value.

- **Fouling of HP EGR cooler.** Since *HP EGR* provide to recirculate raw gases withdrawn directly from the exhaust manifold, these will contribute to the cooler fouling. Due to this, the backpressure at the *EGR cooler* can be different even if the same calibration is set (at the same engine point); this led to a different *HP EGR rate* and so to different λ values.

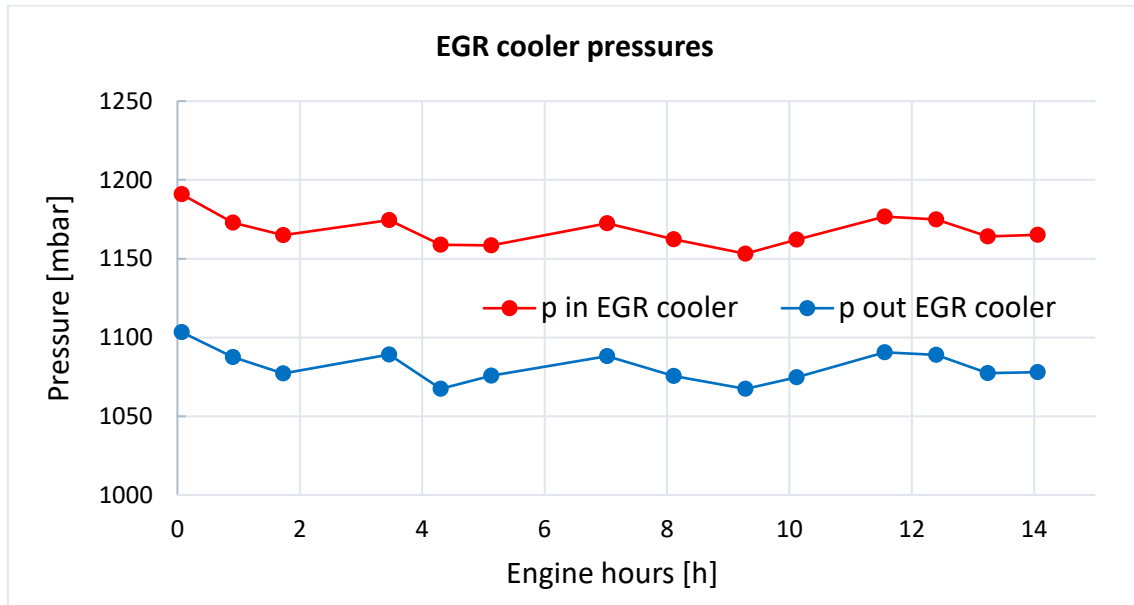


Figure 54 - EGR cooler inlet and outlet pressures of DoE 2250[rpm] x 14.4 [bar] Diesel

In Figure 54 are shown the trends of the inlet and outlet *EGR cooler* pressure of the repetition points of a *DoE*: even if the actuators position is always the same, fluctuations of pressure levels can be seen as a consequence of the fouling phenomenon.

- **Variations of engine coolant water temperature.** The temperature of the engine coolant water may influence the phenomena of heat exchange inside the combustion chamber; this affects not only the air mass inside the cylinder but also the evaporation processes of the fuel and the combustion mechanism. This

temperature is monitored by a *PID* system as described in Chapter 1.5. Errors in electro-valves opening/closing, *PID*'s parameters and its speed of response, may influence the tests, contributing to give further uncertainty to the experimental data.

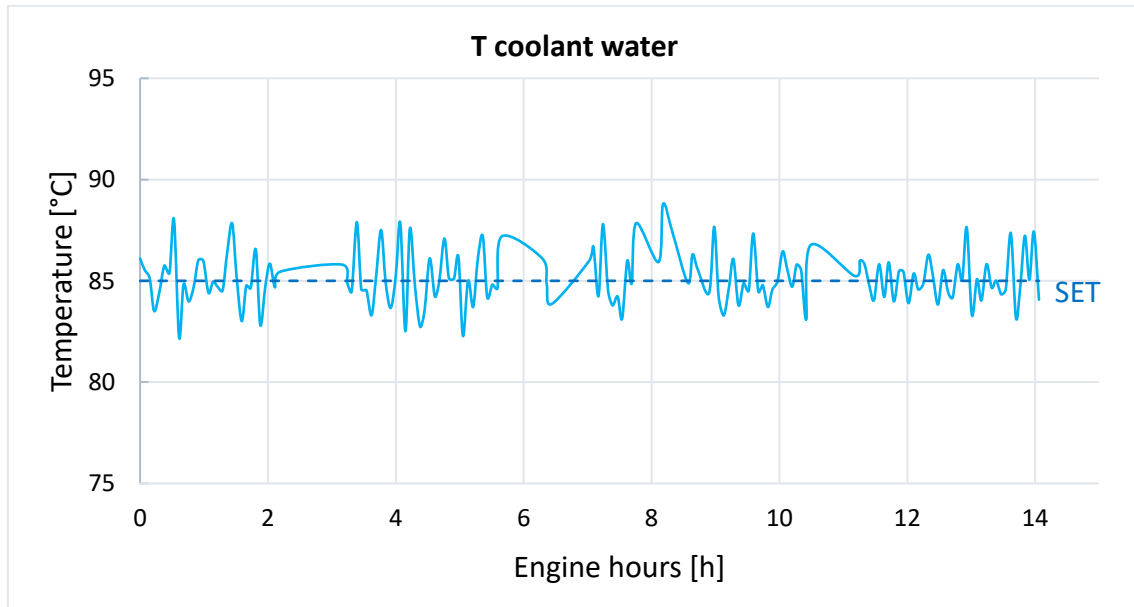


Figure 55 - Coolant water temperature of DoE 2250[rpm] x 14.4[bar] Diesel

In Figure 55 is shown how the coolant water temperature can varies during a *DoE* even if the *PID* control is always set at 85 °C.

All these phenomena lead to a drift of the air drawn by the engine, and it is visible thanks to Figure 56 Figure 56 - Lambda values of the repetition points of the DoE 2250[rpm] x 14.4[bar] Diesel which shows the value of λ during the repetition points of a *DoE*: even if the value should be the same (since the engine calibration is the same), because of all the factors discussed above, it presents a fluctuation and a decrease after the initial value.

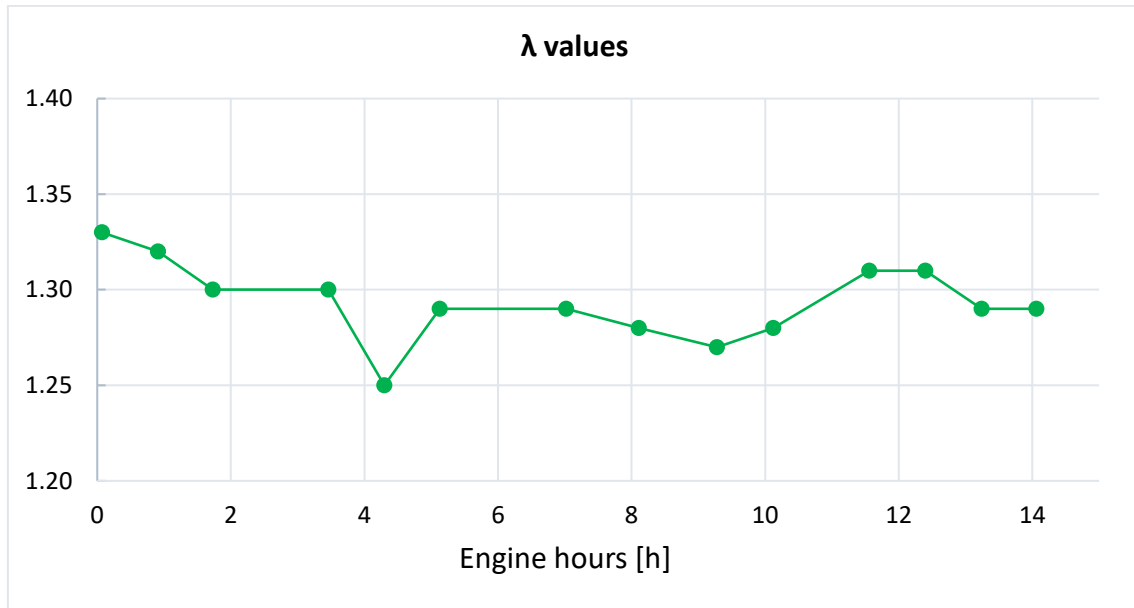


Figure 56 - Lambda values of the repetition points of the DoE 2250[rpm] x 14.4[bar] Diesel

Anyhow, even percentual differences of 20÷25% (or greater) on the *soot* brake specific mass emissions, have a low impact on the results, being the absolute error values in the order of *mg/kWh*. In addition to that, a hypothetical situation can be the one in which, the measured value of the *soot* emission, is greater than the predicted one: being these two quantities in trade-off, this leads almost always to a reduction on NO_x emission; this guarantees, in any case, the obtaining of sensible results, though it was not the desired ones.

Furthermore, each optimization was performed firstly with the same calibration generated by *CAGE* and, if necessary, repeated with the same λ predicted by the model, acting on the *HP EGR* actuator position to reach the target value.

On the other side, quantities that are not strongly influenced by small variation of λ , like *bsfc* and *CN*, show experimental values very similar to the model ones, with differences always lower than 0.7%. For example, *CN* strongly depends on parameters like *SOI*, q_{pil1} , q_{pil2} and *DT* between them, but these values are fixed for a given calibration, so they cannot influence the comparison.

5.8. Diesel and HVO optimal calibrations

Among the many optimizations calibrations executed with *Diesel fuel* and *HVO*, the best ones were chosen for each engine point. The calibrations generated by means of *CAGE* have been created with the aim of minimize the engine-out pollutant emissions, as discussed in Chapter 5.6.

The *percentual variations*, shown in Figure 57, Figure 60 and Figure 63, have been evaluated with Equation (5. 42)(5. 41):

$$Perc. var [\%] = \frac{x_{opt}}{x_{baseline}} \quad (5. 42)$$

The *HRR* and the *MFB* curves, the *MFB10*, *MFB50*, *MBF90* have been evaluated by means of the “*Thermodynamics 1*” block of the *CONCERTO* toolbox “*CalcGraph*”, starting from the in-cylinder pressures signals, filtered by a *low-pass* filter, and averaged on 50 engine cycles on the 4 cylinders. While the *SOC* has been evaluated as described in Chapter 4.3, the *ID* has been calculated thanks to Equation (5. 43):

$$ID = |SOI_{pil2} - SOC| \cdot \frac{60}{n_{eng} \cdot 360} \quad (5. 43)$$

At the 90% of the mass fraction burned, the combustion phase is at the end; for this reason, in this thesis work, as indication of the *duration of combustion* has been taken the difference between the *SOC* and the *MFB90*, as stated in the Equation (5. 44):

$$Combust. duration = |SOC - MFB90| \cdot \frac{60}{n_{eng} \cdot 360} \quad (5. 44)$$

It is obvious that the same time at different speed means different crank degrees: by calculating the *ID* and the *combustion duration* as a time and not as crank degrees, the effect of the rotational speed of the engine n_{eng} has been removed, and this leads to comparable results even at different n_{eng} .

Always in these graphs, the SOI_{pil2} has been indicated simply as *SOI* for clarity's sake.

5.8.1. Calibration optimization: 1250 [rpm] x 2 [bar]

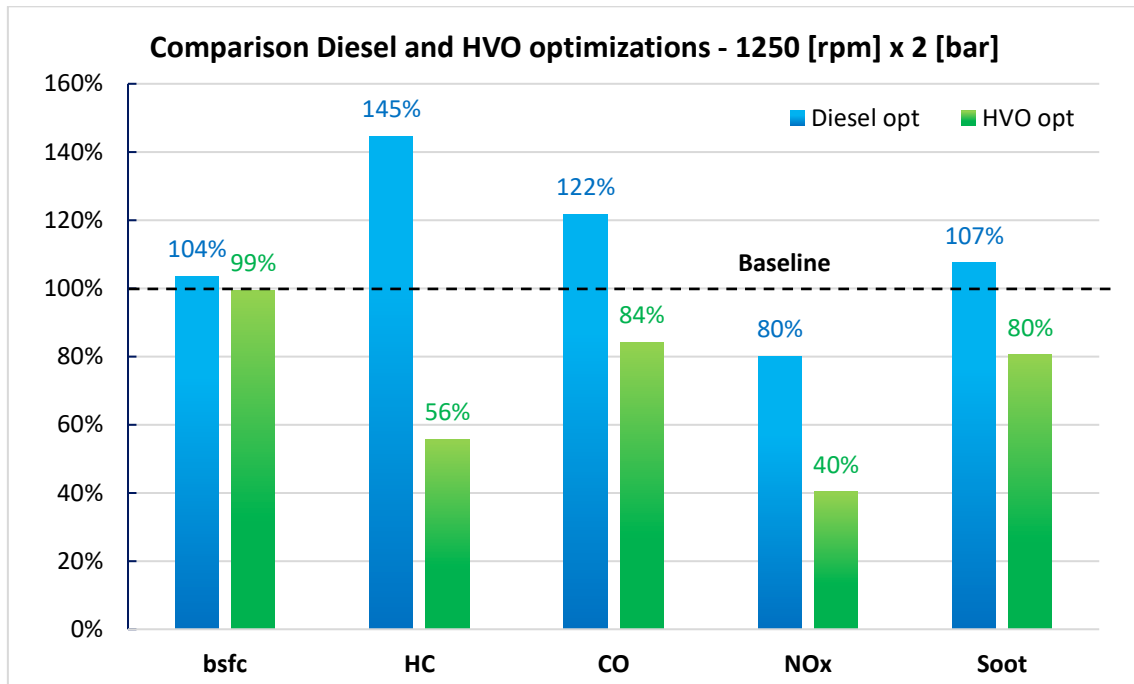


Figure 57 –Variations of Diesel and HVO optimizations respect to baseline @ 1250 [rpm] x 2 [bar]

For this engine point the calibration taken as baseline is the one tested in the *FPT Industrial Research & Development centre* in *Arbon*. The main difference between the calibrations here presented and the one developed in *Arbon* lays in the use of the exhaust flap; from Figure 57 it can be seen that, in order to reduce NO_x emissions with *Diesel fuel*, all the other pollutants have increased, even the fuel consumption. This result has been studied and the main parameters investigated are listed in Table 20. The *baseline* and the *diesel optimization* have more or less the same λ , but this value is obtained differently depending on the calibration: on one side, the baseline, gets that λ value by closing the exhaust flap and this creates a back-pressure in the exhaust line which leads to more *EGR* rate through the *HP* circuit; on the other side, the diesel optimization, gets that lambda value by closing the inlet nozzles of the *VGT*. The use of *VGT* leads to a double effect:

- Back-pressure at the turbine inlet: it causes higher pressure levels during the engine exhaust phase, which lead to a greater *internal EGR*, i.e., higher *residuals*. This is confirmed by the lower temperatures at the intake manifold respect to the baseline.

- Increasing of the rotational speed of the turbocharger: it causes a higher boost pressure; however, this is not a desired effect, since the considered engine point is at low-load, so the *ECU* closes more the *VGT* nozzles to get a greater pressure level at the exhaust manifold in order to recirculate more exhaust gas, but, once again, this makes the boost pressure increase. This loop is a competition between trying to get more *EGR* rate and the effects of the *VGT* closure and it ends when the right λ value is found.

The higher pressure levels during the exhaust phase respect to the baseline, lead to greater *pumping loss* and it is confirmed by the higher value of *IMEP*, being it related to the *BMEP* through the equation (5. 45):

$$PMEP = BMEP - IMEP \quad (5. 45)$$

This could be the reason why the *bsfc* decrease by using the exhaust flap. The lower temperatures at the intake manifold respect to the baseline, lead to lower temperature at the end of the compression phase and so during the combustion process; since the *NO_x*, *HC* and *CO* formation mechanism depend on the temperatures during the combustion, this could be the reason why the *NO_x* emissions decrease without the use of the exhaust flap and, oppositely, the *HC* and *CO* emission increase.

1250 x 2 [rpm x bar]	T_{intake} [°C]	p_{bTC} [mbar]	VGT [%]	n_{turbo} [krpm]	p_{boost} [mbar]	PMEP [bar]
Baseline	60.9	1085	87.7	28.9	17.7	0.97
Diesel opt	46.7	1236	96.0	52.0	21.6	1.03

Table 20 - Differences in the use of the exhaust flap @ 1250 [rpm] x 2 [bar]

During this laboratory activity, a first *1250[rpm] x 2[bar] DoE* with the exhaust flap has been executed but it led to poor results since an additional variable to the regression model was added; in addition, the exhaust flap gave more variability of the pressure levels at the exhaust line: this one, together with the *DPF* fouling, is a further drawback that affects λ control.

Taking into account the *HVO optimization*, even without using the exhaust flap, it is possible to obtain a considerable reduction of *HC* and *NO_x* emission at low-load, respect to the base calibration, keeping more or less *bsfc* constant, and also a reduction of *CO*

emissions. What concerns *soot* emissions, their value is already low, but, however, a decrease has been observed.

The main differences between the *Diesel* and *HVO* optimizations and the baseline calibrations at this engine point are listed in Table 21. It can be noted that, in the optimization with *HVO*, the *SOI* is postponed respect to the *Diesel* optimization: this results in lower pressure levels during the combustion phase, and so lower temperatures, which causes lower NO_x production; in addition, the lower value of λ affects the reduction of this pollutant. The interesting aspect is that, despite the lower λ and temperatures during combustion, the *soot* emissions are also decreased. This suggests an improvement of the combustion process when using *HVO*.

1250 x 2 [rpm x bar]	SOI_m [°bTDC]	p_{rail} [bar]	Flap_{exh} [%]	VGT [%]	HP EGR [%]	LP EGR [%]	q_{pit1} [mg/strk]	λ -
Baseline	-2.9	613	74	87.7	100	0.0	2.0	2.40
Diesel opt	-1.5	540	0	96.0	10	88	2.7	2.34
HVO opt	-3.7	691	0	95.8	46	86	2.8	1.97

Table 21 - Diesel, HVO and baseline calibrations @ 1250 [rpm] x 2 [bar]

1250 x 2 [rpm x bar]	SOI_{pit2} [°aTDC]	SOC [°aTDC]	ID [ms]	MFB 10 [°aTDC]	MFB 50 [°aTDC]	MFB 90 [°aTDC]	Comb. durat. [ms]
Baseline	-14.0	-7.4	0.9	0.7	10.1	31.1	5.1
Diesel opt	-15.3	-7.9	1.0	-1.5	8.6	31.1	5.2
HVO opt	-13.1	-7.4	0.8	0.8	9.4	29.9	5.0

Table 22 – Combustion parameters of optimizations and baseline @ 1250 [rpm] x 2 [bar]

The trends of *in-cylinder pressure*, *HRR* and *MFB* of these three calibrations are shown in Figure 58 and Figure 59, while the main combustion parameters, like *SOI_{pit2}*, *SOC*, *MFB10*, *MFB50* and *MFB90* are listed in Table 22. Since these graphs and tables, it can be seen that, with the *HVO*, the *SOI_{pit2}* has been shifted towards the *TDC* respect to the baseline; nevertheless, the *SOC* is the same, which means a smaller *ID*. Looking at the

MFB90 it is also appreciable a faster combustion process then using *HVO* at this engine point, even if the λ value is lower; however, on one hand, SOI_{pil2} is closer to the *TDC*, which means higher temperature and pressure level during injection events, which affect the *ID* and the *combustion duration*, while, on the other hand, SOI_m is farther away from the *TDC*, which has an opposite effect.

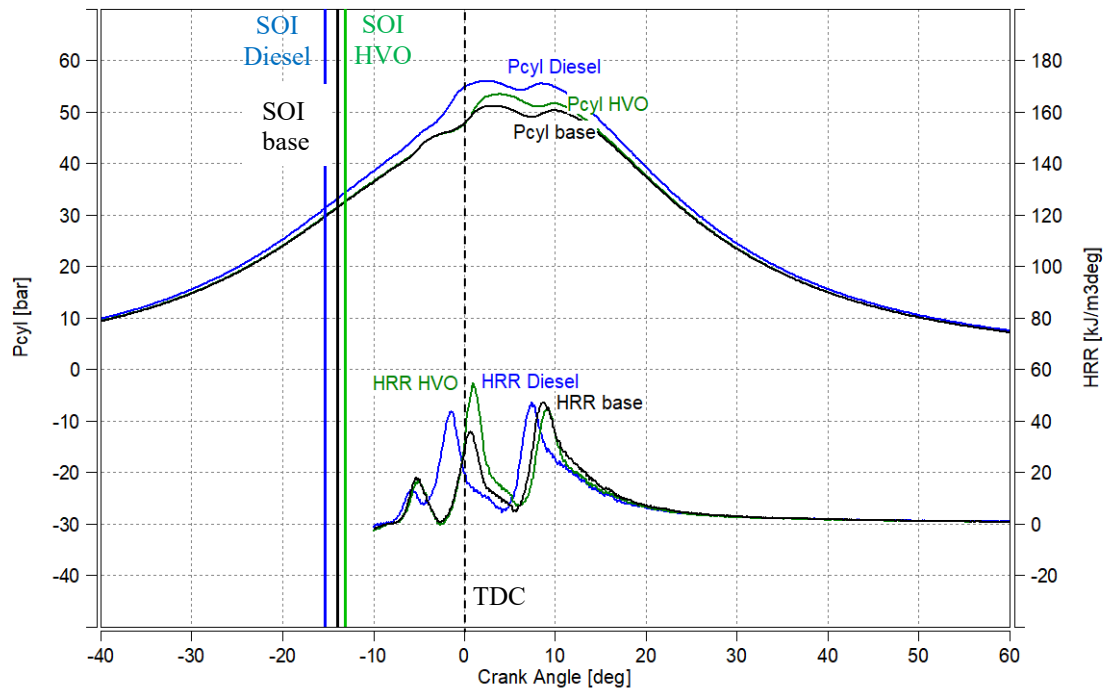


Figure 58 - In-cylinder pressure and HRR of optimizations and baseline @ 1250 [rpm] x 2 [bar]

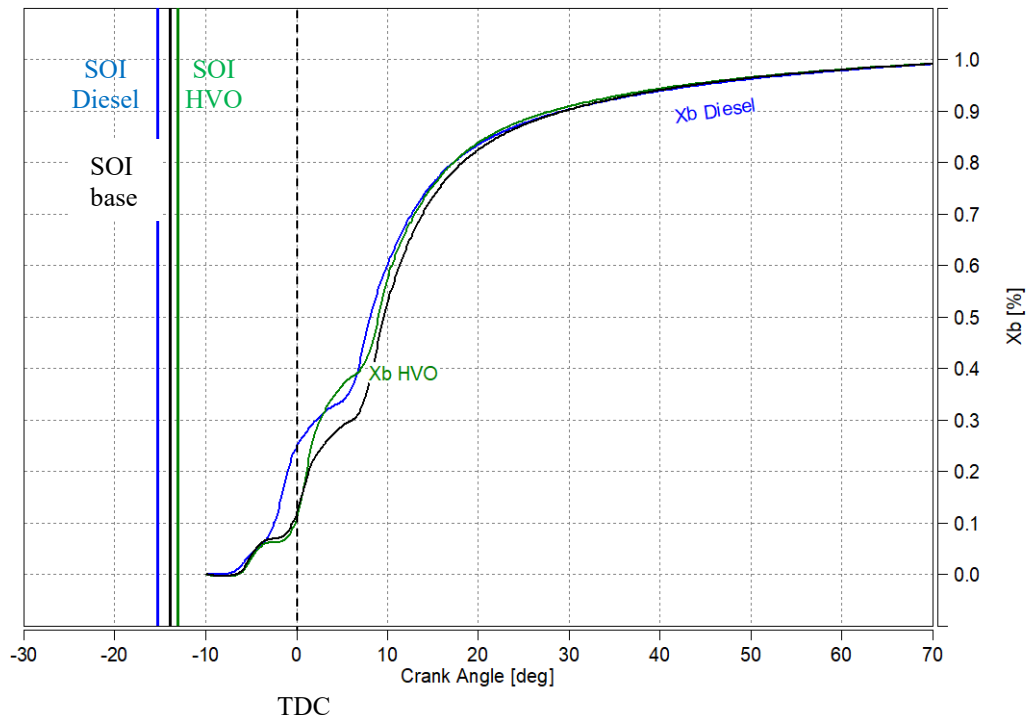


Figure 59 - Mass fraction burned of optimizations and baseline @ 1250 [rpm] x 2 [bar]

5.8.2. Calibration optimization: 2000 [rpm] x 9.6 [bar]

For this engine point the calibration taken as baseline is the one of the engine left completely free, i.e., its original calibration. From Figure 60 it can be seen that, with *Diesel fuel*, a reduction of *CO* and mostly of *soot* and *NO_x* respect to the base calibration has been carried out, keeping more or less constant the *bsfc*. The slight increase of *HC* emission is in the order of magnitude of few *mg/kWh* so it can be assumed as negligible. On the other side, with *HVO*, it is possible to perform a further reduction of *NO_x* emission and a decrease of *HC* emission which was not possible with *diesel fuel*.

The main differences between the *Diesel* and *HVO* optimizations and the baseline calibrations at this engine point are listed in Table 23. It can be seen that, the reduction of *NO_x* emission has been performed by postponing the combustion, i.e., shifting towards the injections train: this causes lower temperature levels during combustion. λ values have been increased in the Diesel optimizations, while, in the *HVO* one, λ is quite equal to the baseline but with a higher rail pressure.

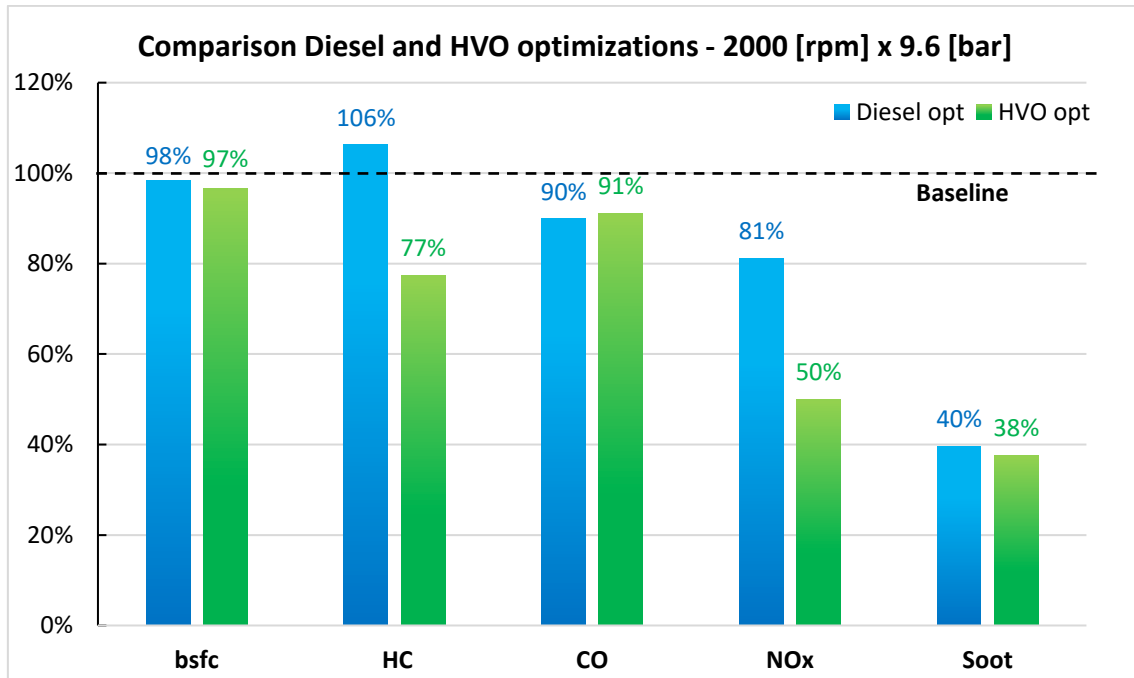


Figure 60 – Variation of Diesel and HVO optimizations respect to baseline @ 2000 [rpm] x 9.6 [bar]

Engine point

2000[rpm] x 9.6[bar]	SOI _m [°bTDC]	p _{rail} [bar]	Flap _{exh} [%]	VGT [%]	HP EGR [%]	LP EGR [%]	q _{pil1} [mg/strk]	λ
Baseline	-2.4	1376	0	81.8	32.5	0	2.5	1.35
Diesel opt	-5.4	1321	0	70.5	0.3	69.5	5.0	1.47
HVO opt	-5.1	1522	0	82.0	3.9	73.0	5.0	1.37

Table 23 - Diesel, HVO and baseline calibrations @ 2000 [rpm] x 9.6 [bar]

The trends of *in-cylinder pressure*, *HRR* and *MFB* of these three calibrations are shown in Figure 61 and Figure 62, while the main combustion parameters, like *SOI_{pil2}*, *SOC*, *MFB10*, *MFB50* and *MFB90* are listed in Table 24Table 22. Since these graphs and tables, it can be seen that, what concerns the *ID*, using *HVO*, it is smaller even if the λ is the same to the baseline; however, on one hand the *SOI_{pil2}* is postponed respect to the baseline one, which helps to reduce the *ID*, while, on the other hand, *SOI_m* is anticipated, which has an opposite effect.

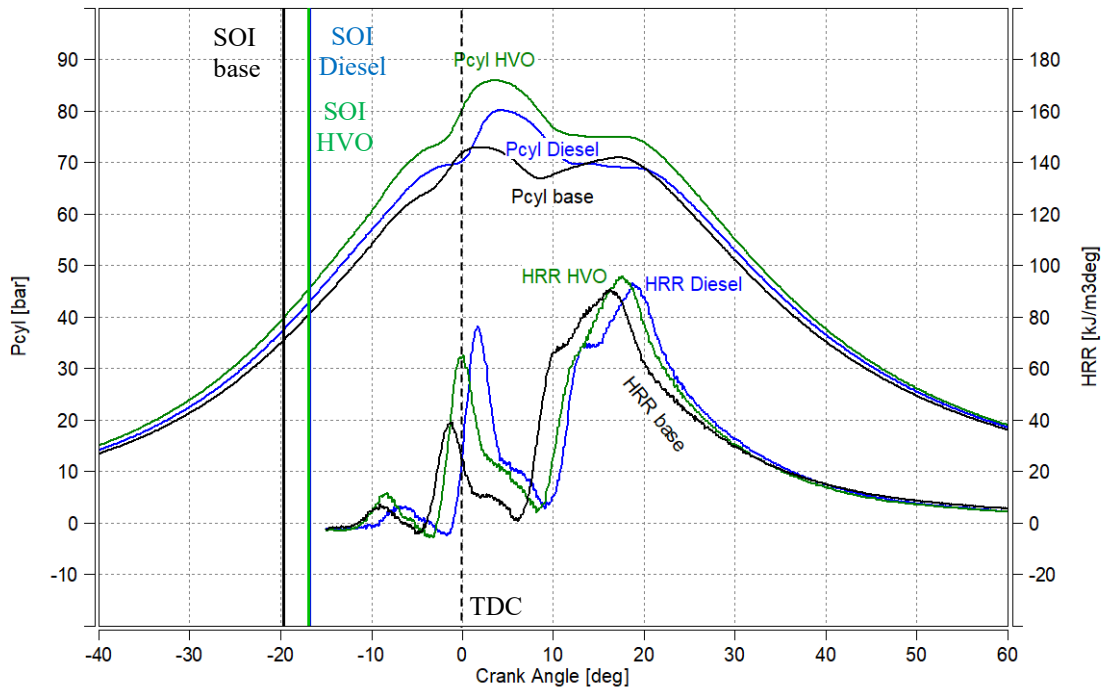


Figure 61 - In-cylinder pressure and HRR of optimizations and baseline @ 2000 [rpm] x 9.6 [bar]

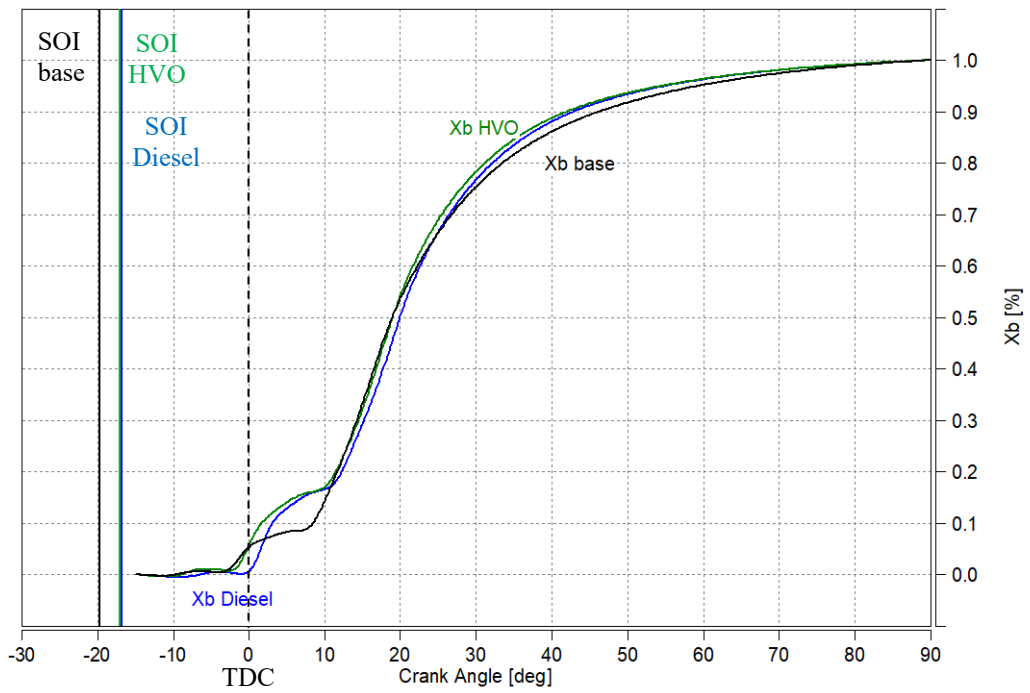


Figure 62 - Mass fraction burned of optimizations and baseline @ 2000 [rpm] x 9.6 [bar]

<i>Calibration</i>							<i>Comb.</i>
<i>2000[rpm] x</i>	<i>SOI_{pit2}</i>	<i>SOC</i>	<i>ID</i>	<i>MFB 10</i>	<i>MFB 50</i>	<i>MFB 90</i>	<i>durat.</i>
<i>9.6[bar]</i>	<i>[°aTDC]</i>	<i>[°aTDC]</i>	<i>[ms]</i>	<i>[°aTDC]</i>	<i>[°aTDC]</i>	<i>[°aTDC]</i>	<i>[ms]</i>
Baseline	-19.7	-12.2	0.6	9.0	19.1	46.5	4.9
Diesel opt	-16.7	-9.2	0.6	3.8	20.3	43.1	4.4
HVO opt	-17.0	-12.2	0.4	2.7	19.1	42.2	4.5

Table 24 - Combustion parameters of optimizations and baseline @ 2000 [rpm] x 9.6 [bar]

5.8.3. Calibration optimization: 2250 [rpm] x 14.4 [bar]

For this engine point the calibration taken as baseline is the one of the engine left completely free, i.e., its original calibration. From Figure 63 it can be seen that a reduction of NO_x and soot emission, keeping the $bsfc$ constant, has been carried out. The 9% of more HC emission can be neglect, since this kind of pollutant at this high-load engine the high temperatures at the DOC promote the HC oxidation.

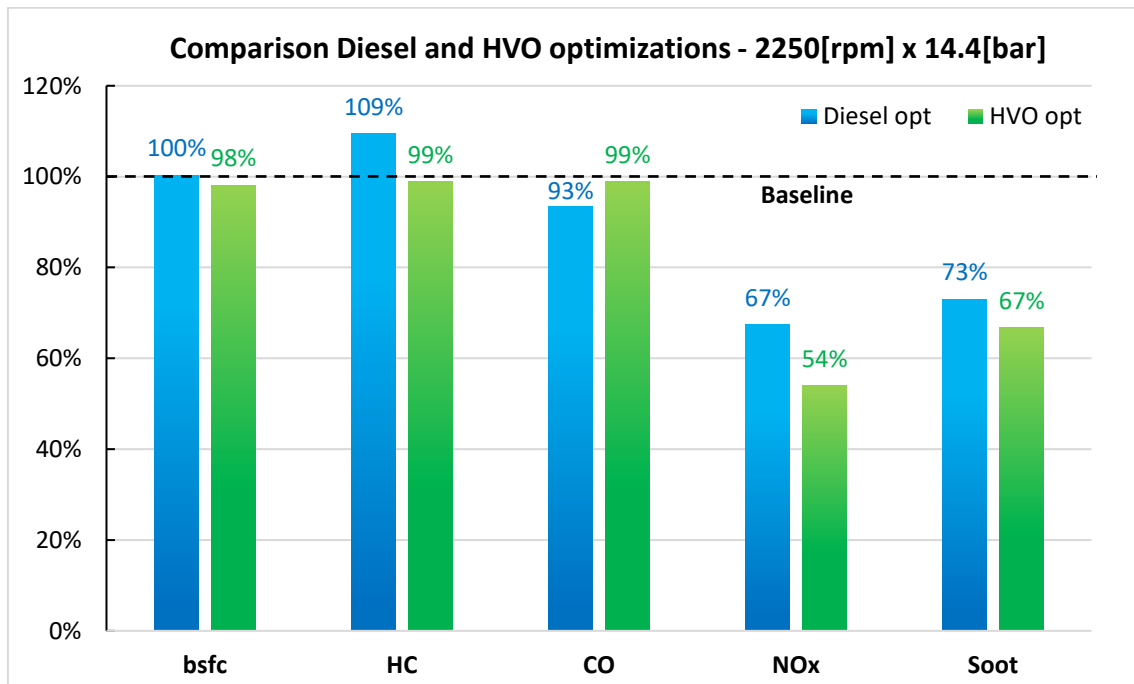


Figure 63 – Variation of Diesel and HVO optimizations respect to baseline @ 2250 [rpm] x 14.4 [bar]

On the other hand, with HVO it is possible to perform a significative NO_x reduction respect to *diesel fuel*, keeping the all the other quantities more or less equal to the baseline, especially considering that, at high-load engine points, the emissions of this pollutant is very important; instead, *soot* absolute values are yet low, but, however, a further reduction

has been seen. Once again, these last considerations should be more comprehensible looking at the absolute values.

The main differences between the *Diesel* and *HVO* optimizations and the baseline calibrations at this engine point are listed in Table 25. In the Diesel optimization the SOI_m has been slightly postponed, while λ value has been increased respect to the baseline. However, what stands out from this table is the *HVO* optimization: λ is greater than the baseline one and the SOI_m is anticipated; in normal working condition (i.e., with Diesel fuel respect to base calibration) an increasing on NO_x emissions would be expected; despite this, an important reduction of NO_x has been seen with the *HVO* calibration.

Calibration								
2250[rpm]	SOI_m	p_{rail}	$Flap_{exh}$	VGT	HP EGR	LP EGR	q_{pil1}	λ
x 14.4[bar]	[°bTDC]	[bar]	[%]	[%]	[%]	[%]	[mg/strk]	-
Baseline	2.4	1451	0	67.3	35.9	0	1.2	1.37
Diesel opt	2.7	1450	0	74.5	0.0	34	1.0	1.47
HVO opt	1.4	1448	0	74.2	0.9	34	1.4	1.46

Table 25 – Diesel, HVO and baseline calibrations @ 2250 [rpm] x 14.4 [bar]

The trends of *in-cylinder pressure*, *HRR* and *MFB* of these three calibrations are shown in Figure 64 and Figure 65Figure 61, while the main combustion parameters, like SOI_{pil2} , SOC , MFB_{10} , MFB_{50} and MFB_{90} are listed in Table 26. Since these graphs and tables it can be seen that, the *Diesel* optimization shows a slight decrease in the *ID*, although no reduction of the combustion process has been highlighted, but this is explained by the higher value of λ and the injection events closer to the *TDC*. What concerns the *HVO* optimizations, they show a smaller *ID* respect to the other two calibrations and also a slight increase of the combustion process; here λ value is the same of the optimal calibration but this could be due to the effect of the injection events closer to the *TDC*.

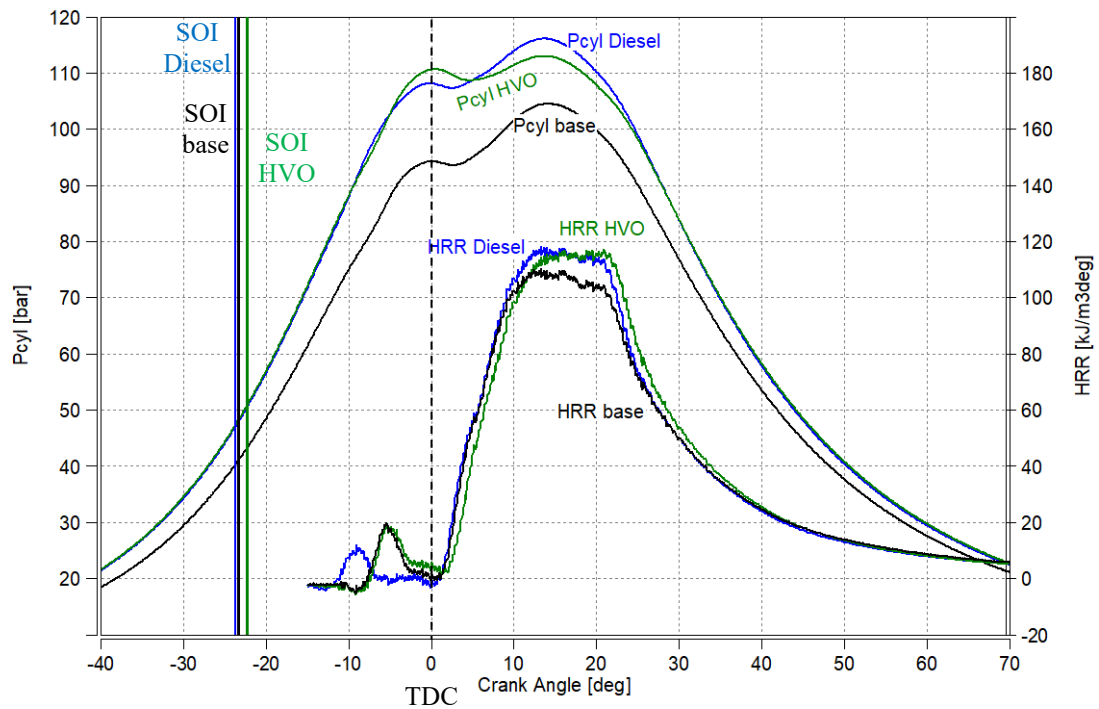


Figure 64 - In-cylinder pressure and HRR of optimizations and baseline @ 2250 [rpm] x 14.4 [bar]

Calibration							Combust.
2250[rpm]	SOI_{pit2}	SOC	ID	MFB 10	MFB 50	MFB 90	duration
x 14.4[bar]	[°aTDC]	[°aTDC]	[ms]	[°aTDC]	[°aTDC]	[°aTDC]	[ms]
Baseline	-23.4	-8.6	1.1	8.0	19.8	46.2	4.1
Diesel opt	-23.7	-11.6	0.9	7.8	19.6	44.2	4.1
HVO opt	-22.4	-8.6	1.0	8.6	20.4	44.6	3.9

Table 26 - Combustion parameters of optimizations and baseline @ 2250 [rpm] x 14.4 [bar]

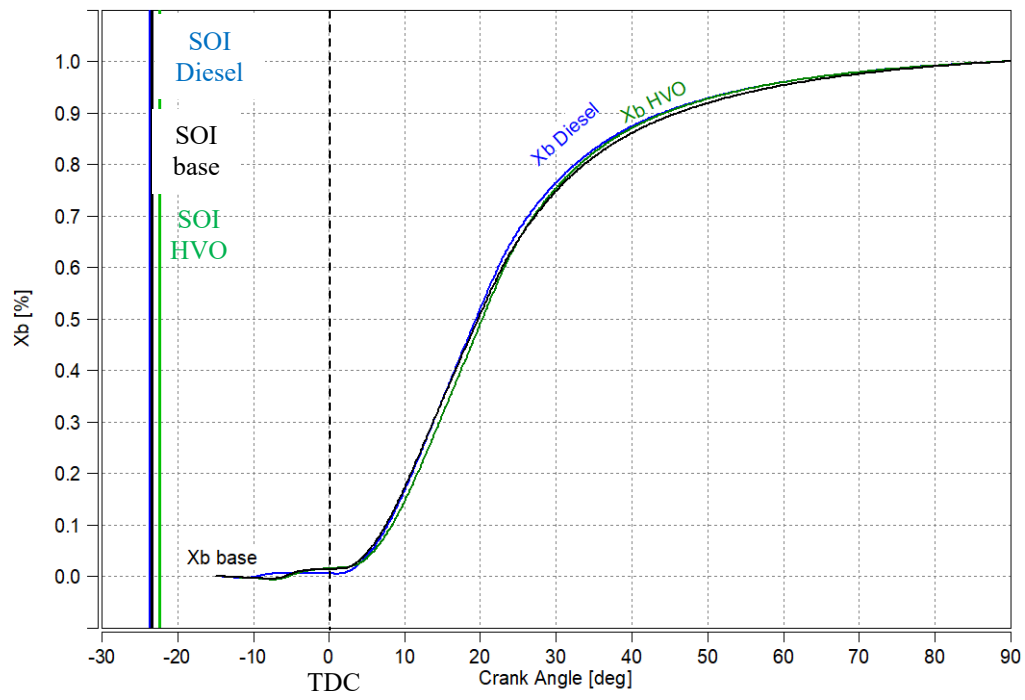


Figure 65 - Mass fraction burned of optimizations and baseline @ 2250 [rpm] x 14.4 [bar]

6. Lambda sweep of optimal calibrations

To highlight the differences between the two fuels, and also to better investigate the domain regions around the optimizations, trade-offs of the best *Diesel* and *HVO* calibrations have been performed. They have been carried out starting from the optimal calibrations and varying λ value: this means to increase/decrease the engine intake air flow and it was performed by acting on the *LP EGR* actuator position.

The experimental results of this procedure are shown in Figure 66, Figure 67 and Figure 68, where the *percentual variations* have been evaluated once again with Equation (5.42) and the optimal calibrations are highlighted with empty symbols. From these graphs it can be seen that, the *HVO* trade-offs show always lower emissions and fuel consumption levels, or at least equal, respect to the *Diesel* trade-offs; only in some cases the *CN* trade-offs seem to be higher: however, this drawback would be not enough to belittle the advantages showed using *HVO*.

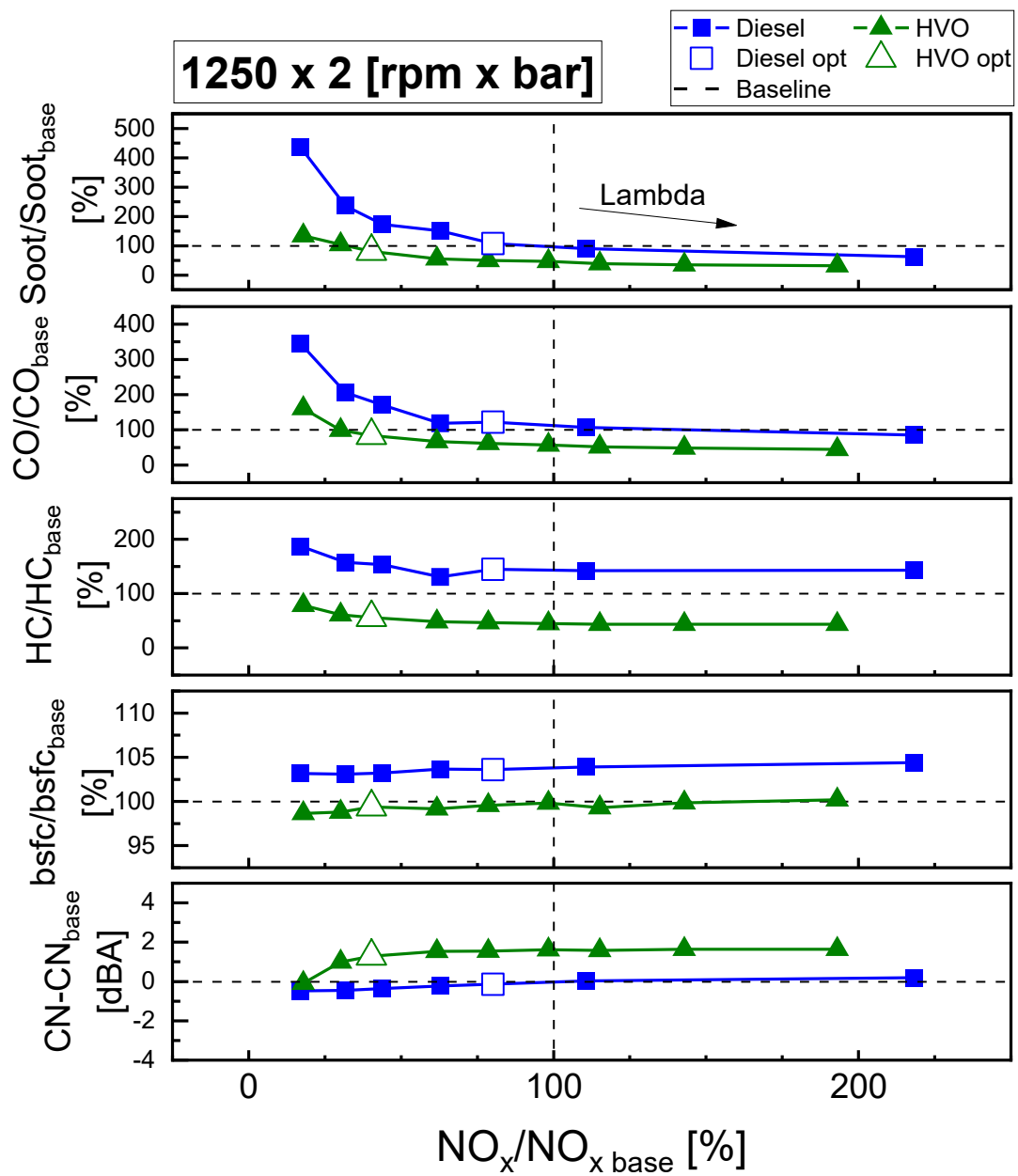


Figure 66 - Comparison of lambda trade-offs of Diesel and HVO optimizations @ 1250[rpm] x 2[bar]

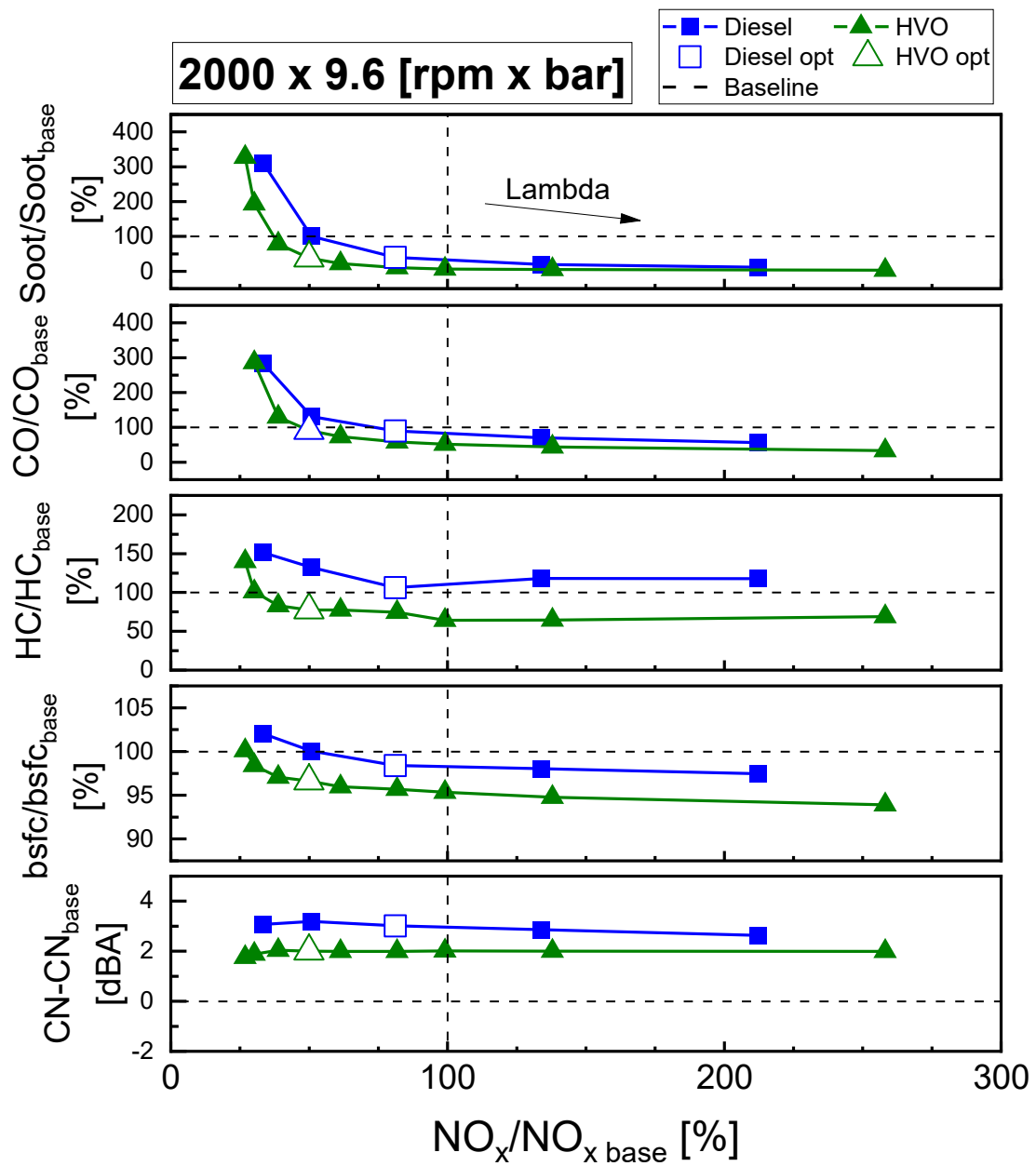


Figure 67 - Comparison of lambda trade-offs of Diesel and HVO optimizations @ 2000[rpm] x 9.6[bar]

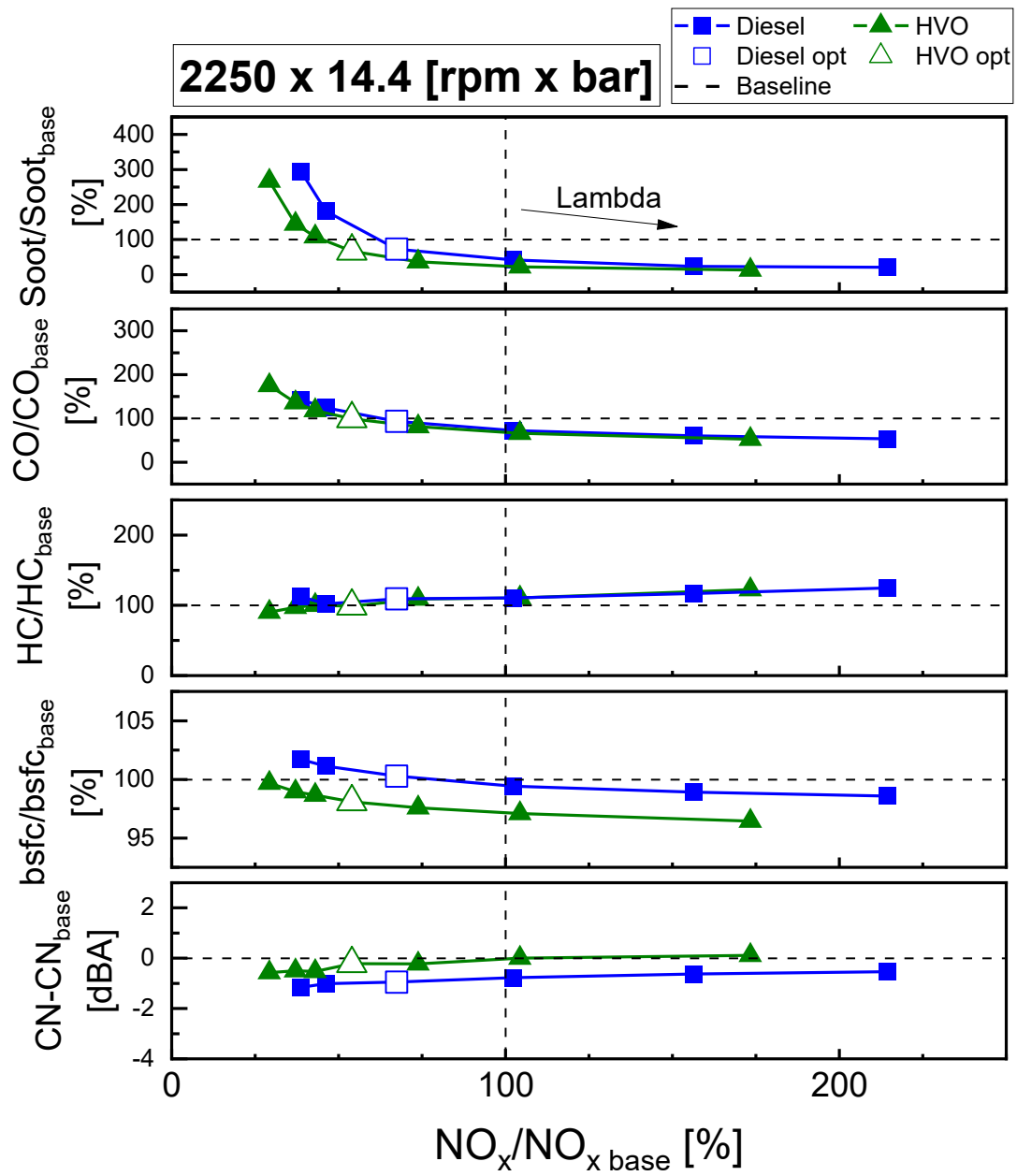


Figure 68 - Comparison of lambda trade-offs of Diesel and HVO optimizations @ 2250[rpm] x 14.4[bar]

7. Conclusions

What concerns the use of conventional *Diesel fuel*, by means model-based calibrations optimizations, good results have been achieved in terms of pollutants emissions regarding the engine points at medium and high load; for the low load one, the use of the exhaust flap seems to be a valid means to obtain better results.

What concerns the use of *HVO* as fuel for a common light duty engine, during this working thesis, smaller *IDs* respect to *Diesel fuel* has been observed, especially at low load, attributable to its higher *Cetane number*, its *chemical composition* and its *surface tension* and *viscosity*; this leads to much time available for the combustion process and lower peak in-cylinder pressure, which allows a NO_x reduction for all the tested engine points.

This makes *HVO* a valid alternative not only to *FAME biodiesel* but even to the conventional *Diesel fuel* itself, especially if the productive process of this fuel and the current alternatives are taken into account.

What concerns *HVO* prices, the common and natural comparison is to benchmark them with conventional diesel ones, since it is the fuel nowadays used; this would put *HVO* on a disadvantages position, since its price sits at around 10 – 15% above the diesel one. However, as *WBGroup* makes notate, we should be looking to compare *HVO* against other future energy solutions to reduce CO_2 and the cost involved with that. With *HVO* there is no upfront investment required, compared to electric or hydrogen, which require a significant amount of investment of not just money, but also time. Although these two fuel sources are the majority of businesses long term objective, in most cases it is not feasible from either a cost or application perspective, and *HVO* can be a real solution that can be called upon now. Once businesses begin to compare the cost of *HVO* with the immediate benefits it brings, and ease of switching compared with electric then the price suddenly becomes more attractive¹³.

The consumption of *HVO* is expected to grow in Europe due to a combination of consumers demand and legislative changes, which will lead to make it a more common and available fuel.

¹³ *HVO – the revolutionary new renewable superfuel: the future of energy or a fashionable alternative?*, WPGGroup, 2021

What concerns the addition of the *LP EGR* system to the original engine layout, it has been noted that, all the founded optimizations, both for *Diesel fuel* and *HVO*, prefer the use of the *LP EGR* circuit instead of the *HP* one; this proved the usefulness of adding this further *EGR* system in order to achieve best results in NO_x reduction, even if this meant to deal with a more complex system. The introduction of the *LP EGR* circuit made necessary the adoption of a further *EGR cooler* and a three-way valve at the intake manifold; this added a further degree of complexity in the λ control, since same engine air quantities could be obtained by acting with different *LP* and *HP* actuators proportions.

Bibliography

- [1] G. Keir, V. Jegatheesan and S. Vigneswaran, “Deep bed filtration: modelling theory and practice,” *Research gate*, 2009.
- [2] General Secretariat of the Council, “CO2 emission standards for cars and vans. Interinstitutional File: 2017/0293(COD),” Brussels, 2019.
- [3] O. P. Bhardwaj, A. F. Kolbeck, T. Kkoerfer and M. Honkanen, “Potential of Hydrogenated Vegetable Oil (HVO) in future high efficiency combustion system,” *SAE Int J Fuel Lubr*, 2013.
- [4] H. Aatola, M. Larmi, T. Sarjovaara and S. Mikkonen, “Hydrotreated Vegetable Oil (HVO) as a Renewable Diesel Fuel: Trade-off between NOx, Particulate Emission, and Fuel Consumption of a Heavy Duty Engine,” *SAE International Journal of Engines*, 2008.
- [5] M. Pechout, M. Kotek, P. Jindra, D. Macoum, J. Hart and M. Vojitisek-Lom, “Comparison of hydrogenated vegetable oil and biodiesel effects on combustion, unregulated and regulated gaseous pollutants and PFF regeneration procedure in a Euro6 car,” *Elsevier*, 2019.
- [6] D. Agarwal, S. K. Singh and A. K. Agarwal, “Effect of Exhaust Gas Recirculation (EGR) on performance, emissions, deposits and durability of a constant speed compression ignition engine,” *Elsevier*, 2011.
- [7] S. A. Alkhayat, G. D. Joshi and N. Henein, “Analysis and correlation of ignition delay for Hydrotreated Vegetable Oil and Ultra Low Sulfur Diesel and their blends in ignition quality tester,” *Elsevier*, 2021.
- [8] L. Miron, R. Chiriac, M. Brabec and V. Badescu, “Ignition delay and its influence on the performance of a Diesel engine operating with different Diesel-biodiesel fuels,” *Elsevier*, 2021.
- [9] P. X. Pham, N. V. Pham, T. V. Pham, V. H. Nguyen and K. T. Nguyen, “Ignition delays of biodiesel-diesel blends: Investigations into the role of physical and chemical processes,” *Elsevier*, 2021.

- [10] G. Zamboni and M. Capobianco, “Experimental study on the effects of HP and LP EGR in automotive turbocharged diesel engine,” *Elsevier*, 2012.
- [11] T. Hulkkonen, H. Hillamo, T. Sarjovaara and M. Larmi, “Experimental study of spray characteristics between hydrotreated vegetable oil (HVO) and crude oil based EN 590 diesel fuel,” *SAE Technical Paper*, 2011.
- [12] E. Spessa, “Trattamento delle emissioni allo scarico nei motori CI,” in *Controllo delle emissioni di Inquinanti*, 2020.
- [13] E. Spessa and C. Maino, “Strumentazione per la misura delle emissioni inquinanti gassose,” in *Controllo delle emissioni di inquinanti*, 2020.
- [14] E. Spessa, “Analizzatori di inquinanti. Strumentazione per la misura del particolato,” in *Controllo delle emissioni di inquinanti*, 2020.
- [15] F. Millo, “Motori diesel: aftertreatment,” in *Propulsori termici*, 2020.
- [16] D. C. Montgomery and G. C. Runger, “Aspects of multiple regression modeling,” in *Applied statistics and probability for engineers*, John Wiley & Sons, Inc., 2003.
- [17] D. C. Montgomery, *Design and analysis of experiments*, John Wiley and Sons, Inc., 2013.
- [18] S. D'Ambrosio, R. Finesso and E. Spessa, “Calculation of mass emissions, oxygen mass fraction and thermal capacity of the inducted charge in SI and diesel engines from exhaust and intake gas analysis,” *Elsevier*, 2010.
- [19] M. Parravicini, C. Barro and K. Boulouchos, “Experimental characterization of GTL, HVO, and OME based alternative fuels for diesel engines,” *Elsevier*, 2021.
- [20] Greenea, *Waste based biofuels, waste based feedstock*, 2014.
- [21] ZERO and Rainforest foundation Norway, *Palm fat acid distillate in biofuels*, 2016.
- [22] A. G. M. Top, “Production and utilization of palm fatty acid distillate (PFAD),” *Lipid Technology*, 2010.
- [23] G. Knothe, *Microalgae-based biofuels and bioproducts*, Elsevier, 2005.
- [24] ENI, “Ecofining: turning organic waste into biofuel,” [Online]. Available: <https://www.eni.com/en-IT/operations/biofuels-ecofining.html>.
- [25] C. Nicolais and A. Del Pia, *Biofuels: NextChem innovative proposition to drive the future of transportation*, NextChem, 2020.

[26] ETIP Bioenergy, *Hydrogenated vegetable oil*, 2020.

[27] *HVO – the revolutionary new renewable superfuel: the future of energy or a fashionable alternative?*, WPGGroup, 2021.